The role of context-dependent metabolic interactions in organizing microbial communities

Thesis by

Steven Alexander Wilbert

In Partial Fulfillment of the Requirements for the Degree of

Doctor of Philosophy

CALIFORNIA INSTITUTE OF TECHNOLOGY

Pasadena, California

2023

(Defended June 9th, 2023)

Steven Alexander Wilbert

ORCID: 0009-0008-4409-8974

ACKNOWLEDGEMENTS

It was only through crossing paths and making connections that I was able to make the progressive steps needed to reach this accomplishment. While I feel deeply impacted by all I have come into contact with along the way, below are some of the most impactful people on my journey. This is by no means an exhaustive list.

Hyla Sweet and Sandra Connelly, thank you for my first opportunities using microscopy as a research tool during my undergraduate degree at Rochester Institute of Technology. Jim McIlvain, thank you for giving me the life altering opportunity to work at the Marine Biological Laboratory (MBL) and for remaining a close friend over the past decade. Gary Borisy and Jessica Mark-Welch, thank you for exposing me to the wonder of the microbial world and for fostering my scientific curiously. Joseph Brzostowski, Carolyn Ott, and Rob Phillips, thank you for your mentorship and giving me the incredible opportunity to help facilitate exciting science in the Physiology course at MBL.

Andres Collazo, thank you for being an irreplaceable mentor, confidant, and friend here at Caltech. Lev Tsypin, Hugo Urrutia, Yuriko Kishi, thank you for your friendship and fellowship, and for all of the cathartic time spent commiserating. Mel Spero, thank you for teaching me basically everything I know about microbiology and genetics, and for being a shining light in some of my darkest times. Chelsey

VanDrisse, thank you for your effortless friendship, being a soundboard, and all of your advice. John Ciemniecki, thank you for opening my eyes to how people with differing skillsets and motivations can create beautiful collaborative work that is fun, fulfilling, and fruitful. Georgia Squyres, thank you for always pushing me to see beyond my current skill set. Darcey McRose, Kurt Dahlsrom, Zach Lonergan, and Rei Alcalde, thank you for all your advice and suggestions. Avi Flamholz, thank you for your unique ability to translate for me between math and biology. You've made it seem more accessible than anyone ever has. Irving, Juan, Ines, Chiara, and all other students I have taught, thank you for expanding my horizons and helping me pinpoint a strong drive and satisfaction that comes from mentoring and teaching. All other lab members, thank you for your feedback, the comradery, and the laughs.

Thank you to my committee, Viviana Gradinaru, Sarkis Mazmanian, and Victoria Orphan for all of your feedback and support over the years. To my advisor, Dianne Newman, thank you for helping me grow as a scientist and person, for never allowing me to give up, and for fostering my creativity.

On several occasions during my PhD, I did not think I would reach the finish line. My motivation, patience, and happiness ebbed and flowed. I knew pursuing a PhD was going to be difficult and a lot of hard work. However, I was unprepared for my biggest hurdles: a lack of self-confidence, imposter syndrome, anxiety, and depression. Caltech Student Wellness center and my therapist, thank you for

helping me recognize areas of myself to work on and to maintain some semblance of a mental health regime.

Finally, thank you to my husband, Michael Piacentino, for always giving me the room I need to breath while ensuring I never felt alone. Thank you for never giving up on me, even when I had. I would not have made it through these past five years without your love and support. Thank you for always being my anchor and best friend.

ABSTRACT

We can image the strikingly beautiful compositions of natural microbial communities, but we still lack an understanding of the factors that shape their organization. Understanding the drivers of these structures at the microscale may allow us to better predict and control large-scale community functions in dynamic environments. In this thesis, I developed quantitative image analysis pipelines for uncovering the spatiotemporal growth of aggregate biofilms within a developing oxygen gradient by expanding upon the Agar Block Biofilm Assay (ABBA). I then developed the Agar Disk Biofilm Assay (ADBA) for improved imaging resolution. These tools push the bounders of laboratory experiments to better capture the complexity of natural environments. Next, I built a synthetic microbial community reflecting a metabolic pathway often partitioned between members found in nature: *Pseudomonas aeruginosa* (PA) strains with a denitrification pathway genetically split at the nitric oxide (NO) node. I characterized the growth of a strict consumer and a strict producer of NO and found that PA metabolizes NO in a manner that supports growth, a previously underappreciated energy conservation strategy. Local oxygen flips this interaction from beneficial to detrimental by increasing toxicity. I found these principles drive context-dependent cellular organization. This work underscores the contributions of partitioned metabolic pathways, redox-active metabolites, and dynamic micro-niches to the organization of microbial communities. Finally, combining my efforts towards method development and an appreciation for how redox-active metabolites drive context-dependent microbial interactions, I show how phenazines promote a

previously unrecognized form of slow growth under nutrient limited environments. Taken together, this thesis highlights the importance of understanding dynamic micron-scale microbial interactions and presents several methodological improvements to capture it.

PUBLISHED CONTENT AND CONTRIBUTIONS

Wilbert S.A. and Newman D.K. 2022. The contrasting roles of nitric oxide drive microbial community organization as a function of oxygen presence. *Current Biology*. https://doi.org/10.1016/j.cub.2022.10.008

S.A.W. conceptualized study, developed methodology, performed experiments, data interpretation, and writing of manuscript drafts under the guidance and editing of D.K.N.

TABLE OF CONTENTS

LIST OF ILLUSTRATIONS AND/OR TABLES

NOMENCLATURE

Aerobic. Referring to microbial growth utilizing oxygen as a terminal electron acceptor during oxidative phosphorylation.

Agathokakological. Being comprised of both good and evil. Used here to illicit the paradoxical sense of how a molecule can be both beneficial and toxic.

Aggregate biofilm. A tight collection of bacterial cells, often representing a progression of growth originating from a single cell.

Anaerobic. Microbial growth in the absence of oxygen. May refer to either oxidative phosphorylation with a terminal electron acceptor other than oxygen or substrate-level phosphorylation via fermentation.

Anoxic. Specification of an environment devoid of all oxygen.

ATP. Adenosine triphosphate, the primary energy currency.

Batch culture. Cells grown under finite nutrient conditions.

Biogeochemical cycle. The process by which an element is transferred between systems of the biosphere.

Clonal domain/expansion. A patch or aggregate of cells originating from a single progenitor.

Co-culture. Two or more cell types grown together.

Colony Forming Units (CFU). A technique used to identify the number of *culturable* cells by sequentially diluting a population until single cells form clonal colonies, manually counting and back calculating an approximation of the total cells.

Consortium. In terms of microbes, a collection of different cell types in an apparent close association.

Denitrification. The sequential reduction of nitrogen oxides from soluble to gaseous substrates, often leading to the loss of nitrogen from biological systems.

Energy conservation. In metabolism, referring to a process that contributes to ATP production.

Fluorescent protein. A molecule which when excited by one wavelength, can emit light energy from another. When integrated genetically into an organism, can be used to identify cell type and or expression levels depending on promotor driving its production. Examples include green fluorescence protein (GFP).

Genetic composition. All of the genes an organism possess.

Genetically engineered. The addition or removal of a gene from an organism. Here, a strain that has a gene cleanly removed from its genome is denoted Δ*gene.*

Hypoxic. Describes an environment that contains less than atmospheric oxygen, but above 0%.

Imaging resolution. The minimum distance between two points discernable by an imaging system.

Inoculum density. A general description of the number of cells used to start an experiment. This can be based on an optical density and or calibrated based on colony forming units.

Lysis. The final stage of cell death. The cell cytoplasm is no longer separated from the outside of the cell.

Metabolic pathway. All of the steps involved in electron transfers between donors and acceptors.

Microbial community. More than one cell within interacting distance from another.

Microenvironment. The chemical environment within immediate proximity to a cell.

Microscale. Scales within a few hundred microns.

Oxic. Being within atmospheric oxygen conditions.

Oxidative phosphorylation. The use of an electron transport chain and a terminal electron acceptor such as oxygen or nitrate to generate a chemical proton gradient driving ATP generation.

Oxycline. The range of an oxygen gradient marked by a critical drop in oxygen.

Phenazines. Colorful redox active metabolites secreted by some organisms and used for a wide variety of uses such as signaling molecules, defense, toxicity, completing redox reaction between the core and periphery of a biofilm and nutrient acquisition.

Pyocyanin (PYO). A phenazine produced by *Pseudomonas aeruginosa* that is blue when oxidized and colorless when reduced.

Quiescence. Inactive cells. Not dividing, but not dead.

Reactive oxygen species (ROS). Free radical forms of molecules that lead to DNA and enzyme damage, and cell death.

Redox active metabolite (RAM). A molecule capable of donating or accepting elections, often contributing to a larger redox cycle.

Sessile. When cells are unable to move freely. Such as adhered to a surface, embedded within or beneath agar.

Sterile conditions. The immediate environment is free from threat of contamination. Practically speaking, this means a process was performed under a flame or within a biosafety cabinet.

Substrate-level phosphorylation. ATP generation without the use of an electron transport chain, typically using fermentation.

Synthetic community. Here used to distinguish between a polymicrobial community (made up of different species) and a community made up of a co-culture of genetically modified strains.

Terminal electron acceptor (TEA). The molecule which is reduced in the electron transport chain allowing the coupling of a chemical gradient to ATP synthesis.

Chapter 1

INTRODUCTION AND BACKGROUND

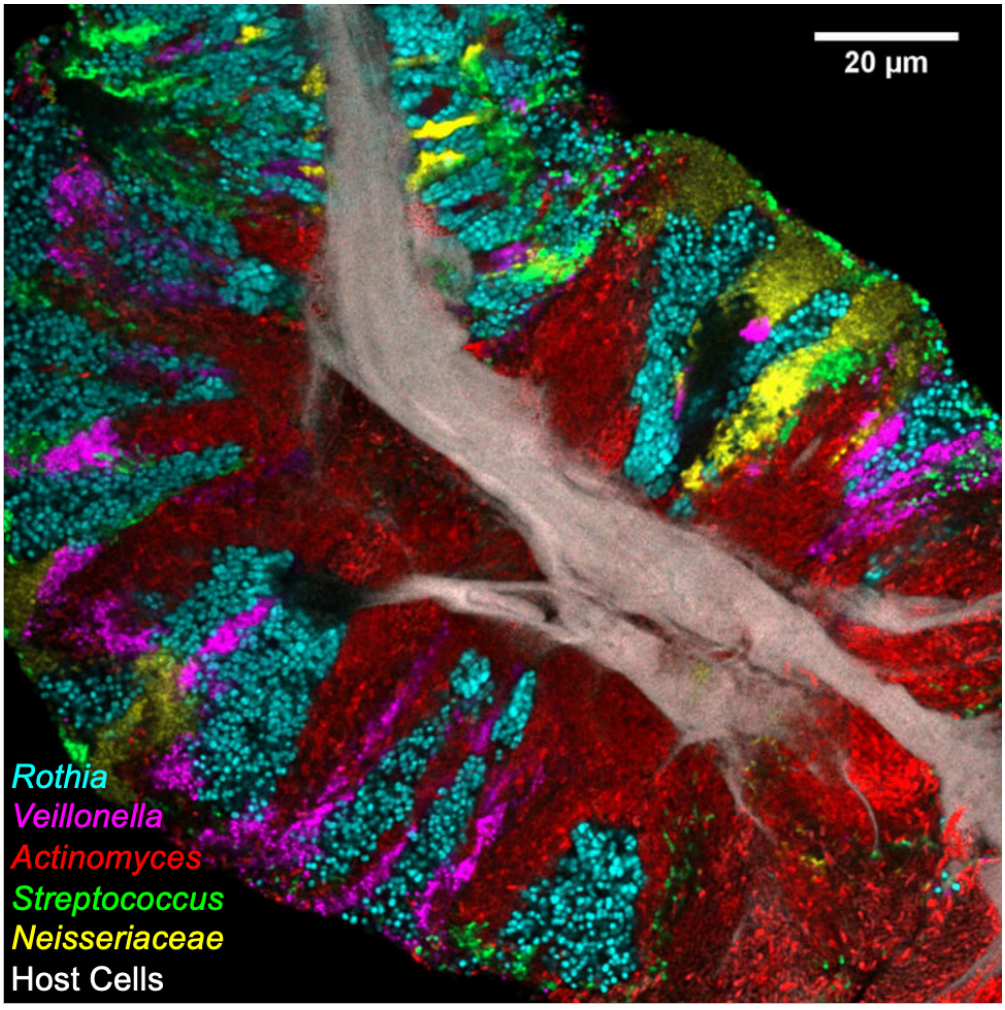

Figure 1. Microbial consortia from the human tongue dorsum motivating understanding the structure-function relationships of polymicrobial comminutes. Image from (Wilbert et al., 2020).

How micron scale spatial patterns bridge our understanding of global biogeochemical cycles and infectious disease

The driving force behind this thesis is to connect the micro and global scales. Microscopy has been a passion of mine for over a decade. Being able to bring into focus the tiny unseen world, capture and share it has always fascinated me. This aimless passion was given direction when I was introduced to the world of microbial ecology. Prior to pursing a PhD at Caltech, I spent several years working towards uncovering the spatial patterns of microbes on the human tongue dorsum in the lab of Gary Borisy (The Forsythe Institute, Cambridge MA). Using a new labelling and spectral imaging approach, I was able to visualize a complex community of organisms forming a beautiful array of spatial patterns (Figure 1). Each dot is a single cell and each color a different kind of cell. It was through this project that I developed a taste for putting in the work, driving the improvement of techniques in order to achieve beautiful and seemingly artistic images of microbes. This labor of love is one of my proudest achievements (Wilbert et al., 2020).

Quickly, however, my need to understand how things work led me to wonder, why? Why these patterns? How did they form? I hope that by the end of this thesis I will have convinced the reader that by using simple imaging tools coupled with a well-defined and genetically controllable interaction, we can visualize such reproducible pattern formation. By mapping key features of

emergent pattern formation, we can start to gain a generalizable understanding of how microbial community interactions can scale to global phenomena.

Chapter 2 lays the groundwork for this thesis by reviewing important concepts and ideas that poise the work that follows. Here I outline conditions microbes face in natural systems, whether they are in soils or infecting human lungs. By doing so, we find that the need to respire leads to more commonality between environments than differences. Therefore, in order to make general claims about how microbes are making a living in these systems, there is a need to adapt laboratory assays to better simulate and encompass the complexities microbes face outside the lab.

Chapter 3 presents several improvements to laboratory assays that allow us to better simulate and visualize microbes under conditions that push the complexity and at a scale that is important. Troubleshooting and assay optimization is a passion of mine, and here I present the most up-to-date versions of analysis pipelines for studying microbes in context. Hopefully these methods will continue to push the field forward.

Chapter 4 is the major hypothesis-driven contribution to my thesis. Here, I genetically engineered a two-strain synthetic microbial community that interacts via nitric oxide (NO). Because NO toxicity is tunable based on oxygen and

proximity, I used these strains and imaging methods to observe spatial patterns in response to the presence of oxygen in the microenvironment. Importantly, the growth of these strains and the influence they have on one another is highly dependent on their genetic composition, but also under which conditions they are grown. The formation of chemical gradients under sessile conditions is thus an important takeaway from this work and prompts future studies to not overlook what is occurring at the microscale.

Chapter 5 is a collaboration with another student in the lab, John Ciemniecki. We recognized the potential to adapt the experimental approach I developed with the NO synthetic community to address how another context-dependent metabolite influences the growth at the microscale: the phenazine pyocyanin (PYO). Here we develop a simple method called Clonal Aggregate Slow Proliferation Assay, or CASPA for short. Using CASPA, we identify a previously unseen promotion of slow cell division in the absence of carbon but addition of PYO. These data again highlight the importance of directly observing growth at the scale it is occurring in order to fully appreciate all contributions to population dynamics.

Chapter 6 is a synopsis of my final thoughts, major take away messages, and what I see as important future directions beyond the work presented here.

C h a p t e r 2

CONTEXT MATTERS: REVIEW OF IMPORTANT CONCEPTS

The microenvironment

If organisms are active, they are acquiring and processing resources. In terms of energy conservation, this is in the form of electron donors and acceptors. As organisms harvest what is available in their local environment, they shape it. We have a great appreciation for vast diversity in the metabolic arsenal of microbes based on decades of laboratory experimentation and prediction from sequencing data. Looking at the specific example from the microbial community found on the human tongue (Chapter 1, Figure 1), we observe spatial patterns that are likely the result of an integration of this metabolic diversity in growth that occurred up until the point of observation. From this perspective, and if we reason individual cells first adhered on the host tissue and grew outward towards fresh nutrients, the shape of clonal domains can be used to hypothesize how growth occurred over the developmental timescales.

For example, some patches appear to start as one cell and progressively occupy more and more space as it reaches the periphery. Such a clonal expansion is indicative of uninterrupted logarithmic growth and has been modeled to show a strong growth advantage over neighboring cells (Hallatschek

et al., 2007). Conversely, we also observe the opposite. As the patch size at the expanding front (perimeter) is smaller than at the core (host tissue), cells must have been outcompeted for nutrients or grew in the reverse direction. These types of patterns can be more difficult to unpack but are likely a response of the metabolic diversity present in the consortium. The red patches, for example, show this pattern of growth and unlike the cyan cells has the ability to breath in the absence of oxygen. So, if an organism can breathe without oxygen, it would have an advantage in that microniche and therefore grow better in deeper anoxic zones, resulting in patterns similar to how the red cells appear.

At this point, perhaps like me you are thinking how this makes sense but is highly speculative. While I have been excited by the perspective of observing microbial growth such as this as an integration of the interactions the cells had with one another and their immediate environment, I feel we should continue to push towards filling in the gaps by directly observing what is happening at dynamic timescales prior to these beautiful, mesmerizing end time point images.

Finally, it is clear that oxygen is a major driver and is an important feature to consider. We know that at the core of biofilms oxygen quickly becomes limiting due to its consumption outpacing its diffusion (Stewart et al., 2016; Wessel et al., 2014). Also, from measurements made in both the lungs of cystic fibrosis patients experiencing chronic bacterial infections and soils subjected to periodic

flooding, we know that oxygen can quickly become a limiting resource that it is highly dynamic (Kolpen et al., 2014; Krichels et al., 2019). Therefore, understanding how microbes respond to changes in oxygen may yield important parameters for better predicting and controlling microbial actives.

Redox-active (aka agathokakological) metabolites

The use of electron donors and acceptors in metabolism are made possible due to redox reactions. The exchange of electrons from one molecule to another changing the redox state is a critical component utilized in energy conservation. From one perspective, the ability to shuttle electrons to complete necessary reactions for metabolism sounds purely beneficial. But such transfers can have a dubious effect as well. For example, during aerobic respiration if oxygen is not completely reduced, radical intermediates form. These so-called reactive oxygen species (ROS) quickly and spontaneously react with iron-sulfur (Fe-S) clusters disrupting enzymic reactions and damaging DNA (Arai, 2011). This will at minimum slow down normal cell function, causing upregulation of costly detox mechanisms, and at worst lead to cell death.

The idea that a single molecule could have such opposing effects on cells depending on its context was a major contributing framework droving me during the course of my PhD. Around the same these ideas were brewing, Dianne received an apt “Word of the day”: Agathokakological, meaning to be composed of both good and evil. To be clear, we use this word to describe the types of

interactions of microbes with their environment we are most interested in, those that are context-dependent and can be the difference between a cell growing or dying. We are cautious to assign sentient morality to molecules or microbes, but rather it is a fun word to say and always engages conversation.

We are gaining an appreciation for how such redox active metabolic (RAM) interactions may act as so called keystone metabolites (Dahlstrom et al., 2020). While others are developing tools and frameworks to use these redox features as metabolic predictors (Thalhammer and Newman, 2023). It was my hope for the work presented here to expand upon our understanding of the types of redox molecules at play (soluble such as phenazines, vs gaseous such as Nitric Oxide) and to improve our ability to directly visualize cells at the microscale while undergoing such agathokakological metabolic interactions.

The need for new methods

Uncovering the full potential for microbial growth and survival will yield better tools to exploit for killing hard to reach populations in chronic infections and preventing fertilizer overuse contributing to global warming. From this perspective, understanding what is occurring at the microscale, can help us better control the macroscale in both instances of human health and our contributions to biogeochemical cycles.

Given the importance of how the microenvironment and redox active metabolites may play in driving microbial community function in biogeochemical cycles and disease, there is a need to develop assays to better encompass these conditions and this was a primary motivator for this thesis. In particular, the need to make the following comparisons drove method development. 1. Cells in the presence and absence of electron donors and acceptors. 2. Cells growing planktonic, sessile, and within biofilms. 3. Cells grown under oxic, hypoxic and anoxic conditions. 4. Bulk vs single cell assays.

It may be difficult to measure all of the chemical changes we would like due to the plethora of complex chemical interactions at play, but you cannot mistake cell division or cell lysis. Therefore, I chose instead to focus on detailing interactions under known chemical conditions that either induce cell growth or lysis. By doing so, we can use the visual queue of division or lysis as a proxy for the microenvironment when we are unable to measure it directly (though it would be very helpful to be able to do so!).

It was not my goal to reinvent the wheel, but rather make sequential improvements. Often these stepwise improvements cost little to no more than standard procedures, and only require basic tools. I hope by taking this approach I have contributed to leading scientific discovery towards a more inclusive and equitable future.

C h a p t e r 3

DEVELOPMENT OF TOOLS TO VISUALIZE CONTEXT-DEPENDENT MICROBIAL INTERACTIONS

This chapter is a collection of unpublished methodological improvements. Technological and intellectual contributions were utilized in publications as indicated.

At time of writing, a Center for Environmental Microbial Interactions (CEMI) grant supports a collaboration between the Newman and Phillips lab in which Gabe Salmon, Avi Flamholz and I are using methods as outlined below to mathematically model context-dependent microbial growth over oxygen gradients. *Work in progress.*

Agar Block Biofilm Assay (ABBA) Analysis

Introduction

Standard laboratory culturing conditions in a well-mixed and rich media is an excellent way of acquiring large quantities of cells in the shortest amount of time. However, these methods often do not recapitulate the metabolic diversity

we know to take place in non-laboratory conditions. In a step towards bridging the complexity of natural systems and the reproducible, well-controlled laboratory conditions, the Agar Block Biofilm Assay (ABBA) was developed (Costa et al., 2017; Spero and Newman, 2018). This relatively simple assay allows us to visualize how a self-induced oxygen gradient influences the growth of cells growing into aggregate biofilms.

While this method had been an established workhorse of the lab, I recognized an opportunity to expand the toolkit. I wanted to push the boundaries of the analysis pipeline from mostly qualitative visualization, to extraction of quantitative metrics. This innovation has led to several publications and has inspired mathematical modeling efforts that seek to better incorporate how the microenvironment (in this case oxygen diffusion) contributes to microbial growth in a more realistic way.

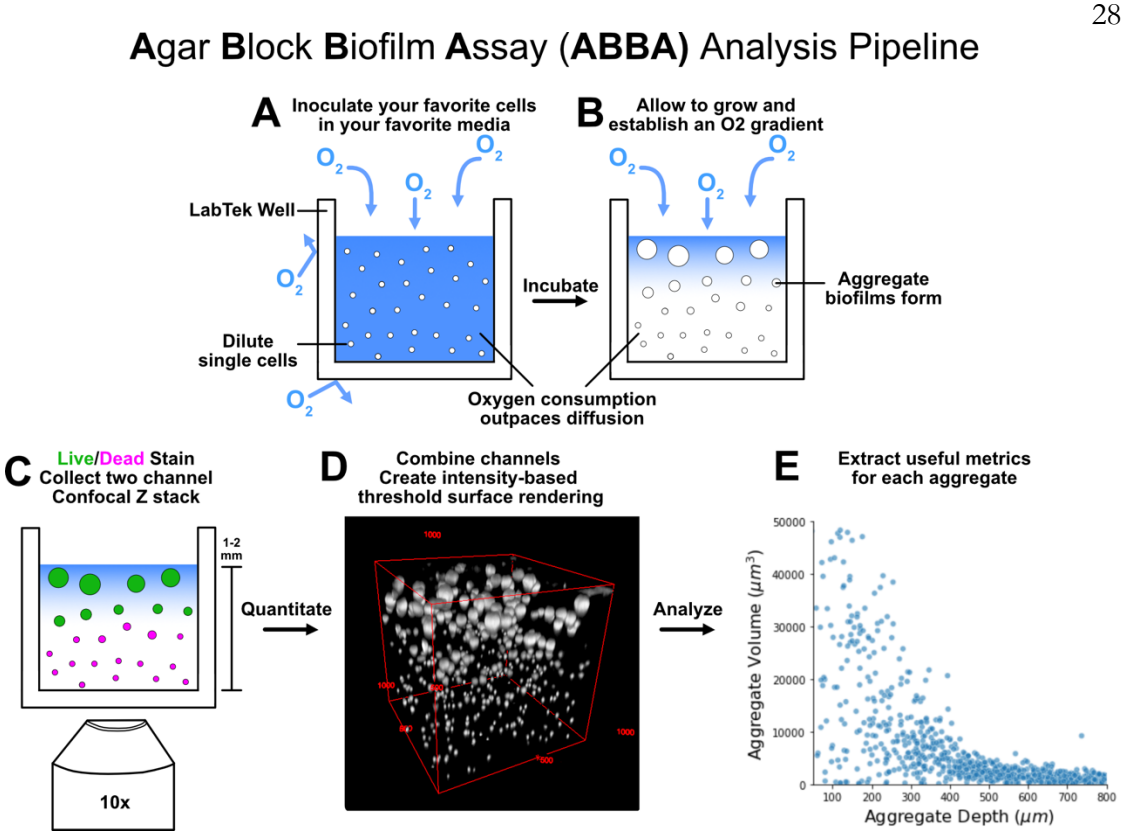

Figure 1. Major steps of ABBA analysis pipeline. (A-B) Prepare ABBA per standard protocols. (C) Stain cells using the Syto9 (Live) and PI (dead) standard protocols and collect confocal Z stacks. (D) Combine channels to create an all-inclusive masking channel, create a 3D surface rendering using Imaris. (E) Extract quantitative metrics from Imaris.

Method

The standard ABBA method involves suspending dilute cells in an autoclaved medium containing a 0.5-2% (w/v) Noble Agar. Noble agar is used in place of standard Bacto Agar, like what is used for plates, because of its purity, reduced light scattering and background autofluorescence. The media and agar mixture may be microwaved and held at 42C in a water bath or heat block to remain molten. Typically, 1 mL of molten media is added to a standard 1.7 mL

Eppendorf tube and placed at 42C until ready (everything should be set up and ready before starting). Liquid overnight cultures are washed and diluted to OD 0.1 either in the same media (minus agar) or 1X PBS. Once ready, this OD 0.1 is further diluted into the molten media and agar solution to a final OD of your choosing. While OD 0.001 has been an ideal starting place optimized for PA14, in practice, this does not scale perfectly to other organisms like *E. coli or S. aureus*. Regardless of the strain used, start by trying several inoculum densities and calibrate with plating for colony forming units CFU, especially when more than one strain is used in order to optimize an equal starting density. Once cells are diluted into the molten agar, cap and thoroughly vortex. Immediately pipette 200 uL of cells suspend in agar into each well of a Lab-Tek imaging dish (Catalog# 155409). Importantly, even if you are preparing multiple wells per strain/media mixture, use a fresh pipette tip for each well as agar quickly solidifies in the tip altering the volume being extracted and or deposited. It is best to slowly eject agar into the well from one corner to the next, quickly popping any bubbles that form with a new dry tip before solidification occurs (Figure 1A).

Once all wells are inoculated, place the lid on the plate and place in a sealed plastic container with a wet paper towel to control humidity. Incubate container as needed. PA14 suspended in a LB agar at 37C will start to form an oxygen gradient (based on visualizing the formation of aggregate size gradients at fixed

time points) around 9 hours and deplete nutrients and therefore cease forming an oxygen gradient at or around 24 hours (based on microelectrode measurements). This timing will change drastically according to strain, inoculum density, and medium used (Figure 1B).

After incubation, cells can be stained with the cell viability kit using Syto9 (cell permeant) to label “all” and or “live” cells in green fluorescence and PI (cell impermeant) to identify “dead” cells in red fluorescence according to manufacturer protocols. Quotations are used to describe the populations labeled as it has been established that redox active metabolites such as phenazines produced by PA can result in quenching of fluorescence dyes (Flamholz et al., 2022). When comparing WT and Δ*phz* strains for PA Syto9 stains Δ*phz* more intensely than WT presumably due to the phenazine quenching. Also, PI has long been considered to label dead cells, but due to the lower membrane charge associated with slow growing or quiescent cells, PI has been shown to also label these populations (Teal et al., 2006). Therefore, while these stains can be extremely useful for labeling live cells and suggesting the metabolic stratification that is occurring within an ABBA, we must be careful in our interpretation of these staining patterns.

All of this aside, stained confocal Z stacks can be acquired. Confocal microscopy is important because of the thick three-dimensional nature of the

aggregates as well as the block that contains them. Widefield fluorescence microscopy suffers from the inability to differentiate between fluorescence coming from one focal plane to another resulting in “blurry” and overly elongated aggregates in 3D data sets. On the other hand, confocal microscopy uses a simple pin hole to deflect away the fluorescence originating from above or below the specific focal plane you are observing at any given Z position. This results in what is called an optical slice. This optical slice image can then be collected step wise throughout the agar block. Starting at the agar surface (it is easy to see by focusing just past where the largest aggregates are, or you can add a dilution of fluorescent beads to mark the surface) and moving deeper within the block collecting several 2D images each representing optical slices through the aggregate throughout the block known as a Z stack (Figure 1C). The interval spacing at which each optical slice is taken in known as a Z step size. Optimally, XY (pixel size) and Z (step size) spacing would be collected intervals based on what is known as Nyquist’s theorem. Often this can be accomplished by selecting “optimal” in the microscope software. But practically, if your optical slice thickness is 12 µm, chose a Z steps size that is less than half of this number with diminishing returns below 2.5 less than the optical slice.

To visualize ABBA data sets, you can open the Z stack in FIJI (Schindelin et al., 2012). As explained and depicted in Figure 1C, the live/dead stains may only stain sub populations because of the differential staining mechanics (often the

larger, top aggregates are brighter in green and the bottom smaller aggregates more in red). Therefore, to visualize all of the aggregates at once, we want to create a single channel that contains the intensity information from both channels. This can be done in FIJI simply by separating the two channels (Image > Color > Split Channels), then combine the two channels into a new third channel (Process > Image Calculator > Operation Add). This new channel can then be used for visualization of all aggregates in 3D (Plugins > 3D Viewer, screenshot displayed Figure 1D). Recombine the three channels into one stack (Image > Color > Combine Channels). Save as a new file. This file can then be brought in Imaris for 3D aggregate quantification.

Briefly, using the “Surface Tool” in Imaris, select the combined channel you created in FIJI and adjust the intensity range until all of the aggregates appear to be enveloped by the 3D mask and click continue. Next, there will be several opportunities to make fine adjustments to your surface rendering and I suggest playing with all of the tools and write down what you have done so you can treat all data sets equally (for example, you may want to exclude aggregates bisected at the edges of the images in your analysis as they will report as artificially smaller than they are in reality). Whatever you do, make sure you know what is being done so that you can be consistent in your image treatment across conditions and others can reproduce your analysis. The beauty of Imaris is that once you are happy with your surface creation and click to finalize it, the

software will automatically calculate several useful metrics for you automatically and just need to be exported as a series of csv files each containing one of these metrics and unique object ID's (aggregate = object) (Figure 1C).

Finally, in your favorite plotting software you can take these exported data from Imaris and make plots of your data. The example plot in Figure 1D shows aggregate size measured in volume (μm^3) compared to its depth within the data set (numbers are distance from agar surface). This is the most basal level of exploratory data analysis possible with this pipeline. Aside from size, the software also extracts fluorescence intensity information from all channels as well as 3D coordinates per aggregate. One could imagine using these data to generate inter and intra-aggregate interaction information.

Results

While a relatively simple example of the analysis pipeline is shown here in Figure 1, it was also the basis for several other quantitative image analysis pipelines I shared with other lab members and contributed to their publications. First, this pipeline was used not only to measure aggregate sizes, but to compare aggregate PI staining over the depth of ABBAs (VanDrisse et al., 2021). Beyond live/dead quantification, this pipeline has also be adapted to

extract mRNA expression levels of aggregates and helped us move towards establishing expression profiles of aerobically and anaerobically respiring cells (Livingston et al., 2022).

Finally, I used this method to compare how the starting cell density influenced aggregate sizes and gradients (Figure 2). Each ABBA was set up as described above only cells were diluted to the final density indicated and using PA14 cells encoding a constitutively expressed GFP reporter. Orthogonal projections displayed in panel A were generated in FIJI by running the following steps: Image > Stack > Reslice (output spacing = Z step size), then Image > Stack > Z Project > Maximum Intensity Projection (MIP) (Figure 2A). The same analysis pipeline was performed as outlined above only instead of directly plotting all data points, for better differentiation and visualization of each dataset aggregates were grouped based on their Z position in 200 μm steps. These binned aggregate volumes were used to generate an average (dark line) and bootstrapped 95% confidence intervals (lighter shaded area) using built in tools in the Seaborn plotting package (Waskom, 2021) (Figure 2B). It is clear from this analysis that starting density plays a major role in the resulting growth of aggregates in ABBA. The smaller the starting density, the larger the aggregates can become likely due to less lateral competition for nutrients.

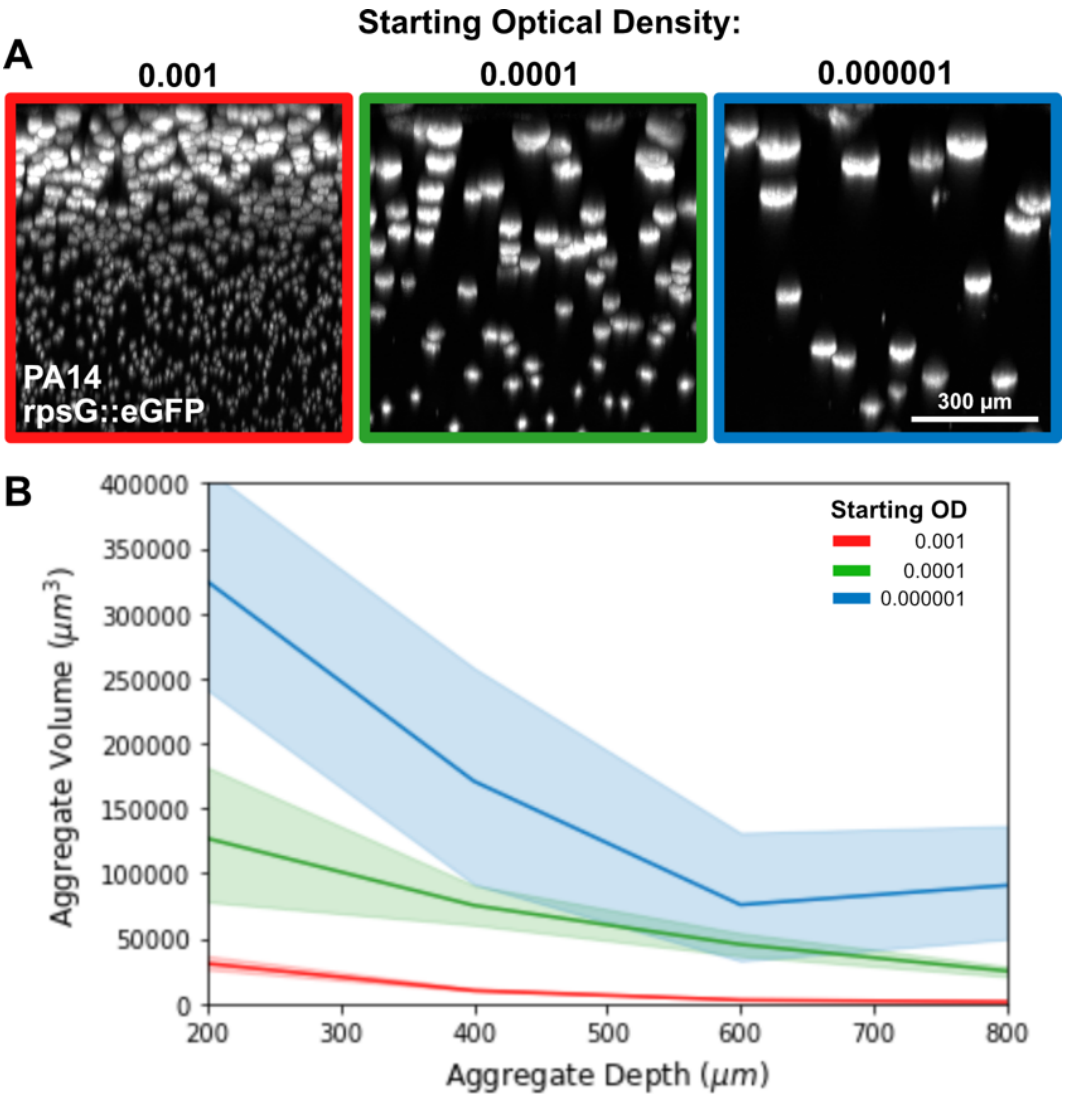

Figure 2. Using the ABBA analysis pipeline to compare how inoculum density sets aggregate size. (A) Orthagonal maximium intensity projections of three ABBA data sets inoculated with different starting cells densities. (B) Results of ABBA analysis pipeline.

Future directions

While this analysis pipeline was a step forward towards expanding the ABBA toolkit, there is still plenty of opportunity for improvements. First, we need better fluorescence markers. GFP and mApple reporters require oxygen to fold. The

ABBA assay is so powerful because we are able to visualize oxygen-mediated metabolic stratification, yet once oxygen becomes low our markers efficacy declines (compare deeper aggregate intensity between densities in Figure 2B). Because oxygen is one of the primary parameters we wish to study, it would be worth the investment to switch to fluorophores that do not relay on oxygen for their maturation such as the LOV proteins (Wingen et al., 2014). However, it is important to note that production of these proteins is often unaffected by oxygen, just rather just have not matured. For example, if you grow GFP expressing cells in the anaerobic chamber devoid of oxygen, taking them out and immediately observing them in the microscope will yield dim cells. However, if you place the cells at 4C to slow further growth but give them time to allow oxygen to fold the proteins, you can then image and identify the fluorescence markers in the cells. I heavily relay on this trick in Chapter 4 in order to retrieve the signal to distinguish single cells as being GFP or mApple populations.

While the aggregate volumes extracted and displayed here are a good estimate, the empirical numbers suffer from optical effects that conflate their size. This is somewhat unavoidable but is made worse by the required use of a low magnification, low numerical aperture (NA) objective so the working distance is long enough to reach the agar surface. I see two ways of overcoming this issue. 1. Add diffraction limited fluorescence beads to the agar, use them to perform a

deconvolution image processing algorithm to computationally correct a large proportion of the conflated aggregate size. While this can certainly work, the downside is more pipeline steps, more time spent processing images, generating even more files (file storage is a major concern). 2. Change the format of the ABBA such that higher magnification and NA objectives can be used, collecting higher quality data sets requiring less processing. Such changes in format are outlined and described later on this chapter.

Finally, 25 μm-sized glass tipped oxygen microelectrodes (Unisense) have been used to take static oxygen gradient profiles of ABBA which can be overlayed with quantitative aggregate size information (Spero and Newman, 2018; VanDrisse et al., 2021). However, as the questions we hope to address become more specific, so should our methods. It will be pertinent to continue developing methods for better understanding what is happening at the microscale within these assays. There are two specific avenues I recommend committing time and energy to. 1. Mathematical modeling of respiration rates within ABBA. I think this is important in order to continue pushing the boundaries of what can be address using this assay such as co-cultures and modulation of nutrients. Such efforts are under way through a collaboration between the labs of Dianne Neman and Rob Phillips supported by a CEMI grant. Gabe Salmon, Avi Flamholz and I have used the data collected here as a jumping off point to better model how this growth is occurring, 2. We need dependable oxygen

measurements at the scale of the aggregates. Microelectrodes are very useful but are an approximation and average of what is likely to be a dynamic and highly variable parameter at the microscale. PA penchant for generating RAMs that interfere with currently available fluorescence oxygen dyes (Flamholz et al., 2022) makes this difficult but nevertheless hopefully motivated the further creation of even better tools that will push the field forward.

Dynamically tracking ABBA growth with time lapse microscopy

Introduction

As soon as an established analysis pipeline was developed to track aggregate size and position, it opened the doors to the possibility of tracking aggregate development dynamically over time. Many of the claims we wish to make about what kind of growth or death is occurring in the ABBA requires looking at an end time point as an integration for what is likely dynamic events. I asked what would aggregate growth look like if we had data more similar to that of a growth curve. Instead of tracing density, I traced the size of aggregates as a proxy for cell growth and relate these data to an aggregates spatial position which we know is impacted by oxygen consumption and diffusion. Therefore, optimization of ABBA time lapse was carried out.

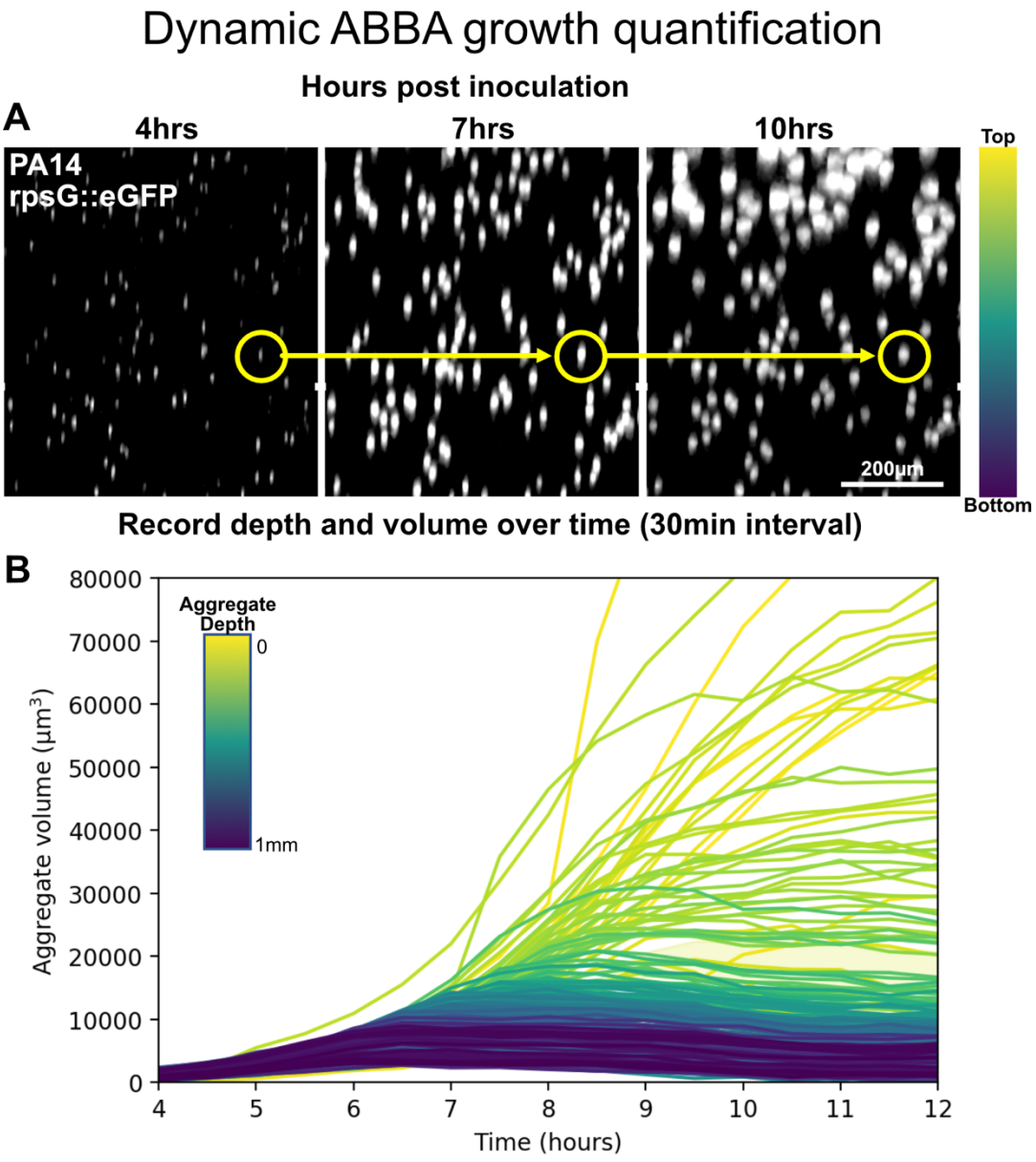

Figure 3. Example of time lapse ABBA data. (A) Single frame orthogonal projection views of the same ABBA inoculated with PA14 WT cells constitutively expressing GFP taken at three different time points. (B) Each aggregates volume is tracked dynamically over time from the data set in A but the trace is colored based on the depth of the aggregate.

Method

To begin, set up ABBA is outlined in previous section but specifically using strains that encode constitutively expressed fluorescence reporters (recall GFP is less sensitive to changes in oxygen compared to mApple, but there is more autofluorescence in the green spectrum and therefore reducing signal to noise making segmentation more difficult).

Controlling humidity is crucial to collecting time lapse data sets. I would recommend adhering to the following precautions I have found to be most beneficial in minimizing agar dehydration and thus signification Z drift during acquisition. 1. Use only the four inner wells of an 8 well Lab-Tek imaging dish, and instead fill the outer wells with 200-400 uL water or buffer to humidify the dish. 2. Seal the imaging dish lid to the base with parafilm (be careful to not over the bottom coverslip). 3. If applicable, use live cell imaging chambers which you can be flooded with humidified air during the time lapse duration.

In my experience, PA can be quite photophobic. For example, if you seed cells and immediately start collecting a time lapse, cells tend to lyse and/or do not grow in the optical path being illuminated with light. To overcome this, pre-grow ABBAs for 3-4 hours in the dark prior to setting up a time lapse. Because aggregates start as single cells and you are using a low magnification objective, pre-growing and allowing small aggregates to form has the added benefit of

allowing you to set up Z stacks and ensure cells are in the field of view prior to walking away.

Finally, set microscope incubation several hours prior to setting up time lapse to allow for thermostabilization, otherwise you are likely to see significant focal drift as the stage and objectives warm up overtime. Next, configure the microscope to acquire Z stacks of several fields of view from each well at an interval of no less than 20 minutes. Keep in mind the time it will take to acquire each Z stack and factor this into your planning so that you can sample at appropriate time intervals.

Due to imaging with low magnification and NA objectives, coupled with poor fluorescence markers, it is often required to pre-process the data before image analysis. A median filter can be applied to minimize noisy pixels. Histogram normalization can also be helpful to standardize aggregate contrast over Z depth but also between time points. As aggregates grow, they will become brighter as there are more cells making more reporters. Pre-processed data sets can then be analyzed in Imaris as described above but ensuring to select “Track Overtime” in the surface creation tool. Keep in mind the file size and computation required to accommodate these files (often at least 1 gigabyte per field of view) on your storage device but also the time it will take to accomplish the analysis. Once complete, the data can be displayed and graphed as in

Figure 3. Here each aggregate is represented by its own line showing its volume over time (reminiscent of a growth curve) and color coded based on its depth in the agar block (Figure 3B).

Results

Looking at the graphed data in Figure 3B, it is fair to assume that yellow traces that are closer to the agar surface have more access to oxygen and therefore grow the largest, fastest and for the longest. While this is not a surprising result, it is nevertheless informative (and satisfying) to observe the full dynamics at play that lead to the aggregate size gradient.

In order to test how such an assay and analysis could aid on our ability to observe growth over a forming oxygen gradient, I next wanted to test what would happen if I modulated the availability of nitrate (NO_3^-) in the media. Because PA can respire NO_3^- when oxygen is limiting, the expectation would be for deeper anoxic populations to grow differentially when NO_3^- is present. ABBAs were set up and time lapse data was acquired as outlined above. After four hours of preincubation, 18 additional hours of growth was recorded of WT PA14 cells in four different media conditions. The media used was LB supplemented with 1% (w/v) Noble Agar as well as specified NO_3^- concentrations (Figure 4A). The top row of graphs shows all aggregates as

individual line traces. The bottom row is the same data, but aggregates were grouped based on their depth in order to more clearly identify which populations (in this case depth, and depth = oxygen). From these data we see that our expectation is correct and there is indeed a dose dependent growth response of deeper aggregates to the presence of NO_3^-. Interestingly, not all depth groups of aggregates show a doubling of size when NO_3^- is doubled, likely indicating which populations are starved for an electron acceptor (in this case O_2 or NO_3^-) but perhaps not carbon.

Finally, I performed the same experiment in LB supplemented with 1% (w/v) Noble Agar and 5 mM NO_3^- but differed in which strain was used (Figure 4B). WT PA14 again showed a clear shift between metabolisms with two distinct exponential phases, likely due first to the utilization and loss of oxygen, the second due to the utilization of NO_3^- reduction. Conversely, the Δ*narG* strain that lacks the nitrate reductase, did not show this type of pattern, indicating it is necessary for the observed growth.

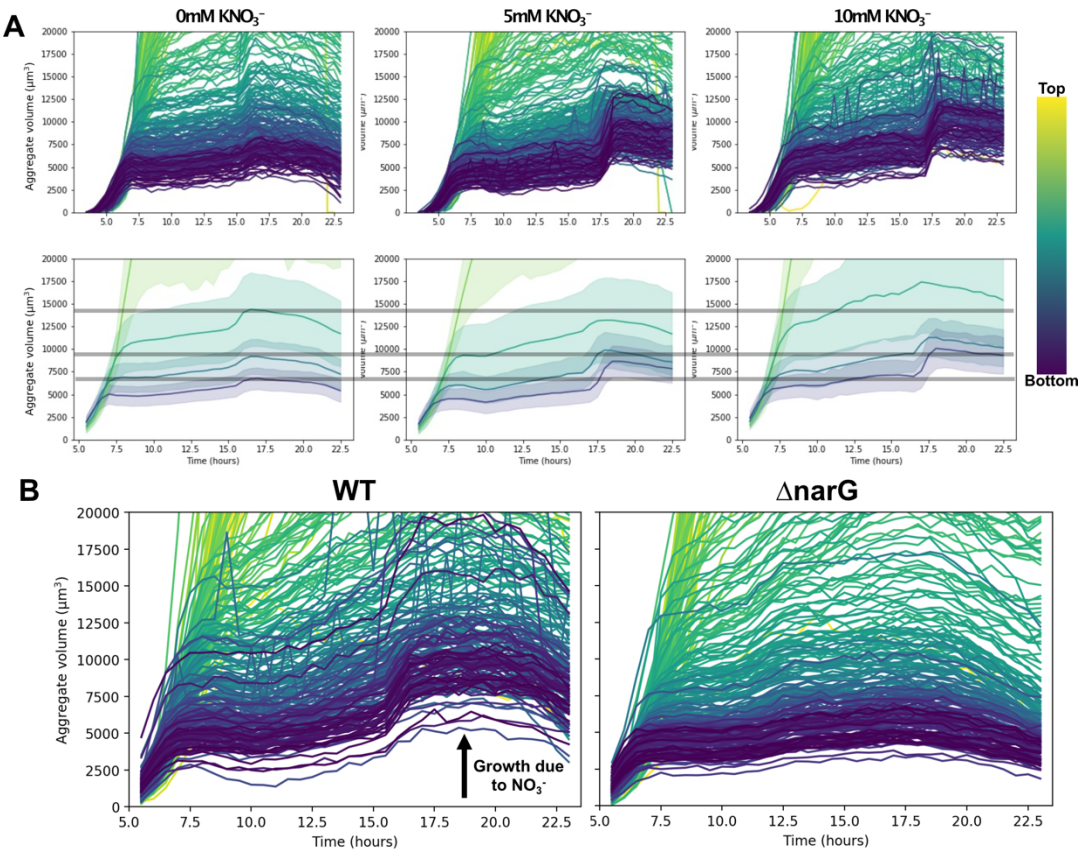

Figure 4. Comparison of aggregate growth when alternative electron acceptors are present. (A) PA14 WT strain containing a constitutively expressed GFP fluorescence reporter was grown in LB agar supplemented with three different concentrations of potassium nitrate (KNO_3^-). Top row of graphs: each trace is a single aggregate. Bottom row of graphs: same data as top but aggregates averaged with four distinct depth bins. (B) WT is compared to a strain lacking nitrate reductase (narG) in media supplemented with 5 mM KNO_3^-.

Future directions

While these data may not have made it into publication beyond the writing here, they have been an incredible source of inspiration for me throughout my graduate career personally, and I have no doubt that they will continue to inspire others and enable exciting discoveries moving forward.

The protocol and analysis pipeline presented here has been significantly optimized, but there is still room for improvements. The Newman-Phillips lab collaboration is currently using such dynamic data to mathematically model growth over oxygen gradients. Thus, it becomes even more important to consider the quality of the volumes being reported. As stated earlier in this chapter, volumes here are conflated due to poor optics used in the current setup. If the questions you are asking with these analyses can be answered by simple comparison of patterns between conditions, the pipeline and analysis is ready for primetime. However, as I have realized thanks to fruitful discussions with Gabe Salmon and Avi Flamholz, in order to mathematically describe and most importantly to predict such dynamic stratified growth it will be evermore important and worth the investment to again either perform deconvolution on these data sets (keep in mind computation costs with these large data set!) or to update the format of acquisition to achieve better data to begin with.

I can only imagine the complexity, but I hope to one day see this method expanded beyond a single growth dynamic to polymicrobial communities coupled with oxygen and or other readouts of the *local* chemical environments (this was the dream that led to my awarded National Science Foundation Graduate Research Fellowship proposal).

Exploring other ABBA formats for higher imaging resolution

Introduction

Each section in this chapter so far has made sequential improvements upon the ABBA method in order to continue to push its capabilities. However, a common theme that arose during these method developments was a desire for increasing image resolution. Because the agar-oxygen interface in ABBA is millimeters away from the coverslip, we are required to use objectives with long working distances. These are typically low magnification and low NA lenses. For comparison simple qualitative comparisons (aggregates are larger in this media verses another for example), the current assay works beautifully and is an incredibly simple and quick way of addressing these types of questions. However, our thirst for more quantitative metrics requires more accurate measurements.

Early on in my PhD I was entranced by the ABBA assay. We always talk about gradients, but we rarely get to see them, and this visual method was like candy to the eyes. However, the microscopist in me was immediately unsatisfied by the requirement to use low magnification and low NA objectives. I thought, what if there were a way to change the format of the ABBA such that the oxygen-agar interface was instead up against the coverslip instead of millimeters away?

Figure 5A graphically represents this idea. Again, ABBA require long working distance objectives (represented by the block lines). If instead we made a disk that is sandwiched between glass, as in the ADBA example, we should be able to use any objective we want since a smaller working distance can capture the same type of information. The following data show only a few examples of my experimentation with this endeavor and I hope if nothing else inspires others to get creative.

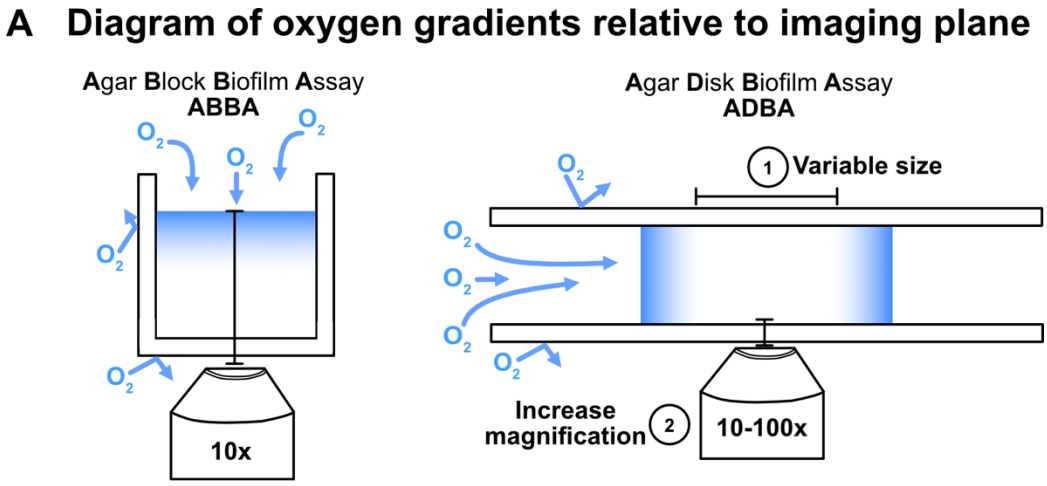

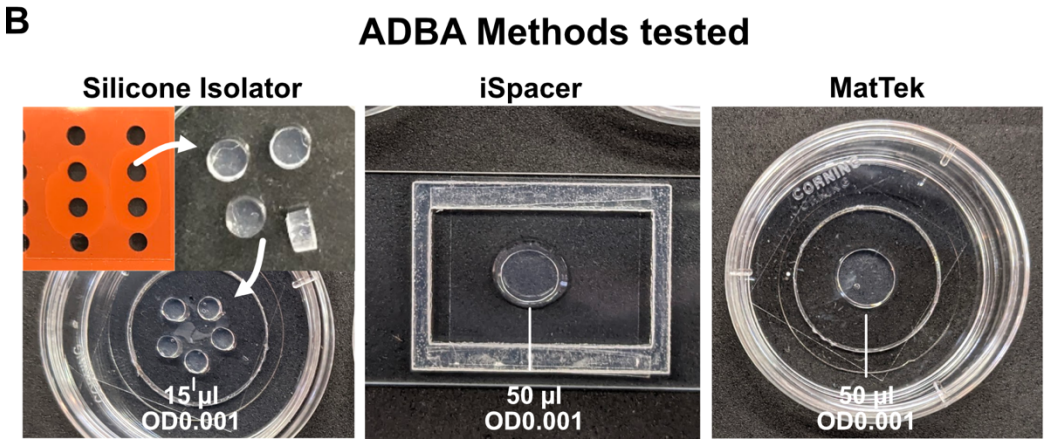

Figure 5. Agar Disk Biofilm Assay methods. (A) Graphical comparison of ABBA and ADBA. (B) Images of agar disks produced using specified tools.

Method

Three different techniques were used to compare how they influence the formation of aggregate gradients in this disk form (Figure 5B). As in all ABBA methods outlined in detail earlier, cells are diluted to a sparse final OD. Here that final OD was 0.001, though I would recommend you try several different dilutions depending on the questions you are addressing.

If you use the “Silicone Isolator” method, clean the isolator with ethanol and or by autoclaving. Press the isolator on a clean standard glass slide to seal one side. You should now have a well. Depending on which isolator you are working with (pictured here is the smallest available) add your cells in molten agar to the well you have created with the isolator. Working quickly, fill several wells to make as many replicates as you would like. Place another slide on top. There should be just enough agar peeking out of the well that when you place another slide on top it completely seals and no bubbles form (note in Figure 5A the access agar that overflowed under the second glass slide). Next, let the agar solidify either at RT or 4C to speed it up. Once solidified, push off one of the glass slides carefully. With small forceps, peal back the isolator. The molded agar disks should be left on the bottom slide. If not, try bending the isolator at

each well position to pop them out. It is helpful to make several and just collect the one that come out smoothly. The agar disk can now be picked up (I found a metal pallet knife to be an excellent tool for this) and placed in a MatTek coverslip bottom imaging dish. Finally, gently place a 22x22 coverslip on top of the agar disks.

The “iSpacer” and “MatTek” are very similar. Instead of molding an agar disk, it is created by directly sandwiching a molten inoculated agar droplet between coverslips. The challenge to this method is controlling the height the agar disk. For a specific, measurable and reproducible height I recommend the iSpacer (available commercially in several thicknesses). Pictured is an iSpacer that is one millimeter in height. However, you can also take advantage of the ledge created when the hole in the bottom of MatTek dishes is cut for the coverslip. The challenge with these methods is reproducibility. You need to commit when placing the coverslip onto of the agar droplet, if you hesitate, make contact and pick it back up you will ruin the disk. Bubbles are also easily formed (see MatTek picture).

Finally, as with any of these methods involving agar, humidity is important. Make sure to incubate the ADBAs in a sealable container with a wet tissue. I have not attempted to perform time lapse microscopy of an ADBA yet, but I would imagine controlling humidity will become even more important.

Regardless of what you do, be consistent. I, and others, have gone down several rabbit holes chasing phenotypes that seems to change from day to day but may be primarily driven by keeping track of which container is used, how much water is added to the container, which incubator is used, where in the incubator the container is placed and how often that incubator is opened and closed during the incubation period.

Results

While this method is still in its infancy and will require further optimization, while exploring the different methods for disk formation I noticed how the aggregate growth gradient was impacted by the different techniques. Figure 6A shows whole tile scan images (taken at 10x for speed but can image aggregates up to 100x!) as well as the volume of each aggregate relative to its distance from the disks center complied using the same analysis methods outlined above.

Based on the inoculum density comparison from Figure 2, and because all three disks shown here in figure 6A were made from the same inoculum density, I expected the aggregate sizes to be similar. However, the agar disk size appears to be yet another major contributing factor on this parameter. From the images it is clear that the XY density is fairly consistent across each disk. However, one feature of these disks that is not shown and difficult to represent is the height of the disks. Even though the disks are presented from smallest diameter to

largest, in fact the mold disk of the Isolator technique is in fact the tallest around two millimeters. The iSpacer is around one millimeter tall and the MatTek disk is the thickness of the plastic of the dish, roughly 0.5 millimeter. This difference in disk thickness is clearly an important feature to control and consider when making disks. This is likely due to more (when thicker) or less (when thinner) oxygen consumption (by aggregates) above those pictured at the coverslip surface. Thus, agar disk radius is a useful parameter to play with in order to increase or decrease the anoxic population.

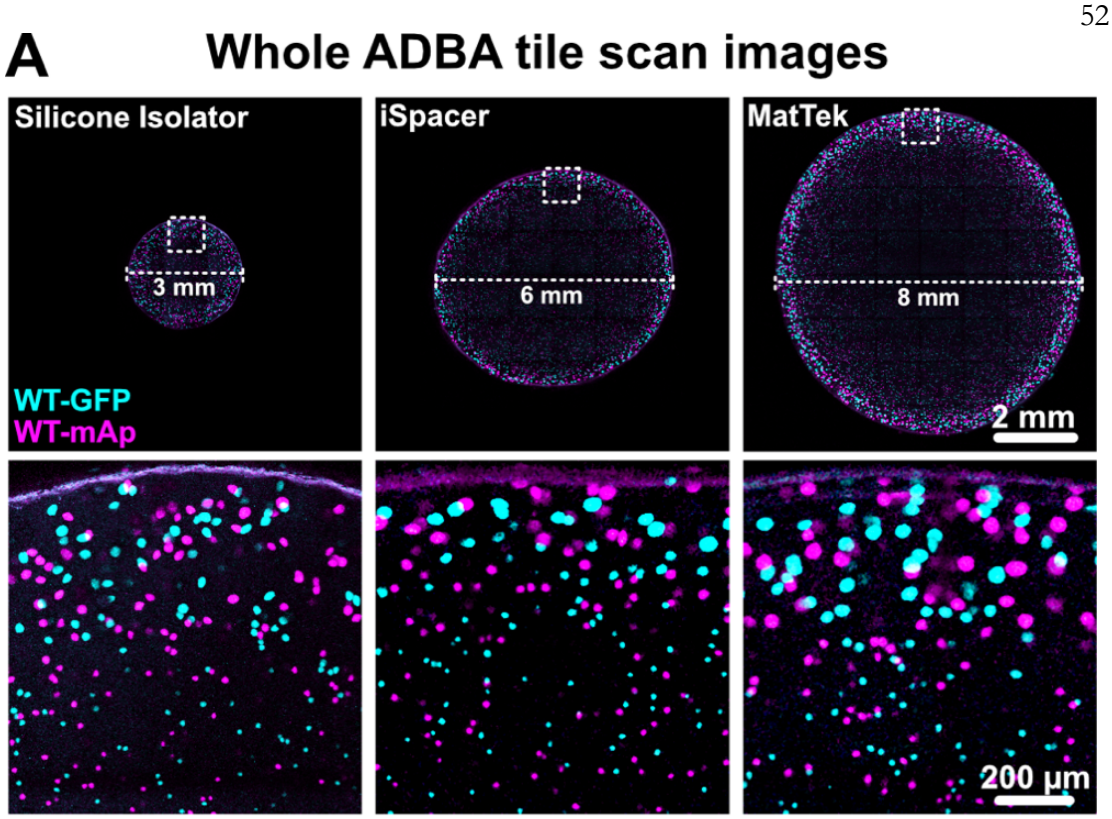
A
Whole ADBA tile scan images
Silicone Isolator
iSpacer
MatTek
3 mm
6 mm
8 mm
WT-GFP
WT-mAp
2 mm
200 µm

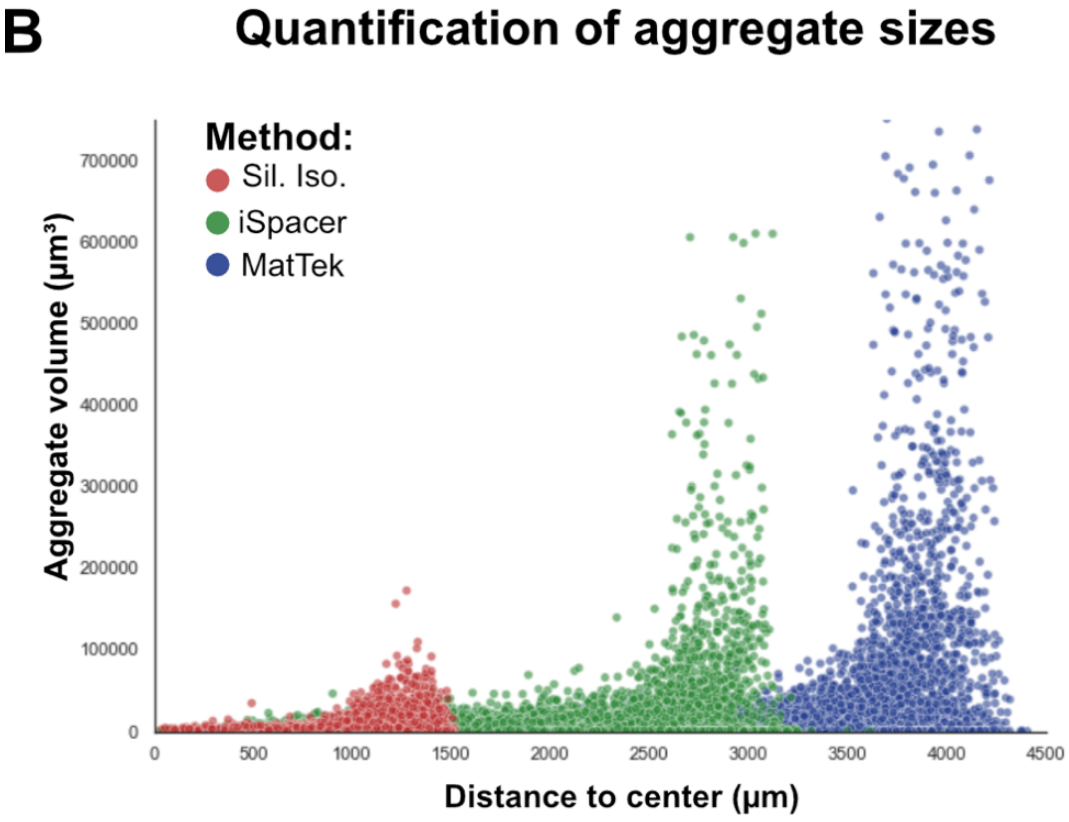
B
Quantification of aggregate sizes
Method:
Sil. Iso.
iSpacer
MatTek
Aggregate volume (µm³)
700000
600000
500000
400000
300000
200000
100000
0
0
500
1000
1500
2000
2500
3000
3500
4000
4500
Distance to center (µm)

Figure 6. ADBA method aggregate comparison. (A) Whole agar disk tile scan images scaled for comparison as well as well as high magnification call outs showing the formation of microbial aggregates gradients. (B) Quantitative comparison of aggregate volumes.

Future Directions

ADBA is a clear and simple extension of ABBA that can use most of the same tools and analysis pipelines for answering similar questions. However, ADBA improves upon ABBA with more freedom to control the size of aggregates, gradients and can be imaged with a more flexible selection of objectives which makes it uniquely adaptable to your specific questions.

That said, there are still hurdles to overcome with the method and situations where ABBA will still out-perform ADBA from a practice standpoint. First, ABBA can easily be stained without perturbation because buffers can simply be added to the top of the block (this is not to say that doing so does not cause a change in growth and thereby a change in oxygen gradient). Stains can be introduced to ADBA, but there is a risk of perturbing the agar disk and or the coverslip thereby allowing oxygen to flush to areas that otherwise would not have access potential interfering with results.

Profiling oxygen with microelectrodes is difficult and precarious regardless of what you are profiling. However, because the gradient being measured is upright in ABBA, the standard machine that steps the microelectrode through your sample can be used. I cannot imagine a way to get the electrode into an

agar disk sandwiched between coverslips. While this is clearly an issue and prevents oxygen measurements this way, I hope that it continues to motivate the devolvement of reliable optical oxygen measurements as they would overcome this issue and lead to more precise characterizations.

Finally, all these methods have something in common that will always need to be considered: they are batch cultures. Once nutrients run out, cells will slow metabolism. We can use this to our advantage in interpretations such as the observation that aggregates in the core of the agar are smallest because they have less access to oxygen. However, they have less access because cells above them are reducing it. But once they stop, oxygen will flow deeper leading to a complex and dynamic microenvironment. This is all well and good if you keep these dynamics in mind when interpreting results and without dynamic oxygen measurements. However, I think an avenue to continue exploring would be to make an ADBA contained within a flow chamber. The Babbin Lab at MIT has a system that pushes these techniques in a direction that will be transformative to understanding such context-dependent microbial physiology and I highly recommend digging into their work (Ciccarese et al., 2022).

Imaging in context: preserving microbe-host interactions

Introduction

Suspending cells in agar and allowing them to grow, shaping and being shaped by their local environment under laboratory conditions is often motivated by the pursuit to mimic and therefore better understand what is happening in natural systems. We often cannot visualize what is happening in places such as plant root surfaces without destroying structure. In a step towards developing a pipeline similar to those outlined above in terms of ease, reproducibility, and information gained I developed a protocol for setting up, growing and imaging bacteria on plant roots, the so-called rhizosphere.

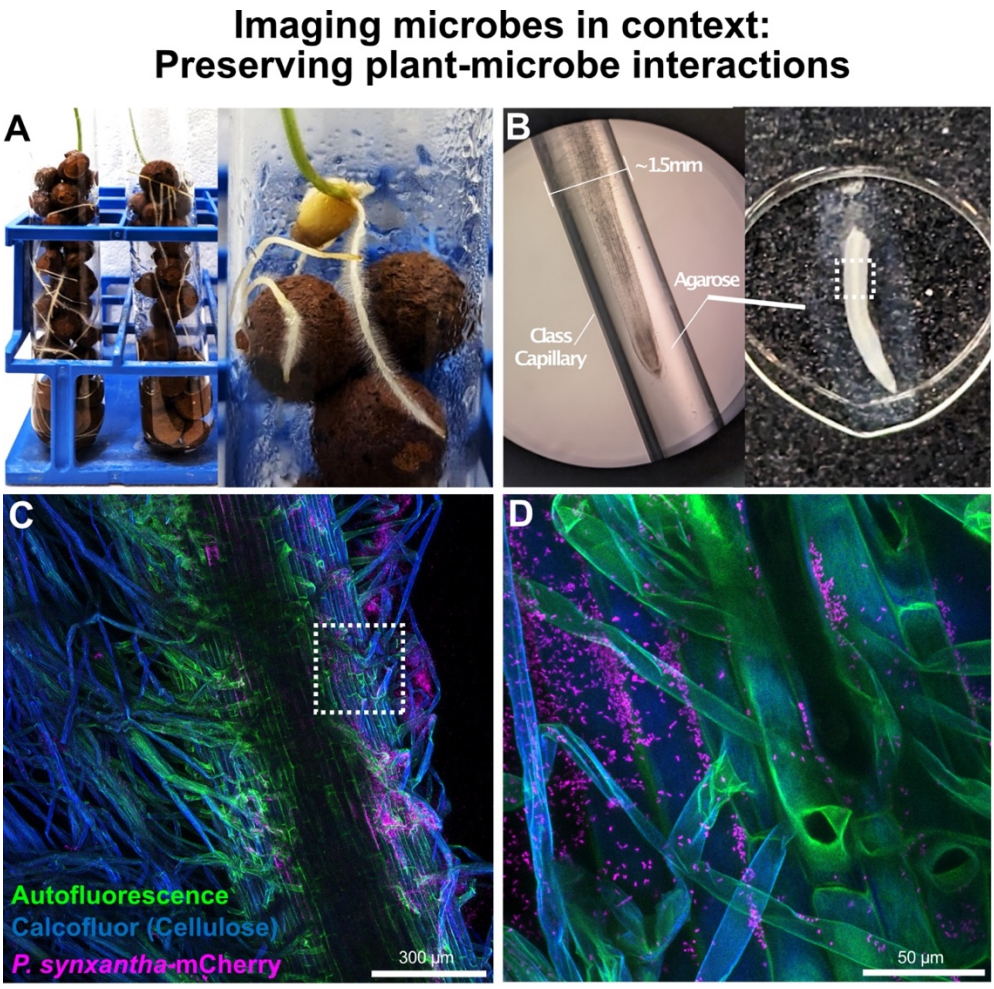

Figure 8. Plant-microbe imaging protocol. (A) Wheat seedlings are placed in large glass culture tubes containing inoculated culture media and lightweight expanded clay aggregate (LECA). (B) After incubation, plants are removed from tubes, roots are cut, suspended in low melt agarose, mounted for imaging. (C-D) Example confocal image of a freshly prepared root sample stained for cellulose (blue) and harboring *Pseudomonas synxantha* cells (magenta).

Method

Wheat seeds should be sterilized according to standard procedures. I found the best results (majority of seeds germinating) when seeds were placed in a solution of 50% Bleach and 0.1% triton x for 3 minutes, then rinsed three times in water. Rinsed seeds were then lightly pressed embryo side down into standard agar plates prepared with 0.5X MS media and 0.6% phytagel within the biosafety cabinet to ensure sterilization. Plates should then be sealed and place at 4C for a day or two (this helps sync germination by allowing all seeds time to soak up water and split open). Once the majority of seeds have begun germination, the plate can be placed in a warmer place for one additional day. At this point, the seedlings should look as seen in Figure 8A (the close-up image, this may take more or less time depending conditions).

Under sterile conditions, seedlings can either be dipped in a solution of bacteria in media or the bacteria can be added to culture tubes (depends on if your question involves wanting to see if the bacteria are attracted/will find the plant root or not). Lightweight Expanded Clay Aggregate (LECA) is a consumer product often used in semi hydroponic agriculture. Here is used as a growth

medium due to its high porosity resulting in effective water flow throughout the height of the tube allowing roots to remained humid and hydrated without allowing them to become overly embedded or tangled within the growing media as would be the result of growth in soil or small glass beads. In most experiments, including that which is shown in Figure 8, the wheat seedlings were placed upon the LECA surface in the tubes that had an inoculum of PS cells driving a constitutive mCherry fluorescent reporter.

After a few days, seedlings can be carefully removed from the tubes and placed in a sterile surface. Using a scalpel, cut root section and place in a solution of molten 1% low melt agarose (LMA) and 1X PBS. Quickly, using a plunger within a small glass capillary suck up root piece encased in the molten agarose. Once it has solidified, the plunger can be used to push the root encased in agar out and root pieces can be collective in an Eppendorf tube.

If your cells have a constitutive fluorescent reporter, the root piece can be taken immediately to a microscope and imaged. However, roots encased in agar have the added benefit of being able to be further treated due to the entrapment of the root in agar, there is less worry about perturbing microbial structure. The samples can be fixed with paraformaldehyde (PFA), and labeled later using Hybridization Chain Reaction (HCR) or Fluorescence *in situ* Hybridization

(FISH) probes all while maintaining microbial structure through several rounds of rough washing.

A temporary imaging mount can be created as follows and shown in Figure 9A. When ready to image, place agar embedded root on a slide. As to not squish the sample by directly placing a coverslip on top, gently scoop each corner of a square 22x22 sized coverslip into some clay (hobby quality is fine). The coverslip can then be place on top of the sample and clay will act as a spacer that holds the sample under the coverslip with enough pressure to hold stiff but not enough to compress and destroy. A droplet of clear nail polish can be added to a corner for added security. This is a temporary imaging chamber that allows you to image and then recollect for later used if needed and or to flip the root over if needed. It is very forgiving and is especially useful in the beginning as you get to know your samples.

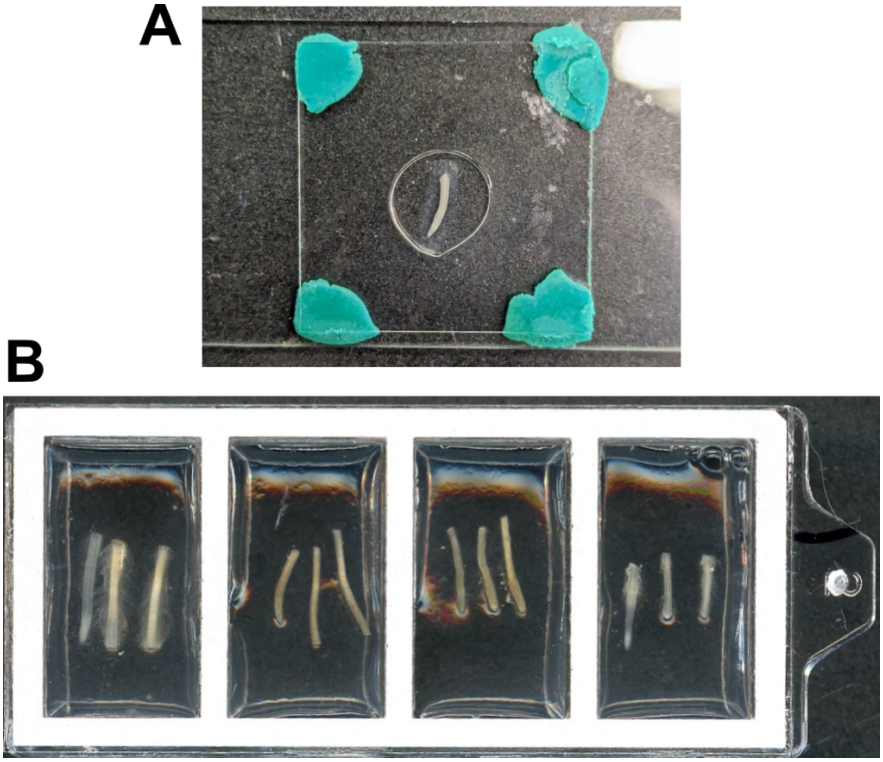

Figure 9. Wheat roots prepared for imaging. (A) Clay feet imaging preparation for agar embedded plant root. (B) Three sequential cuts of the longest root each of four individual seedlings were made and placed in the four well LapTek dish. Drops of low melt agarose in 1X PBS were placed on top to adhere roots to surface.

Another option for maintaining structure, and which helped especially in maintaining the mucus layers perturbed by the suction in the glass capillaries, is to instead place cut roots on the coverslip surface of an imaging dish as show in Figure 9B. Here, root pieces are placed in the bottom of the well, and a few drops of molten LMA are placed on top to hold them in place resulting in samples that have been minimally disrupted and held close to the coverslip for high magnification imaging. Again, the embedded roots can be imaged immediately or fixed with PFA for later use.

Future Directions

Under my mentorship, a rotation student, Chiara Berruto, was able to help develop this method and use it to visualize a six-member wheat rhizosphere community comprised of the following strains: *Arthrobacter pascens* DSM 20545, *Arthrobacter woluwensis* strain 1551, *Chryseobacterium ginsenosidimutans* strain THG 15, *Chryseobacterium shigense* strain DSM 17126, *Pantoea agglomerans strain* DSM 3493, and *Pseudomonas synxantha* strain NBRC 3913. The strains were those isolated from a wheat field and tested by a previous graduate student in the lab (Perry and Newman, 2022).

A clear next step would be to use this method to further characterize the spatial organization of a model microbial community with using 16S FISH as Chiara and I did, or even more excitingly, using SeqFISH methods to elucidate the spatiometaboilc activities of microbes in association to plant roots. (Dar et al., 2021)

Chapter 4

ENGINEERING A NITRIC OXIDE (NO)-DEPENDENT MICROBIAL INTERACTION

This chapter is adapted from:

Wilbert S.A. and Newman D.K. 2022. The contrasting roles of nitric oxide drive microbial community organization as a function of oxygen presence. *Current Biology*. https://doi.org/10.1016/j.cub.2022.10.008

Abstract

Microbial assemblages are omnipresent in the biosphere, forming communities on the surfaces of roots, rocks, and within living tissues. These communities can exhibit strikingly beautiful compositional structures, with certain members reproducibly occupying particular spatiotemporal microniches. Despite this reproducibility, we lack the ability to explain these spatial patterns. We hypothesize that certain spatial patterns in microbial communities may be explained by the exchange of redox-active metabolites whose biological function is sensitive to microenvironmental gradients. To test this, we developed a simple community consisting of synthetic *Pseudomonas aeruginosa* strains with

a partitioned denitrification pathway: a strict consumer and strict producer of nitric oxide (NO), a key pathway intermediate. Because NO can be both toxic or beneficial depending on the amount of oxygen present, this system provided an opportunity to investigate whether dynamic oxygen gradients can tune metabolic cross-feeding and fitness outcomes in a predictable fashion. Using a combination of genetic analysis, controlled growth environments and imaging, we show that oxygen availability dictates whether NO cross-feeding is deleterious or mutually beneficial, and that this organizing principal maps to the microscale. More generally, this work underscores the importance of considering the double-edged and microenvironmentally tuned roles redox-active metabolites can play in shaping microbial communities.

Introduction

Given the diversity of microbial metabolic strategies and that microbes rarely live alone, the potential for metabolic interactions is vast (Zuñiga et al., 2017). Metabolic interactions can be positive or negative and can have profound effects on the surrounding environment, from contributing to nutrient flux to stimulating the immune system of an infected animal or plant. Numerous ecological models have been developed to better understand how such interactions influence the growth of a community (Goldford et al., 2018; Niehaus et al., 2019; Ratzke et al., 2020). However, these models typically focus on

simple growth kinetics involving a shared or exchanged beneficial metabolite and do not consider how changing microenvironments over small spatial scales might influence the initiation and/or quality of the interactions. Yet it is a well-documented ecological phenomenon that microbes are confronted with changes in important nutrients that can tune these interactions, such as oxygen, in both space and time (Dal Co et al., 2020; Krichels et al., 2019; Lowery and Ursell, 2019; Stewart et al., 2016). How such spatiotemporal environmental changes impact the biological function of exchanged metabolites is often overlooked in these models.

Diffusible, redox-active metabolites, be they organic or inorganic, are particularly interesting to consider in this context, as these molecules' reactivity is highly sensitive to local chemistry. Recent work has called attention to the fact that certain redox-active metabolites have the potential to be both toxic (i.e., generate reactive oxygen species under oxic conditions) or beneficial (i.e., contribute to energy conservation under anoxic conditions), thereby having the potential to play different and dynamic roles in the development of a microbial community (Dahlstrom et al., 2020). Such double-edged effects may be particularly important when the metabolite in question is an intermediate in a common metabolic pathway. For example, if two microbes are reliant on each other for growth due to an intermediate that can be toxic to the producer but is essential for the consumer, it stands to reason that their growth and subsequent environmental impact will depend on microenvironmental conditions that affect

the properties of the exchanged intermediate. The potential for variable local interactions due to shifting environmental gradients would therefore be expected to determine when, where, and how certain microbial interactions would manifest spatiotemporally.

As a step toward testing this hypothesis, we sought to create a simple synthetic model system in which to explore the effect of the microenvironment on the interactions between two bacterial partners linked via an exchanged redox-active metabolite. Four criteria guided our development of such a system. First, we required that the metabolite be “agathokakological,” a word derived from Greek roots meaning “composed of good and evil.” In other words, a metabolite that is predictably “double-edged”: beneficial or harmful according to its environmental context. Second, we needed to be able to measure and perturb the most important environmental parameter—oxygen—that affects its physiological impacts. Third, we aimed to control the production and utilization of this metabolite via the generation of mutant strains from an isogenic background in order to focus strictly on the capacity to make or use the metabolite. Finally, we sought a metabolic exchange that is of broad ecological relevance across many environments.

The exchange of nitric oxide (NO) met all of our criteria. NO is known in both the eukaryotic and microbial worlds as a potent signaling molecule and a highly reactive nitrogen species that can damage a variety of cellular components

(Toyofuku and Yoon, 2018). In the absence of oxygen, NO is toxic at high concentrations by antagonizing Fe-S centers and causing DNA damage; yet in the presence of oxygen, much lower levels of NO can be toxic due the generation of peroxynitrite (Beckman and Koppenol, 1996; Zumft, 1997). Microbes have numerous mechanisms to deal with low levels of NO toxicity such as flavohemoglobin proteins (Fhp) that can reduce NO to nitrous oxide (N_2O) or mediate its oxidation to nitrate (NO_3^-) depending on the environment (Arai, 2011; Koskenkorva et al., 2008), and other dioxygenases can sequester NO (Sasaki et al., 2016; Yoon et al., 2007). However, as its concentration rises, and if producing cells or neighbors are unable to reduce it to nitrous oxide (N_2O), it reaches toxic levels and leads to local growth inhibition or death (Brunelli et al., 1995; Yu et al., 1999).

NO production is a landmark step in denitrification, where the soluble substrate nitrite (NO_2^-) is reduced to gaseous NO. Denitrification *sensu stricto* plays a critical role in the loss of nitrogen in soils (Fang et al., 2015; Krichels and Yang, 2019; Tian et al., 2019). If an organism contains a full pathway to sequentially reduce nitrate (NO_3^-) > NO_2^- > NO > N_2O > nitrogen gas (N_2), harmless N_2 will be released into the environment where it can eventually become recycled by nitrogen fixing species (Kuypers et al., 2018). However, it is becoming more clear that the complete reduction of NO_3^- to N_2 may occur as a polymicrobial community effort in which different members contain only a subset of the denitrification pathway (Gowda et al., 2022; Hester et al., 2019; Lycus et al.,

2017; Rich et al., 2003). Synthetic pseudomonads have previously been shown to exchange nitrite under strictly anoxic conditions, leading to predictable spatial patterns that are sensitive to pH-dependent abiotic nitrite reduction to toxic nitrogen species (Borer et al., 2020; Goldschmidt et al., 2018; Goldschmidt et al., 2021; Lilja and Johnson, 2016). In an independent study, environmental isolates that naturally differed in their possession of denitrification genes were used to create a model that predicted interactions via denitrification intermediates (Gowda et al., 2022); yet, in this case, NO production was only considered for its potential toxicity rather than any potential for energy conservation. Because PA uses a NO reductase that does not directly contribute to proton translocation (qNor), it is often considered only for its detoxifying potential (Toyofuku and Yoon, 2018). However, physiological studies have shown that NO reduction in other, qNor-containing strains can contribute to ATP synthesis as the sole terminal electron acceptor (TEA) (Carr et al., 1989; VoBwinkel et al., 1991). To our knowledge, the ability for NO to be exchanged between cells in a manner that supports growth has not been demonstrated.

In this study, we utilized different mutations to the denitrifying organism *P. aeruginosa* strain PA14 to test the hypothesis that the spatial interactions of strains exchanging NO can be predictably altered as a function of oxygen in the microenvironment. *P. aeruginosa* is a cosmopolitan organism, notorious for being an opportunistic human pathogen, but is also found in sediments and soils (Arai, 2011). *P. aeruginosa* is also a classic denitrifier that encodes all enzymes

necessary for the complete reduction of nitrate to nitrogen gas and can be easily genetically manipulated, permitting the creation of a synthetic NO cross-feeding community. Our findings with this model community provide a conceptual lens through which to interpret more complex microbial community patterning in nature and disease involving the exchange of agathokakological metabolites.

Results

Design and characterization of a synthetic NO cross-feeding community

The PA14 genome contains a full suite of respiratory enzymes for the complete dissimilatory reduction of NO_3^- to N_2 (Nar, Nap, Nir, Nor, Nos) (Figure 1A) (Arai, 2011). Previous studies have shown that these steps occur sequentially and thus intermediates can build up and leak from the cell (Carlson and Ingraham, 1983). Because the PA14 NO reductase (Nor) does not directly contribute to proton translocation and in fact requires the consumption of protons for its reaction, it is often dismissed for contributing to energy conservation. However, if we trace the flow of electrons (Figure 1B, gray dashed lines) originating from the oxidation of NADH by the Nuo NADH dehydrogenase, through the quinone pool to the bc_1 complex, a total of six protons are translocated prior to NO reduction (Chen and Strous, 2013). If we account for the two protons consumed by the reduction of two NO molecules to one N_2O and one H_2O (Figure 1B, solid line), four protons still remain per NADH oxidized that could contribute to the

proton motive force. Electron flow to the N_2O reductase (Nos), which reduces N_2O to N_2, is also thought to follow the same pathway (Chen and Strous, 2013). Thus, when considering the full electron transport chain, we expect for each NADH oxidized, a net of $4H^+$ to be translocated per NO reduced all the way to N_2. Accordingly, there is good reason to expect NO to be able to support sufficient energy conservation to power growth under anoxic conditions, provided its toxicity under these conditions is managed.

To determine how the wild type (WT) PA14 strain responds to NO exposure, we incubated it with a common NO donor molecule called DEA NONOate under both anoxic and oxic conditions (Figure 1C). DEA NONOate releases 1.5 moles of NO per mole of parent molecule. WT cells were grown to mid-exponential phase, washed into anoxic buffer (pH 7.4) with and without a final concentration of 50μM NO donor (~75 μM NO). This concentration was chosen to exceed that which has been shown to be tolerated by NO reductase (Nor) deficient mutants (~15 μM) with the expectation that the WT strain could detoxify using its Nor (Yoon et al., 2007). Cultures were incubated at room temperature in an anoxic glove box for one hour (donor half-life ~16 minutes). After incubation, cultures were washed in fresh anoxic buffer and plated for colony forming units (CFUs) which revealed a 50% NO killing compared to an untreated control (Figure 1C). Next, we hypothesized that incubating cells with NO donor under oxic conditions would increase the toxic effects. After repeating this experiment under a normal atmosphere, NO exposure killing increased to 90% of the population (Figure

1C). These results suggest that NO as the sole TEA has the potential to contribute to energy conservation if certain conditions are met: that its concentration be maintained in the sub 75 μM range and that oxygen not be present in the microenvironment.

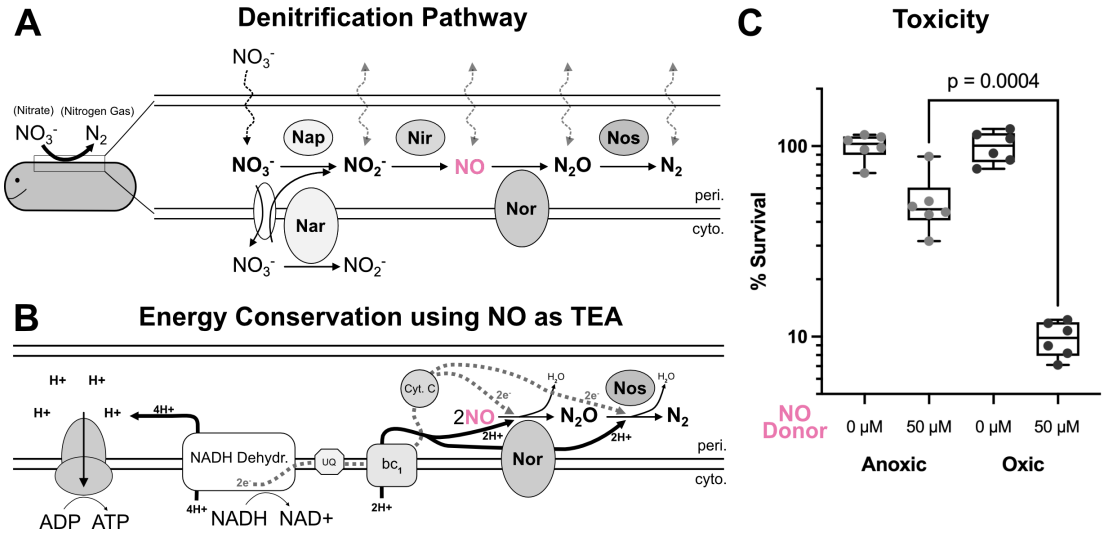

Figure 1. The agathokakological roles of nitric oxide in *Pseudomonas aeruginosa* growth. (A) WT PA14 sequentially reduces nitrate to nitrogen gas using five major enzymes. (B) Proposed mechanism of energy conservation using NO as the sole starting terminal electron acceptor (TEA). (C) WT PA14 survival after exposer to a short burst of an NO donor molecule under anoxic or oxic conditions. P value from unpaired t-test. Each dot represents one replicate, n=6 per condition.

To generate NO at the microscale, we partitioned the PA14 denitrification pathway between two strains, a NO producer and a NO consumer, to make a synthetic community that could catalyze the complete denitrification reaction (Figure 2A). We reasoned that such a community would allow an NO producing strain to supply a low but steady concentration of NO to its partner consumer strain, minimizing toxicity issues and circumventing the need to work with NO

donor molecules. Because of the sequential nature of the denitrification steps, we began by creating and characterizing several single, double, triple and quadruple clean deletion mutants to split the first and second half of the pathway at NO between two strains (Figure S1). After several iterations, we settled on a co-culture consisting of two strains that allowed us to observe NO cross-feeding via the presence or absence of growth under anoxic conditions (Figure 2A, co-culture 4 from Figure S1A). The NO producer strain, magenta outline, lacks both the NO reductase (Nor) as well as the N_2O reductase (Nos). Compared to WT (black) under anoxic growth with nitrate (Figure 2B), the producer strain shows a dramatic defect in growth. This is consistent with previously characterized Nor mutants that can accumulate upwards of 15 μM NO before triggering a negative feedback loop that represses further nitrate and nitrite reduction, preventing further NO production (Yoon et al., 2007). To ensure NO would be the sole TEA available for use, we designed the NO consumer strain to lack both the nitrate reductases (the proton pumping, membrane bound Nar and the redox balancing, periplasmic Nap), and nitrite reductase. Compared to WT, the consumer strain (cyan) also shows a dramatic growth defect, but unlike the producer strain, without NO inhibition, shows slight growth likely due to small amounts of carryover oxygen or built-up energy stores from the inoculum (Figure 2B). When these two strains are co-cultured to complete the pathway (dark blue), we see a large increase in total growth, as would be expected if the producer were relieved of deleterious NO build-up, and the

consumer were provided with a low-level supply of an otherwise toxic TEA. (Figure 2B).

To verify that the growth of the strains in the anoxic co-culture was due to the removal of NO from the producer by the consumer, we functionally replaced the consumer with the chemical NO scavenger, c-PTIO, and grew the NO producer strain in its presence or absence. Compared to growth without the addition of c-PTIO restored NO producer growth, supporting the interpretation that NO reduction by the consumer drives growth in the co-culture (Figure 2C). Further, to address whether the consumer's reduction of NO in the co-culture caused it to grow, we removed the NO reductase (Nor) from the consumer strain (Figure S1C). While this deletion did not alter the growth of this strain alone (Figure S1C, cyan), co-culturing this strain with the NO producer not only prevented, but also appeared to hinder co-culture growth completely (Figure S1C, dark blue). Finally, we asked if substrate level phosphorylation via pyruvate fermentation, a means of ATP generation for long term anaerobic survival in PA (Eschbach et al., 2004), might contribute to consumer growth by using NO in a redox balancing role as occurs for phenazines, another redox-active metabolite made by PA (Glasser et al., 2014). As with Nor deletion, removal of genes responsible for substrate level phosphorylation (*ackA* and *pta*) did not have a measurable effect on maximum OD reached using a plate reader (Figure S1D, cyan). However, unlike Nor removal, the co-culture's maximum OD was unaffected by the consumer's ability to perform this process (Figure S1D, dark blue),

suggesting consumer growth may be attributed to energy conservation from NO reduction as graphically depicted in Figure 1B.

These experiments suggest there is a net community benefit to strains in planktonic co-culture with a partitioned denitrification pathway under anoxic conditions compared to monoculture. To unpack this bulk phenotype and discern the effects of co-culture on the two members, we co-cultured the NO producer and consumer expressing constitutive fluorescence markers (GFP or mApple) for 48 hours. To track each strain's growth in the mixed population, we performed serial dilutions of the anoxic culture and plated for CFUs under oxic conditions. Using a fluorescence microscope and image analysis, we calculated the change in starting cell numbers and ratio of the two strains at the final time point (Figure 2D). Alone, the NO producer, regardless of the fluorescence reporter used, showed no change in CFU after 48 hours (Figure 2D). This indicates NO production under these conditions reached inhibiting levels, but not necessarily enough to cause death. The NO consumer in the absence of the producer exhibited slight growth (Figure 2D), as seen in the growth curves (Figure 2B). Finally, we measured the growth dynamics of each strain in the co-culture. Regardless of the starting ratio (more producer, more consumer, or equal) both strains grew significantly, converging on an even ratio of producer to consumer by 48 hours (Figure 2D). These results demonstrate that NO, when supplied at a low but steady level, can serve as a TEA to support slow anoxic growth. This exchange promotes a mutualistic interaction where growth

inhibition of the producer is alleviated by the consumer, which in turn gains a TEA; together, they flourish.

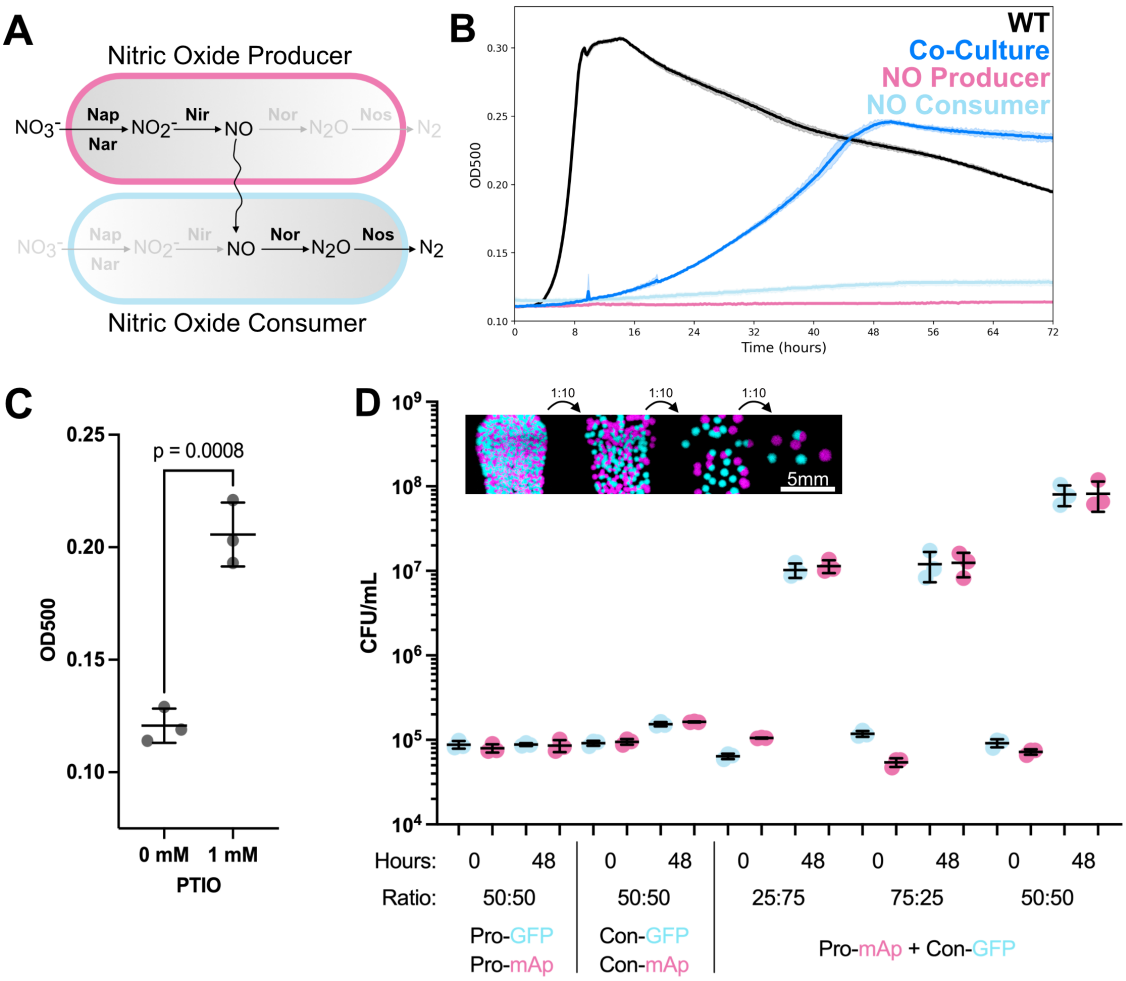

Figure 2. Design and characterization of synthetic nitric oxide cross-feeding community. (A) Schematic of NO producer (magenta) and consumer (cyan). Genes that have been cleanly deleted are grayed-out, and those remaining are shown in black. The pathway partitions where NO is produced and reduced. (B) Growth curve of strains in (A) grown individually and in co-culture (partitioned pathway), compared to WT (full pathway), over 72hrs under anoxic conditions with 5mM nitrate as sole provided terminal electron acceptor (TEA). Each growth curve represents n=4 replicates. (C) Growth rescue of producer strain using the chemical NO scavenger c-PTIO. Line and error bars represent means and standard deviations; P value from unpaired t-test. Each dot represents one replicate, n=3 per condition. (D) Different mixtures of the producer and consumer strains constitutively expressing either a GFP or mApple fluorescence reporter were grown as in (B) but at the beginning and end of a 48hour incubation were plated for colony forming

units. Consumer strain is Δ*narGHJI*Δ*nirS*Δ*napAB*Δ*ackApta*. Producer strain is Δ*norCB*Δ*nosZ*. See also Figure S1 and Table S1. Each dot represents one replicate, n=3 per condition.

NO cross-feeding under anoxic and sessile conditions is mutually beneficial and proximity dependent

Next, we wondered how spatial structure might influence the growth of the producer and consumer given that NO is a highly reactive and diffusible molecule. We hypothesized that, unlike under shaken planktonic growth conditions in which the whole population benefits, under spatially constrained anoxic conditions, proximity determines the success of community members. To test this prediction, we mixed fluorescently labeled cells of the same or differing genotypes in equal ratios, diluted the cultures, and sandwiched them between a coverslip and a nitrate-supplemented agar medium pad such that single cells were randomly distributed from one to dozens of cell lengths from each other. From these starting points, single cells could develop into aggregate biofilms over a 48-hour period. Figure 3A graphically represents the strain mixtures shown in Figure 3B as well as their predicted interactions based on the results of our planktonic growth experiments. As controls, we mixed WT with WT to explore how two cells with the full pathway and no growth defects would interact under these conditions, as well as the consumer and producer strains with themselves. Finally, the producer and consumer strains were mixed to visualize their interaction.

Using widefield microscopy, we observed the two strains (GFP/mApple) in the WT mixture grew as large clonal expansions with little single cell intermixing, indicating neither was impacted by the other (Figure 3B-3C) (Ciccarese et al., 2020; Panmanee et al., 2019). In contrast, both the Pro+Pro and Con+Con mixtures showed a dramatic reduction in aggregate size (proxy for total growth accumulation until observation, 48 hours) compared to WT (Figure 3B), in line with the inability of these strains to reduce nitrate, the supplied TEA. Interestingly, in order to observe this low baseline of growth for the consumer strain when grown with itself, it was necessary to use a consumer strain deficient in pyruvate fermentation. Whereas optical density was unable to resolve a difference between consumer strains +/- fermentation capability, this single cell imaging approach significantly increased our growth detection sensitivity, enabling measurement of subtle, but significant, differences (Figure S2A-2C, compare with Figure S1D, cyan). If we compare the WT (Figure 3C) and co-culture (Figure 3D) under these conditions, most strikingly we observe an increase in single cell intermixing between the two strains for the co-culture (Figure 3B vs 3D). The two WT strains (GFP/mApple) appear to grow as clonal expansions, pushing against one another rather than maximizing cell-cell contact (Figure 3C). Conversely, the co-culture shows slower growth compared to WT (same under planktonic growth), but appears to favor cell-cell contact between strains, forming mixed aggregates (Figure 3D), suggestive of a reliance of each partner on one another for continued growth (Momeni et al., 2013).

These mixed aggregates likely resulted from close starting positions of producer and consumer cells.

In addition to intermixed co-culture aggregates, we also observed a difference in aggregate size between single genotype mixtures and the co-culture (Figure 3E). If we compare producer aggregates (Pro+Pro, GFP or mApple dots) to the producer aggregates when grown with the consumer strain (Pro+Con, mApple dots) we see a significant increase in aggregate size (Figure S2D); thus, even when the producer is not in direct contact with the consumer, it appears to benefit from NO removal at distance. The consumer strain (Con+Con, GFP or mApple dots) also showed a small but statistically significant increase in size even when not in direct contact with the producer (Pro+Con, Cyan dots) (Figure S2D). However, the largest aggregates were those that contained a mixed population of producer and consumer strains (blue dots) (Figure 3E and Figure S2D).

Importantly, the increase in aggregate size even when the co-culture strains where not in direct contact indicates that while single cell intermixing can occur when the two strains are seeded at close initial starting positions (Figure 3D), without a proximal sink, NO can diffuse outward from producer cells to reach consumer cells thereby increasing the interaction range. NO's ability to rapidly traverse the distances separating source from sink cells in our mixed cultures is not surprising given prior results showing that NO can diffuse over 100 μm

within 1 second (Lancaster, 1994). To determine whether diffusion alone could explain our results, we measured the Euclidean distance between the centers of each aggregate at 48 hours in producer-alone, consumer-alone and co-cultures. When we compare the minimum distance between each aggregate and its closest neighbor, we find that all are within 100 μm of each other, with the majority between 20-60 μm (Figure 3F). Notably, there is a slight decrease in distances between co-cultured aggregates, likely due to better growth given the exchange of NO. Together, these results extend our planktonic growth observations into a spatial context, revealing how community members with a partitioned denitrification pathway can interact under anoxic conditions where NO can freely diffuse.

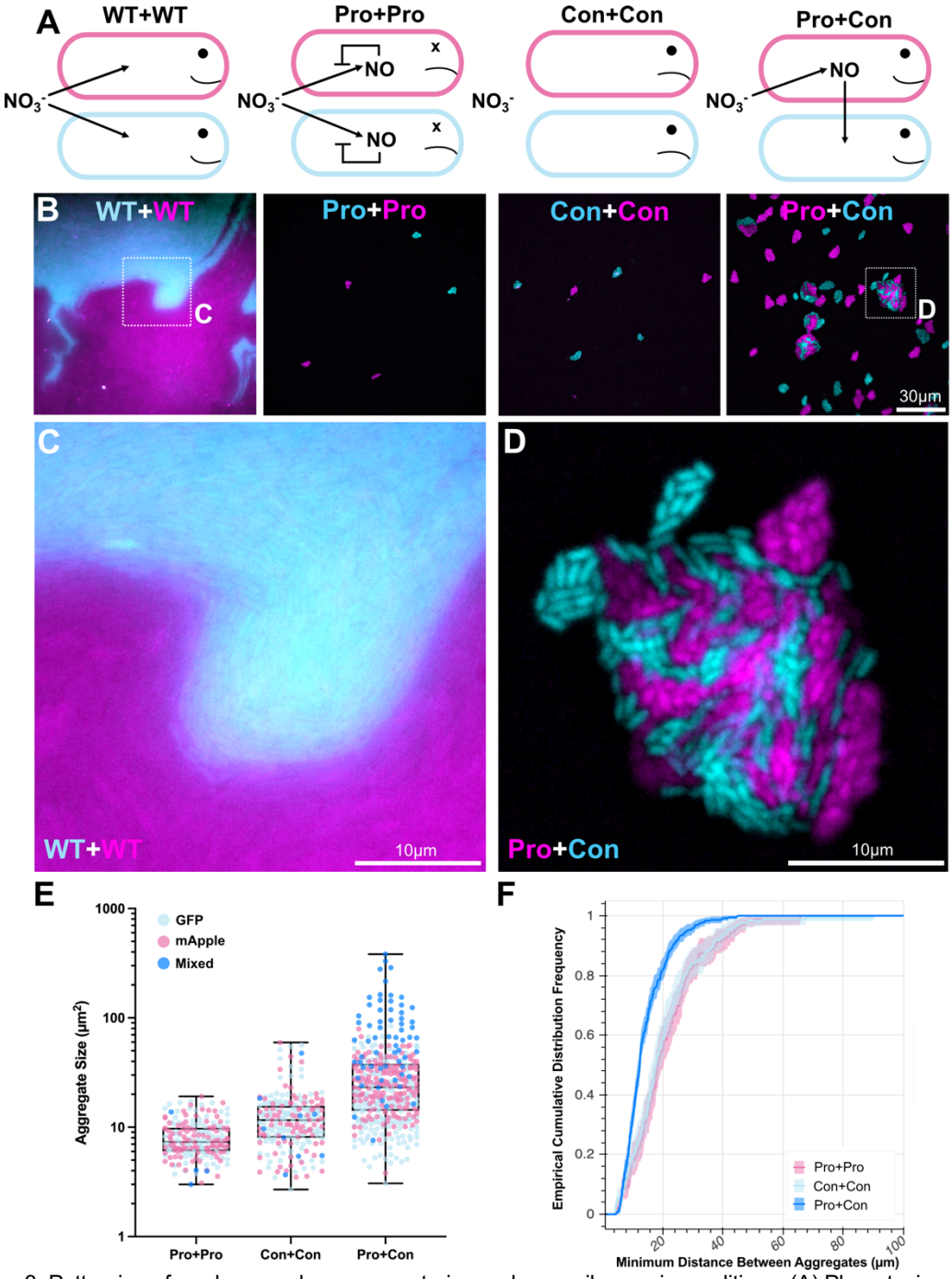

Figure 3. Patterning of producer and consumer strains under sessile anoxic conditions. (A) Phenotypic predictions. (B) Representative images showing growth patterns of indicated strain mixtures constitutively expressing either GFP or mApple after anoxic growth for 48hrs under an agar pad with nitrate provided as sole TEA. (C,D) Zoom-in of WT mixture showing strains growing as clonal patches (C) compared with zoom-in of the co-culture showing intermixing (D). (E) Quantification of each aggregates (dots) size and

color-coded based on whether the aggregate contained just GFP, mApple or both (mixed) cells. (F) ECDF plot of the Euclidean distance between each aggregate and its closest neighboring aggregate. Consumer strain is Δ*narGHJI*Δ*nirS*Δ*napAB*Δ*ackApta*. Producer strain is Δ*norCB*Δ*nosZ*. E and F display values from at least 190 aggregates measured from at least 25 images per condition, pooled from two independent replicates. See also Figure S2.

Oxygen availability enhances NO toxicity, thereby changing the nature of the co-culture interaction

Recognizing that oxygen presence increases NO toxicity (Figure 1B) and that many environments where denitrification occurs experience dynamic changes in oxygen and nitrate consumption coupled to increased production of nitric and nitrous oxide (Krichels et al., 2019; Krichels et al., 2022), we wondered what would happen to the NO producer strain and co-culture when grown in a heterogeneously oxygenated environment. Strains such as PA14 are facultative anaerobes, meaning they preferentially respire oxygen when it is available (oxic conditions), but when oxygen is limited, they induce pathways (such as denitrification) that permit energy conservation using alternative TEAs. A classic example of this phenomenon is when cells grow planktonically but are not shaken during growth. Cells at the surface of the medium reduce oxygen faster than it can diffuse into the culture, resulting in an oxygen gradient (Figure 4A, left) (Price-Whelan et al., 2007). To expand our understanding of when, where and how NO-cross feeding operates, we exploited this phenomenon and measured growth in shaking or standing “oxic” cultures. We hypothesized that strains harboring a partitioned denitrification pathway would exhibit growth that

depends on the amount of oxygen and nitrate present, in a manner reflecting the agathokakological effects of oxygen and NO on cells.

To test this hypothesis, we first observed how stagnantly grown cultures created an oxygen gradient by measuring the oxycline of both the WT and co-culture at multiple time points using an oxygen microelectrode (Figure 4B). The oxycline was present and consistent between strains and time points. As a baseline, we tracked the growth of the producer and consumer strains, alone and in co-culture, over 48-hours in a continuously shaking plate reader to prevent an oxygen gradient from forming. In the absence of nitrate all strains grew similarly, as expected, indicating the genetic modifications had no off-target effects (Figure 4C). Conversely, with 5 mM nitrate added to the medium, the consumer showed a slight growth defect compared to the WT and the producer displayed a brief growth arrest midway through exponential phase, with growth then paralleling that seen for the WT or mixed producer + consumer cultures (Figure 4D). Despite continuous shaking, at these cell densities, we surmise from prior work that these strains began to experience oxygen-limitation during mid exponential phase (Price-Whelan et al., 2007).

To further induce hypoxia, we performed the same planktonic growth experiment without the plate reader shaking, mimicking the conditions leading to the oxycline shown in Figure 4B. Again, in the absence of nitrate, we did not see a difference between the strains (Figure 4E). However, in the presence of

nitrate, all but WT showed a slight lag in growth (Figure 4F). Importantly, even without the ability to reduce nitrate, the consumer was able to eventually reach the same final OD as WT. Conversely, the producer strain showed a dramatic decrease in OD later in the growth curve, suggestive of cell lysis. To check whether this reduction in OD was due to a reduction in viable cells, we counted CFUs. Compared to WT viability at the 48hr time point, there was a significant reduction in producer CFU (Figure S3A). To confirm whether growth and prevention of cell death in the co-culture was caused by NO consumption, we repeated the growth curve but this time with a consumer strain lacking the NO reductase (Nor) (Figure S3B). When the Nor deficient consumer strain was co-cultured with the producer under hypoxic conditions, we observed a reduction in OD similar in timing and amount to the producer growth alone. Because the consumer alone reaches the same final OD as WT, yet would otherwise die if it lacked NO reduction ability in the co-culture, we propose that under hyp(oxic) conditions the consumer plays a beneficial role in the mixed community.

Finally, to assess whether concomitant aerobic respiration and denitrification were occurring under these conditions, we tracked the accumulation of superoxide (O_2^-) and NO. O_2^- is a by-product and intermediate of oxygen respiration that is typically removed by superoxide dismutase (SOD) (Figure 4A, right). However, NO readily reacts with superoxide (O_2^-) to form the reactive nitrogen species, peroxynitrite ($ONOO^-$), which can out-compete superoxide for SOD leading to an accumulation of reactive oxygen species and lead to

oxidative stress (Figure 4A, right) (Brunelli et al., 1995). Thus, we reasoned that the increase in cell death observed under hypoxic conditions for the NO producer might correlate with an inability to scavenge superoxide. To test this idea, we used a O_2^- sensitive dye (CellROX, Figure 4G) and an intracellular NO sensitive dye (DAF-2DA, Figure 4H) to detect their production. Both O_2^- and NO increased over the growth curve in the producer strain when grown alone (Figure 4G-4H), with a rise in signal around 30 hours, correlating with the drop in OD (Figure 4F, arrows). This decrease in OD and increase in O_2^- signal likely occurs due to cell death and thus a collapse of the oxygen gradient leading to a cascade of further ROS production.

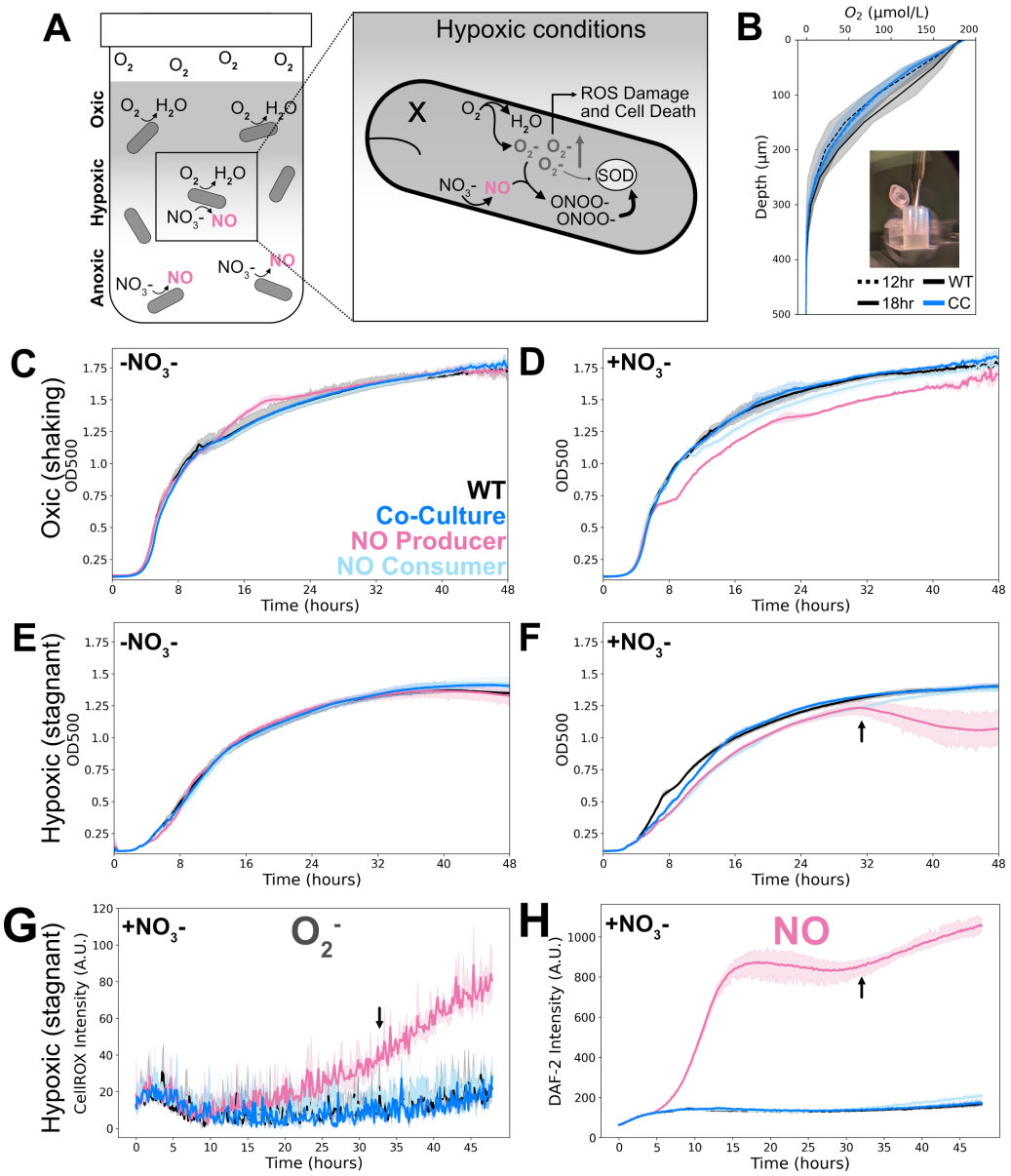

Figure 4. Oxic vs hypoxic growth of planktonic cultures supplemented with and without nitrate. (A) Graphical prediction of the heterogeneously oxygenated environment created by stagnate liquid culture incubation (left). Expected consequences of the NO producer growing under this environment (right). Superoxide (O_2^-) produced during aerobic respiration is kept below toxic levels by superoxide dismutase (SOD). The byproduct of NO and O_2^-, $ONOO^-$, can out-compete O_2^- for SOD causing an accumulation of O_2^-. (B) Oxygen profiles from non-shaking cultures of the WT compared to profiles from the co-culture at two time points to confirm heterogeneity. Each trace represents n=3 replicates. (C-F) 48hr growth curves cultured under the indicated conditions. Evenly oxygenated environments ("oxic-shaking") were achieved by shaking cultures during incubation (C,D), while unevenly oxygenated environments ("hypoxic-stagnant") were

achieved by culturing without shaking (E,F). (G-H) Fluorescent dye readings of superoxide (G) and nitric oxide (H) accumulation over a hypoxic growth curve with nitrate (as in F). Consumer strain is Δ*narGHJI*Δ*nirS*Δ*napAB*. Producer strain is Δ*norCB*Δ*nosZ*. Each trace in C-H represents n=3 replicates. See also Figure S3.

NO cross-feeding under (hyp)oxic and sessile conditions leads to spatial behavioral patterns

Unlike under anoxic conditions where the consumer strain gains a TEA that allows it to grow, we wondered what role its reduction of NO would play under heterogeneously oxygenated, sessile growth conditions. To achieve this, we grew diluted cells on agar pads under oxic conditions into aggregate biofilms (Figure 5A). Unlike the anoxic experiments, here cells initially had full access to oxygen and thus we expected them to behave as in planktonic oxic growth conditions. Over time, we expected cell density to rise and oxygen to diminish, prompting greater nitrate reduction to NO by the producer strain, as seen under planktonic hypoxic growth conditions. The question became: how would the fixed organization of NO producers and consumers in space influence their behavior over time?

To visualize interactions between NO producers and consumers, we mixed the strains with themselves or each other and incubated them under oxic conditions on nutrient agar pads containing nitrate. After 24 hours of growth, we observed with widefield fluorescence microscopy that WT, like under anoxic conditions, grew into aggregate biofilms; however, rather than monolayers, these biofilms appeared thicker perhaps due to their access to oxygen and ability to support

both oxic and anoxic populations (Figure 5B). Strikingly, the producer only mixture (Pro+Pro) also showed clonal patches (outlined with a dotted white line, Figure 5B) but with very few cells remaining fluorescent. To investigate further, we examined fluorescence and corresponding phase channels more closely (Figure S3C-3E). Cells that maintained their fluorescence after this incubation period also maintained their opacity in the phase channel. Cells no-longer showing fluorescence appeared transparent, leading us to conclude that they have undergone cell death and lysis as seen under hypoxic planktonic growth (Figure 4F). Conversely, the consumer only mixture (Con+Con) grew into clonal patches, (note much larger than under anoxic conditions due access to oxygen as a TEA) though they did not appear as dense as WT owing to their inability to support anoxic growth with nitrate.

The co-culture, however, provided several new insights. First, there was an increase in single cell intermixing (compare Figure 5C (no mixing) and 5D (mixing)). Second, unlike under planktonic growth conditions where the whole co-culture population benefits from interacting, here there appeared to still be lysis of producer cells when not in proximity to consumer cells (Figure 5D, Figure S4A shows lysis overtime). This indicates that spatiotemporal, microenvironmental changes induce metabolic dynamics that unlock a spatial niche where cross-feeding provides a selective advantage as protection from lysis for the producer strain. Such protection spatially patterns in several ways (Figure 5E): producer cells follow the consumer contour; others appear to be

protected by a pocket formed by consumer cells; and still others are protected in regions of high intermixing. Knowing that the producer cells would lyse without local NO depletion under hypoxic conditions (Figure 4F) permits us to link such cellular spatial arrangement to physiological activity.

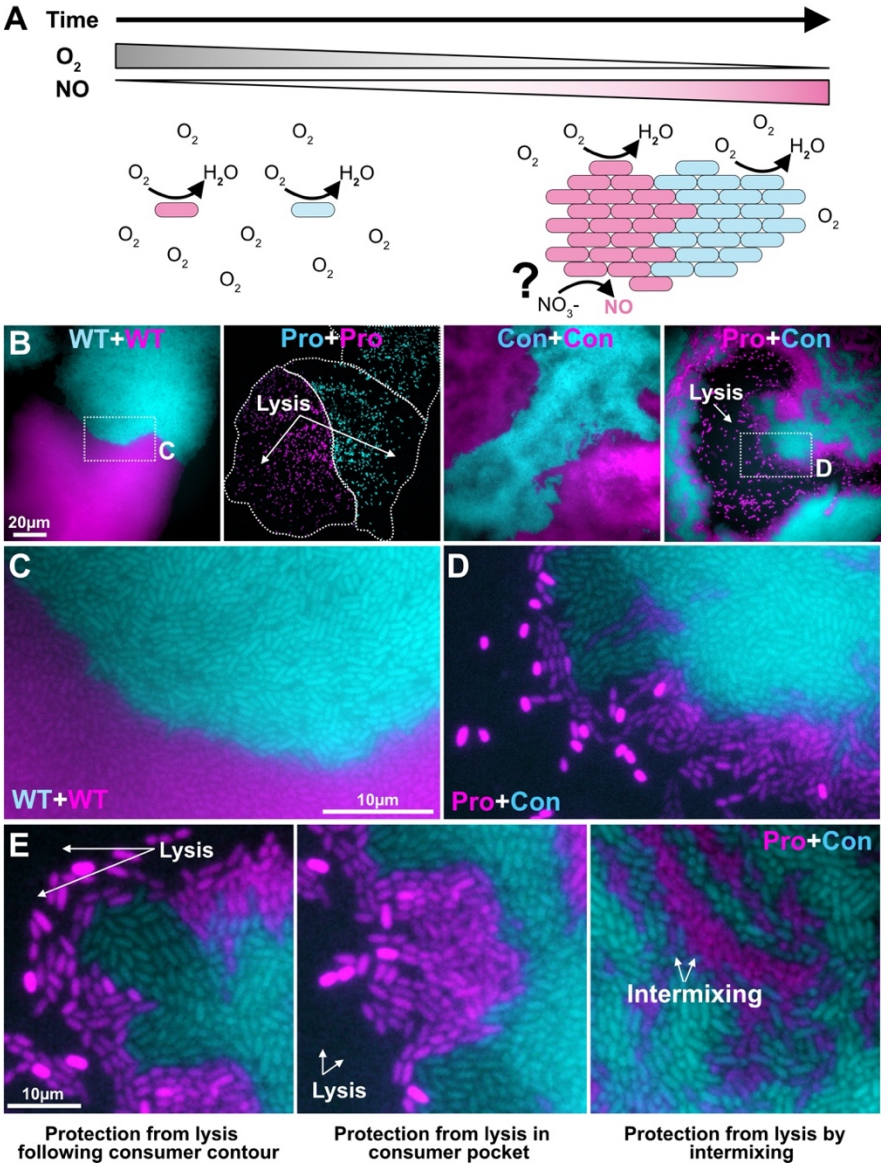

Figure 5. Patterning of producer and consumer strains under sessile oxic conditions. (A) Graphical prediction for NO producer and consumer strains growing initially in the presence of replete oxygen. Overtime oxygen consumption will lead to hypoxia and presumably a higher and higher production of NO.

(B) Representative images of indicated strains grown as biofilms for 24hrs under oxic conditions in the presence of nitrate. (C) Zoom-in of WT clonal expansion showing no intermixing. (D) Zoom-in showing producer survival adjacent to the consumer expansion interface; note that cells appear brightest prior to lysis. (E) Three additional high magnification callouts to spotlight specific structural features. Consumer strain is Δ*narGHJI*Δ*nirS*Δ*napAB*. Producer strain is Δ*norCB*Δ*nosZ*. See also Figures S3 and S4.

NO-dependent, co-culture interaction patterns dynamically reflect changes in the microenvironment

To test our predictions about how these spatial patterns arise, we repeated agar pad imaging as in Figure 5, but varied whether or not the consumer strain encoded the nitric oxide reductase (Nor). First, we asked whether the presence of Nor decrease ROS stress by preventing the downstream generation of superoxide. To address this, we included CellROX in the agar from the beginning of the experiment to visualize super oxide accumulation using confocal microscopy (Figure 6A-6D). The consumer channel was used to generate a mask and measure CellROX fluorescence intensity of the consumer only space (illustrated in Figure S4B). Comparing the results of consumer strains with (Figure 6A) and without (Figure 6B) Nor, we found a dramatic increase in CellROX staining at the border between the strains, and a measurable increase in the consumer cells surrounding the producer cells. This suggests NO diffusion leads to ROS generation in the absence of NO reduction by the consumer. Next, we asked how the consumer affects the producer cells in these biofilms by measuring the remaining producer cell area as a function of available, non-consumer space (inverse of consumer mask, illustrated in Figure

S4B). The results show a dramatic reduction in producer area when the consumer lacks the ability to reduce NO (Figure 6D).

Finally, these end time point measurements assumed where the border between consumer and producer started. The increase of CellROX staining at the border when the consumer lacked NO reductase suggests it could be undergoing lysis itself. This led us to ask if the consumer lysis when NO cannot be reduced matches the protection afforded to the producer when it can be reduced. We performed time lapse microscopy of the two co-cultures (consumer +/- Nor) both pre- and post-lysis. This allowed us to mark the initial border (Figure 6E, solid line) between the strains and draw a line indicating the extent of protection (Con + Nor) or induction (Con - Nor) of lysis (Figure 6E, dashed line). Indeed, the consumer strains without Nor undergo lysis at the border with the producer (Figure 6F), suggesting the major role for its NO reduction under these conditions is first to protect itself from toxicity, with a secondary benefit for the producer. Quantifying this phenomenon, we measured the range of protection (distance) conferred to the producer by the consumer (arrows, Figure 6E; pink line-Figure 6G). When the consumer lacks NO reduction capacity, all of the producer is vulnerable to lysis and the equivalent protection range manifests as a lysis range in the consumer population due to NO diffusion (Figure 6F, cyan line-Figure 6G). Overall, these ranges (2-12 μm) are much shorter than the interaction distances observed under anoxic growth conditions (20-60 μm, Figure 3F). We interpret this to be a consequence of NO’s high reactivity with

oxygen effectively shortening its diffusive range. Figure 6H graphically depicts our working model, showing how initially non-interacting cells can develop a high stake interaction with respect to fitness as the microenvironment changes.

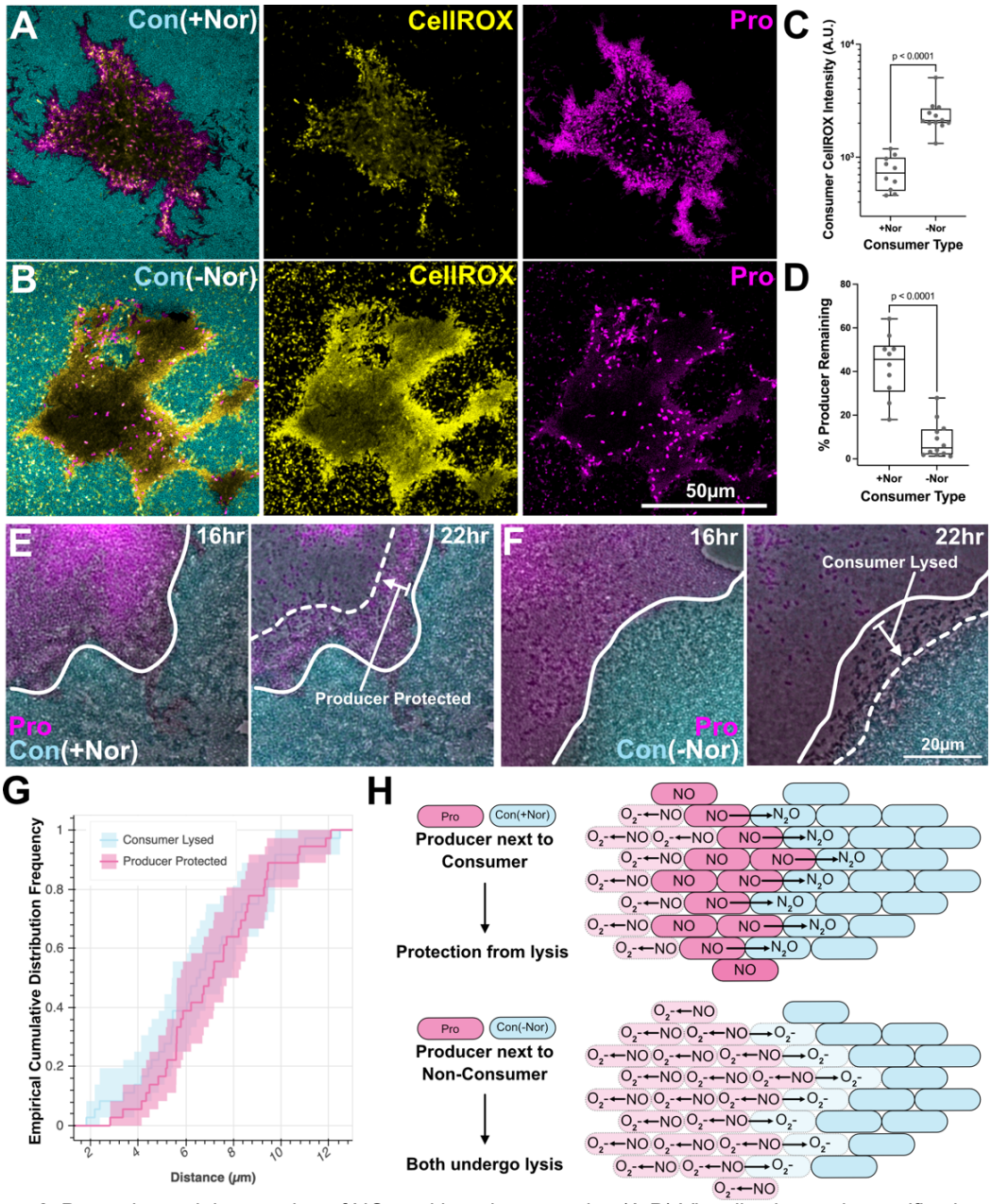

Figure 6. Dynamic spatial patterning of NO partitioned community. (A-D) Visualization and quantification of spatial superoxide production and lysis as a function of NO consumers presence (+Nor) or absence (-Nor) of the NO reductase. Specified strains were grown as in Figure 5 but including the superoxide sensitive dye

CellROX (Yellow). (C) Mean CellROX intensity of consumer cells was measured whether it contained the NO reductase (A) or not (B). (D) Using the inverse of the consumer region as a pre-lysis producer area mask compared to the remaining producer area (unlysed), a % remaining metric was obtained. P values from unpaired t-tests in C and D. Each dot represents measurements from single images ($n \geq 10$). (E-F) To measure lysis range in the presence or absence of NO reductase, time lapse imaging was performed from pre- and post-lysis. (G) ECDF of lysis/protection from lysis range was measured from 12 regions each from three aggregate co-culture interfaces (between solid and dashed lines as drawn in E and F, n=36). (H) Proposed model in which the NO producer and consumer strains both grow clonally until the microenvironment changes such that the producer begins to produce NO and lyse. The consumer acts as a sink for NO in close proximity to the producer, relieving NO toxicity and preventing the producers and own lysis. Consumer strain is Δ*narGHJI*Δ*nirS*Δ*napAB*. Producer strain is Δ*norCB*Δ*nosZ*. See also Figure S4.

Discussion

Awareness of the diversity of microbial metabolic interactions is expanding with improved techniques for identifying new pathways and observing interactions (Cordero and Datta, 2016; Dar et al., 2021; DePas et al., 2016; Pessi et al., 2022; Wilbert et al., 2020; Zuñiga et al., 2017). In the face of this progress, gaining a better understanding of how these interactions may shift as a function of dynamic oxygen gradients is an important goal. We developed a synthetic microbial community linked by the exchange of NO, an agathokakological molecule whose biological effects are tuned by the presence of oxygen, as a step towards this end. Our work shows that the interactions that drive NO intercellular exchange and reduction are induced and sensitive to the genetic content of community members and microenvironmental gradients, knowledge of which leads to predictable organizational outcomes.

Given denitrification may be a community effort (Gowda et al., 2022), and that each community member may contain a different suite of relevant enzymes, our studies with a synthetic community suggest that certain agathokakological intermediates, such as NO, may play an outsized role in structuring natural microbial communities. Linking environmentally-dependent metabolic interactions to microscale microbial organization is an important goal (Fuhrman, 2009; Gralka et al., 2020; Kuhns et al., 2015; Ma and Cordero, 2018; Proctor and Relman, 2017; Widder et al., 2016). Our findings spotlight dynamic changes in local oxygen for its ability to tune both the nature and need for a cross-feeding relationship. In our example case, NO can generate toxic byproducts under oxic conditions, leading to cellular growth arrest. Yet under anoxic conditions, NO can be a lifeline, serving as a TEA and promoting energy conservation and growth. These agathokakological effects are important because oxygen exhibits steep environmental gradients over small spatial scales (Kolpen et al., 2014; Krichels et al., 2019). Our work draws attention to the fact that oxygen gradients can shape microbial interactions both in planktonic and sessile communities, with the scales over which these interactions occur being set by the proximity of interacting cells and their local microenvironment, which they in turn alter in space and time.

An important next step will be to determine whether mixtures of natural isolates with partitioned metabolic pathways play by the same rules. Our work gives rise to testable predictions about when and where NO cross-feeding may occur. For

example, it is well appreciated that NO is an important intermediate species in the nitrogen cycle (Kuypers et al., 2018), whose turnover rates may decide the fate of soil nitrogen stores. Interestingly, recent metagenomic studies indicate that within certain habitats, there an enrichment for organisms that can only reduce NO to N_2O, an important greenhouse gas (Pessi et al., 2022). Thus, an understanding of what constrains NO reduction may provide insight into a metabolic process with important environmental consequences. Recent studies have drawn attention to the potential for partitioned pathways to influence the rate of nitrogen flux in soils by resident microbes (Gowda et al., 2022; Pessi et al., 2022). Our work attempts to directly link structure and function of such partitions as is suggested by the genomic content of environmental isolates (Pessi et al., 2022). In an entirely different context, our finding that *P. aeruginosa* can thrive by reducing NO provided by another cell lends credence to the hypothesis that PA may survive the host immune NO attack by its reduction to N_2O, and may correlate with the appearance of N_2O in the breath gas of cystic fibrosis patients (Kolpen et al., 2014). Importantly, *P. aeruginosa* can be found proximal to host immune cells in these infected environments (DePas et al., 2016).

Finally, we note that NO is only one of many agathokakological molecules, both organic and inorganic, that may help structure microbial communities over small spatial scales as a function of oxygen availability. For example, other redox-active metabolites such as phenazines can function as natural toxins or

beneficial agents of nutrient acquisition and/or redox homeostasis, depending on the context (Dahlstrom et al., 2020). Similarly, sulfide has long been known to play nuanced roles in nature, with its concentration-dependent toxicity influencing which phototrophic species are able to thrive (Findlay et al., 2015), and where different energy-conserving processes can occur within microbial mats (Jungblut et al., 2016; Prieto-Barajas et al., 2018). We hasten to note that many other parameters may be subject to similar dynamic spatiotemporal gradients, such as carbon, pH and light, and are likely to also play important roles in determining the niches where cross-feeding or other types of metabolic interactions can occur ((Goldschmidt et al., 2018; Goldschmidt et al., 2021; Zhang et al., 2021)). Towards the goal of gaining a predictive understanding of why diverse microbial communities are structured the way they are, a constructive next step will be to model these interactions in light of fluctuating environmental parameters, iterating with experiments until cross-cutting principles can be identified with predictive power.

Materials and Methods

Bacterial strains

All strains used are clean deletion mutants originating from the wild-type (WT) *Pseudomonas aeruginosa* UCBPP-PA14 strain as described below in the Method Details. Strains were stored as 25% glycerol stocks at -80°C.

Bacterial growth conditions

Before use, strains were streaked from frozen stock onto Bacto agar (BD, Sigma) plates containing LB (Miller, BD, Sigma) or LB supplemented with 50 µg/mL gentamicin (GoldBio) to select for retention of expression cassettes within fluorescent strains, and grown overnight at 37°C. From streak plates, a dab of culture was used to inoculate 5 mL liquid cultures in LB or LB plus 50 µg/mL gentamicin liquid media. Cultures were shaken at 250 RPM at 37°C overnight until fully saturated at stationary phase. To standardize inoculum sizes between strains, each strain's optical density (OD_{500nm}) was measured by spectrophotometry (Beckman Coulter). Strains were then each washed and diluted to an OD of 1 via centrifugation and resuspension in phosphate buffered saline (PBS). Strains were then either further diluted directly, or first mixed at equal ratios for co-culture experiments and then diluted to final experimental concentrations. For all experiments, a Low Salt LB (LSLB) was used instead of standard LB powder due to microelectrode reactivity to the high NaCl concentration. The composition of LSLB was 141 mM Tryptone (BD, Sigma), 16mM Yeast Extract (BD, Sigma), 45mM NaCl (Fisher Chemical), which were dissolved in Mili-Q water and autoclaved. Nitrate was supplemented into media where indicated by diluting from a 1M stock of KNO_3 (Fisher Chemical).

Construction of mutant bacterial strains

Table S1 contains a full list of primers used in the creation of deletion constructs and mutant strains used in this study. Briefly, a 1kb fragment up- and downstream of the target gene was amplified via PCR and cloned into the pMQ30 (Shanks et al., 2006) plasmid using Gibson assembly (NEB) and transformed into *E. coli* cells as previously described (Spero and Newman, 2018). Deletion constructs were then introduced to parent strains (WT PA14 and or deletion strains of PA14, see Table S1) via triparental conjugation. *E. coli* plasmid and helper strains were selected against by bead plating on VBMM containing 50 µg/mL gentamicin (Choi and Schweizer, 2006). Roughly 50% WT and 50% clean deletion colonies were then obtained by bead plating on a 10% sucrose plate to induce homologous recombination with the construct containing the regions up- and downstream, but lacking the targeted gene locus (Basta et al., 2017). Clean deletion strains were confirmed via PCR genotyping using primers that span the deletion region and sequencing of the amplified product. Finally, anaerobic growth challenges revealed expected physiological effects (e.g., Δ*nirS* was unable to grow on nitrite, etc.). Fluorescence strains were created as previously described using plasmids driving GFP/mApple expression under control of the constitutive ribosomal promoter rpsG introduced into the Tn7 site of specified strains using tetra-parental conjugation (Basta et al., 2017; Panmanee et al., 2019). *E. coli* helper strains were again selected against using VBMM containing 50 µg/mL gentamicin. Confirmation of insertion was

performed via microscopy, visualizing colonies in both green and red fluorescence channels, and selecting those that were bright in their respective channel above background autofluorescence.

Serial dilution and colony forming unit (CFU) counting

Liquid cultures were plated for colony forming units and back calculated to assess number of cells. Typically, 100 µL of culture was placed into the well of a 96 well plate (at least three technical replicates were assessed). 20 µL of culture was then diluted seven times in serial 1:10 dilutions in PBS. 10 µL of the dilutions were then plated on a LB agar plate using a multichannel pipette. The plates were then slanted vertically and tapped to allow the 10 µL to spread in a line. All dilution plates were incubated under normal atmospheric conditions, in an incubator at set to 37°C for roughly 24 hours. After incubation, colony counting was performed either manually or with an imaging and image analysis pipeline (when fluorescence imaging was used, see below). Dilutions with 100-200 colonies were used to calculate colony form units (CFU/mL) by multiplying this number by the dilution factor.

Growth curves

Anoxic growth curve media was placed in anaerobic chamber 72 hours prior to experiment to allow time for oxygen to degas from media. 1 OD_{500nm} cultures were brought into chamber and further diluted to 0.005 OD_{500nm} in anoxic media. Growth curves were performed using a BioTek Synergy 4 plate reader stored in

an anoxic chamber and set to 37°C with shaking and measured OD_{500nm} every 10 minutes. Oxic (shaking) and Hypoxic (stationary) growth curves were set up as above but under normal atmosphere. Oxic growth curves were performed using a Tecan Spark 10M set to orbital shaking. Hypoxic growth curves were performed using a Spectramax M3 (Molecular Devices) plate reader set to not shake. Each condition was performed in technical triplicate or quadruplicate. Each well contained 200 µL of culture with 40 µL of autoclaved mineral oil added to the top of each well to prevent evaporation of 48-72-hour growth curves. Traces from growth curves were analyzed and presented by plotting mean OD_{500nm} over time (dark center line) and 95% confidence intervals from technical replicates (shaded area) using Seaborn(Waskom, 2021) plotting packages in Python (Van Rossum et al., 2009).

Nitric oxide and superoxide quantification

Levels of nitric oxide and superoxide were quantitated using fluorescent dyes during hypoxic growth curves. NO was quantitated using 50 µM DAF-2DA (Calbiochem, Sigma) which is internalized by cells where esterases free DAF-2DA to interact with NO producing a green fluorescence signal (Wany et al., 2020). Superoxide was quantitated using 5 µM CellROX Deep Red (Thermo), which is non-fluorescent in a reduced state but exhibits a strong induction of fluorescence upon oxidation with reactive oxygen species (McBee et al., 2017). The Spectramax plate reader was configured to measure green fluorescence (Ex. 488 nm, Em. 520 nm, DAF-2) and far-red fluorescence (Ex. 640 nm, Em.

665 nm, CellROX). For pad imaging assays, CellROX was supplemented to the agar pads directly at a final concentration of 10 μM and imaged after significant biofilm growth had occurred to reveal superoxide localization. DAF-2DA was also used to visualize NO; however, due to weak single-cell signal and strong background autofluorescence in the green channel, we were unable to visualize the signal convincingly.

Oxygen profiling

To confirm the presence of oxygen gradients in standing cultures, we employed a 25 μm diameter oxygen microelectrode (Unisense), which was calibrated as previously described (Spero and Newman, 2018). Briefly, LSLB media incubated at 37°C was used to calculate the high point O_2 concentration. A zero-point calibration was obtained by dissolving 2 g Sodium Ascorbate in 100 mL 0.1 M NaOH, which scavenges O_2 from the medium. Using the Unisense Sensor Suite Software to save calibration values and control a motorized micromanipulator for profiling, O_2 was measured from the surface of hypoxically incubated planktonic cultures in 1 mL Eppendorf tubes. The surface was set by eye and confirmed by a reduction in mV signal. O_2 was then measured over a 1 mm distance below the surface at 50 μm intervals. Two measurements were taken at each position, and three technical replicates were averaged and displayed as the mean value with 95% confidence intervals (Figure 4B). Cultures were prepared as in growth curves but maintained as 1 mL volumes in

tubes rather than aliquoting into 96-well plates. Mineral oil was not added due to potential incompatibility with electrodes.

Agar pad imaging assay

We determined that OD_{500nm} cultures diluted to a starting concentration of 0.001 OD_{500nm} was sufficient to obtain single cells randomly distributed under agar pads. Agar pads were made by combining LSLB media with 2% w/v Noble Agar (BD, Sigma). Prior to use, the agar was melted by microwaving. To make equally sized agar pads, 100 µL was pipetted into each of several square isolators (16-7 mm X 7 mm X 1.6 mm Depth ID, 25 mm X 75 mm, Grace Bio Labs), placed between two glass microscope slides, and allowed to solidify at 4°C until use. Anoxic pads were made 72 hours in advance and placed in an anaerobic chamber to degas. 5 µL of 0.001 OD_{500nm} dilution culture was added to the well of an 8-well LabTek dish (Thermo). Agar pads were then placed on overtop. Dishes were incubated at 37°C for 24 hours (oxic) or 48 hours (anoxic) in a sealed container (6.7 oz, Systema). When additional humidity was added, instead of distinct aggregate biofilms, cells appeared as under intermixed planktonic conditions; thus, additional humidity was not added. Time lapse imaging was performed incubating pads as described above, but just before lysis would occur (~18 hours), dishes were sealed with parafilm and placed in the heated microscope incubation chamber for imaging. Anoxically-incubated cells were not initially fluorescent due to the inability for fluorophores to fold in the absence of oxygen. To overcome this, pads were placed at 4ºC without lids

for one to two hours prior to imaging resulting in sufficient signal recovery to differentiate GFP and mApple positive cells.

Microscopy

All imaging was performed either using a Nikon Ti2 widefield fluorescence microscope or a Zeiss LSM800 microscope. End time point agar pad images were collected using the Nikon with a Plan Fluor 100x/1.30 oil phase objective and time lapse images were collected using a Plan Apo 40x/0.90 dry phase objective. GFP channels were collected using a 488 nm LED excitation light source and emission was collected with a FITC filter. The mApple channel used 561 nm LED light source and emission was collected with a TRITC filter. For time lapse imaging, an OKO Labs cage incubation unit was set to 37°C several hours before imaging to equilibrate the microscope stand and used for the duration. Images were collected every 20 minutes from multiple stage positions. Time indicated in figures represents time since the pads were inoculated. Both fluorescence CFU counting images from Figure 2D and the CellROX/Producer mass quantification images from Figure 6A-6B were collected using the Zeiss LSM800 confocal with an EC Plan-Neo Fluor 1.25x/0.03 and Plan-Apochromat 63x/1.4 lens, respectively.

Image analysis

All images were analyzed and prepared for display using FIJI (Schindelin et al., 2012). Brightness and contrast were adjusted on a per image basis in order to

best display cell positions and identifications, unless otherwise noted (e.g., CellROX intensity in biofilms imaged and displayed the same for comparison of intensity (Figure 6A-6B)). For time lapse imaging, agar pad XY drift was accounted for by performing an image registration in FIJI using the StackReg plugin with the Rigid Body option. For CFU counting and aggregate biofilm size measurements, images were segmented following a background subtraction, contrast enhancement, and median filter. The processed fluorescence channels were segmented using the Auto Local Threshold function. Segmented objects were counted using the Analyze Particles function with a size filter set to the average size of the specified objects. The XY image position was recorded and used to find the Euclidian distance between aggregate biofilms on a per-image basis. Empirical Cumulative Distribution Function (ECDF) plots (Figure 3F and Figure 6G) display 95% confidence intervals and were generated in Python using iqplot (Bois, 2022).

CellROX intensity was measured from a subset of the images in Figure 6A-6B by generating an intensity-based threshold binary mask of the consumer space (GFP channel). The producer space was then found by inverting the consumer space. Finally, the producer remaining was found by thresholding the producer channel (mApple). By finding the difference between the producer space and producer remaining, a percentage was calculated (Figure 6D, Figure S4B). Finally, to assess the distance in which the producer was saved from or induced

consumer lysis, the intensity profile of a line was drawn between the two points and used to mark start and end and recorded for several images.

Quantification and statistical analysis

Quantification and analyses are described in the Method Details. Briefly, experimental values were compiled and explored in Python and results were plotted using either Seaborn, iqplot, or exported and displayed in GraphPad Prism v9. Statistical tests were performed in GraphPad Prism v9, and the relevant statistical test and sample size is described in the appropriate figure legend.

Supplemental Material

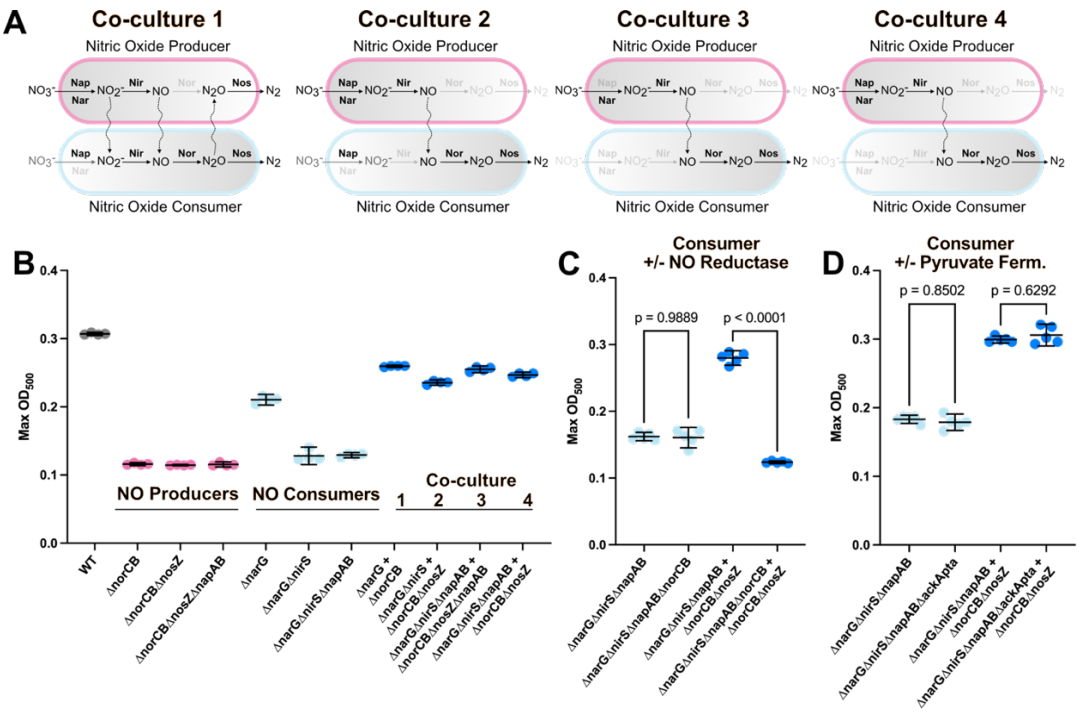

Figure S1. Synthetic NO cross-feeding co-culture comparisons. Related to Figure 2. (A) Schematic representation of genomic identity and subsequent cross-feeding of different NO producer and consumer strains. Wiggly arrows indicate intermediates that can be exchanged. Grayed-out gene name indicates a clean genomic deletion. (B) Max OD for specified strains/co-cultures from growth curves performed identically to those in Figure 2B. (C) Comparison of consumer and co-culture growth when consumer has the nitric oxide reductase (Nor). D) Comparison of consumer and co-culture growth when consumer has the ability to generate ATP via pyruvate fermentation (ackApta). (B-D) Max OD reached over the course of 72-hour growth curves supplemented with 5mM nitrate. Each dot is an independent well (technical replicate, n=4 (B) or n=5 (C,D) for each condition). Each graph is from an independent experiment. Line and error bars in graphs indicate mean and 95% confidence intervals; P values reflect one-way ANOVA with Tukey's multiple comparisons test.

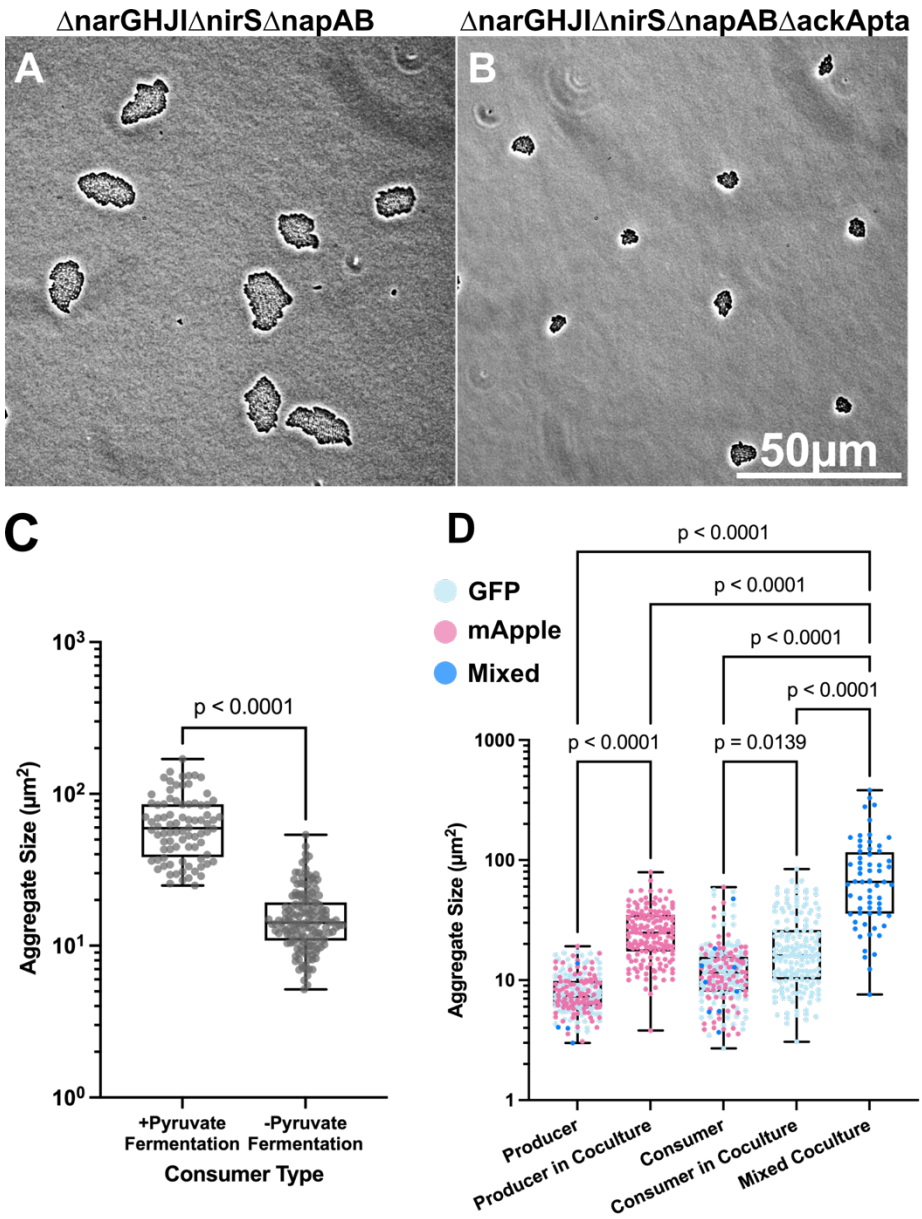

Figure S2. Single cell aggregate imaging increases ability to observe subtle slow-growth differences. Related to Figure 3. (A-B) Comparison of consumer strains differing only in their ability to perform pyruvate fermentation (ackApta) grown under agar pads as in Figure 3B. (C) Quantification of aggregate sizes. P value from unpaired t-test. Each point represents one aggregate (n=84 consumer + pyruvate fermentation, n=153 consumer – pyruvate fermentation) measured from 10 images per condition, (D) Breakout of aggregate size quantification from Figure 3E. P values reflect one-way ANOVA with Tukey's multiple comparisons test.

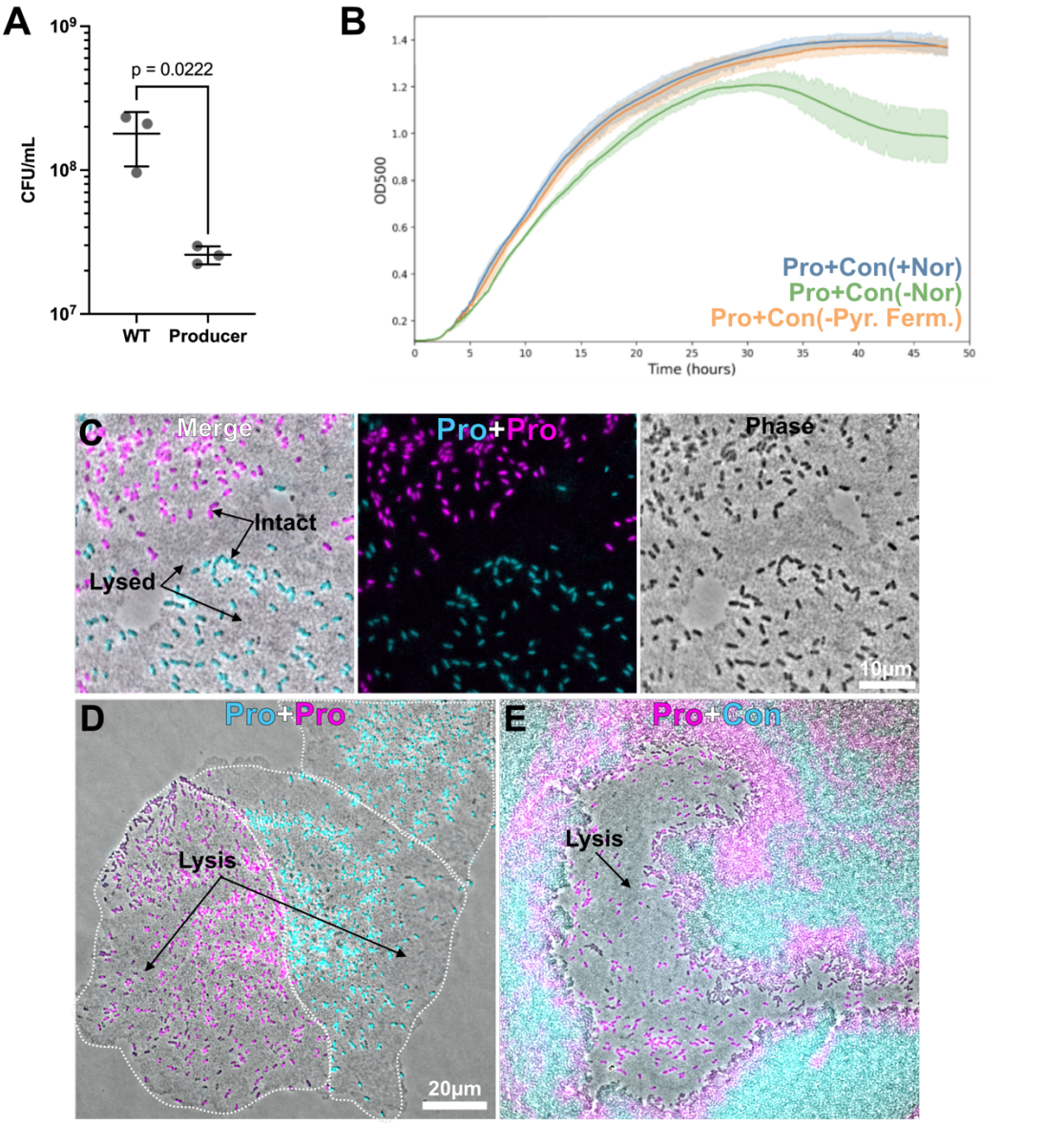

Figure S3. Confirming the cause of reduction in OD under hypoxic growth conditions. Related to Figures 4 and 5. (A) Specified strains grown under identical conditions to Figure 4F (hypoxic-not shaking, with nitrate) were plated for colony forming units (CFU). NO producer strain reduction in CFU is consistent with observed reduction in OD and cell death interpretation. Each point represents one replicate (n=3 per condition). Line and error bars indicate mean and standard deviation; P value from unpaired t-test. (B) Comparison of NO producer co-cultured with different consumers under hypoxic growth conditions. A rescue from cell death (reduction in OD) during co-culture is not observed when consumer lacks NO reductase (Nor). Each line represents the mean of n≥4 replicates per condition. (C) NO Producer comparison of fluorescence and phase channels used to interpret visual lysis. (D-E) Fluorescence and phase channel overlay of Pro+Pro and Pro+Con representative images in Figure 5.

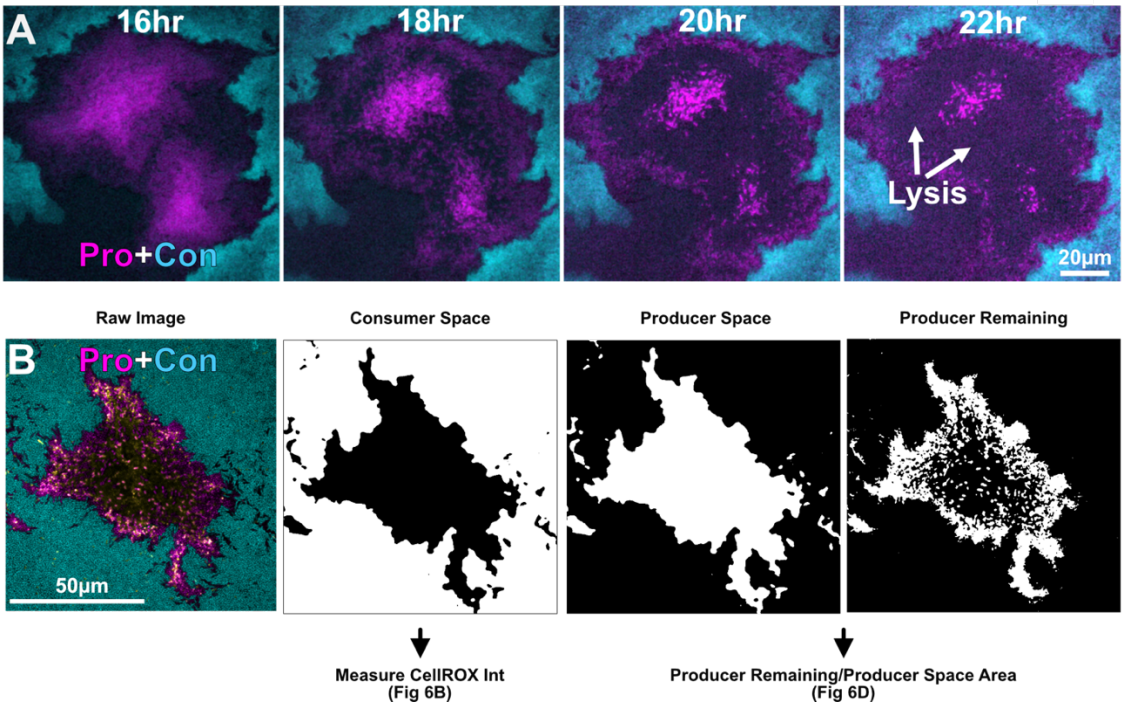

Figure S4. Full patch time lapse and image analysis example. Related to Figures 5 and 6. (A) Time lapse of a NO producer patch showing temporal lysis patterning occurring in the absence of consumer contact. (B) Example of image analysis masks used to quantify metrics in Figure 6 panels C and D.

Deletion Construct	NarGHJI
Function	Membrane bound nitrate reductase
Up F	TAAAACGACGGCCAGTGCCACGTACTGGGTGTTCGCCCTG
Up R	CGCGCAGGGTCTTGATCTCCTCACCCGGTC
Dn F	GGAGATCAAGACCCTGCGCGGCCGGCGCAT
Dn R	CATGATTACGAATTCGA GCTGCTGGCGCGGCAGGAAGCGC

Plasmid	pMQ30
Cut Sites	HindIII, SacI
Published	Spero et al 2018
Deletion Construct	**NapAB**
Function	Periplasmic nitrate reductase
Up F	ACGACGGCCAGTGCCAAGCTTCTACAGTCGCCTGCATAGA
Up R	GTGCTTTCATGCGGCCTCCCCGATTGTCTCCTCGGGCGAG
Dn F	CTCGCCCGAGGAGACAATCGGGGAGGCCGCATGAAAGCACTCA
Dn R	CATGATTACGAATTCGAGCTTCCTGCCGACCGGGGCCCAG
Plasmid	pMQ30
Cut Sites	HindIII, SacI
Published	This study
Deletion Construct	**NirS**
Function	Nitrite reductase
Up F	ACGACGGCCAGTGCCAAGCTTGTCGATGCGCTGGGCCAGCA
Up R	GGCTCCTGAGGAGATAGACCGACCCGCGTGCGGGGCACGC
Dn F	GCGTGCCCCGCACGCGGGTCGGTCTATCTCCTCAGGAGCC
Dn R	CATGATTACGAATTCGAGCTTATCAGGCGACATGGAGATC
Plasmid	pMQ30
Cut Sites	HindIII, SacI
Published	This study
Deletion Construct	**NorCB**
Function	Nitric oxide reductase
Up F	TAAAACGACGGCCAGTGCCATGATCCTCGGCTGGCTGG
Up R	GAAGGCCATCGCGGCCTCCTGGAATGGG
Dn F	AGGAGGCCGCGATGGCCTTCGCCGTCGAG
Dn R	CATGATTACGAATTCGAGCTCCGGGCAATCGTCCAGCG
Plasmid	pMQ30
Cut Sites	HindIII, SacI
Published	This study
Deletion Construct	**NosZ**
Function	Nitrous oxide reductase
Up F	ACGACGGCCAGTGCCAAGCTACGTACTTGACCTGCTGGCG
Up R	GCCCTTGAGGACGACACGAGTCCACTCAGCGCGGTCGATG
Dn F	CATCGACCGCGCTGAGTGGACTCGTGTCGTCCTCAAGGGC
Dn R	CATGATTACGAATTCGAGCTGAGGAACTGGCCGCCCTGGA
Plasmid	pMQ30

Cut Sites	HindIII, SacI
Published	This study
Deletion Construct	**AckA-Pta**
Function	Pyruvate Fermentation
Up F	ACGACGGCCAGTGCCAAGCTTTCAGGCTGCAGAAGGACTG
Up R	GCCCACTGGGCGGCGTTCCTTCACTGCTCCTTGGTCTGCT
Dn F	AGCAGACCAAGGAGCAGTGAAGGAACGCCGCCCAGTGGGC
Dn R	CATGATTACGAATTCGAGCTTACTGATCGCGGCCTGGAAGAAAAAGC
Plasmid	pMQ30
Cut Sites	HindIII, SacI
Published	This study

Table S1. Primers, plasmids, cut sites and strains used to make the mutants used in this study. Related to Figure 2.

Chapter 5

CRYPTIC PHENAZINE-DEPENDENT GROWTH EXPOSED BY CLONAL AGGREGATE SLOW PROLIFERATION ASSAY (CASPA)

This chapter is adapted from a collaboration with John Ciemniecki in which the CASPA method was developed and utilized to address the role of the phenazine PYO in anaerobic growth. *Manuscript in preparation.*

Introduction

Typically, when we envision microbial growth, we picture it as exponential. One cell becomes two, two becomes four and so on. But if this were the status quo of all microbes you can imagine how quickly the world would be filled to the brim with bacteria. The reason that is not the case is because once cells no longer have enough resources, they stop dividing (thankfully!). Logic would dictate that most microbes must instead be limited for resources. However, under such conditions it can be surprisingly difficult to distinguish between cells that are in a quiescence state, those that are dead or if they are still able to divide, just extremely slowly. Given that such a state is likely to be the primary growth phase of microbes, new methods need to be developed that allow us to resolve such slow growth.

Many of the mechanisms of attack antibiotics rely on are involved in an active metabolic state and bacterial division, and therefore less effective in treating slow growing populations (Hassett et al., 2002; Spero and Newman, 2018). Therefore, a better understanding of factors that contribute to slow growth may turn out to be useful and noble targets for chronic infections. Second, understanding what factors contribute to the start, progression and prolonging of slow growth and survival will help accurately predict microbial contributions to global nutrient cycles. Given we cannot always observe or trace all activity directly, such models need to have as much accuracy as possible. *Pseudomonas aeruginosa* (PA) is considered a facultative anaerobe that requires a terminal electron acceptor (TEA) to perform oxidative phosphorylation. Oxygen is its preferred TEA but can also use nitrate NO_3^- in its absence. Substrate-level phosphorylation via fermentation has been considered to insignificantly contribute to energy conservation and especially cell growth.

Beyond strategies for cell division and growth, cell survival has been notably observed with an interaction of PA and its colorful, redox active pigments known as phenazines. In a previous study, long-term anaerobic survival was observed when PA was incubated in a system that allows a redox cycle between phenazines and an electrode in the absence of oxygen (Glasser et al., 2014). This survival showed a dependence on the presence of phenazines, the phenazines being redox cycled and interestingly pyruvate fermentation. The

way survival was measured was through periodic sampling of the culture and plating for colony forming units (CFU) in aerobic conditions. CFUs remain similar for upwards of a week before a decline starts and last longer when the redox cycle is carried out with a positive change active at the electrode surface. At the time, it was unknown exactly how phenazines were contributing to this survival, but it was hypnotized that through a redox balance coupled to fermentation, cells could survive longer. Recently, it has been shown that reduction of phenazines can occur at NADH dehydrogenases (Ciemniecki and Newman, 2023) leading to the potential for contribution to proton translocation and therefore a proton motive force (PMF) and energy conservation through an oxidative phosphorylation mechanism as well.

Getting the same CFU count from one time point to the next supports the conclusion that cells are surviving, but it this may not report cell divisions. This result could also indicate there was an equal number of cells dividing as there was dying. Another tricky thing with plating for CFUs is that you require the cells to be able to regrow under the plate growing conditions. Here, we are talking about taking deep stationary phase cells from conditions lacking any oxygen or nutrients and placing them on high nutrient oxic plates. The shock of the sudden change in conditions could lead to a skewed result.

Finally, hidden away in the supplemental material of the previous chapter lays a piece of data that brings all of the above thoughts into focus and initiated a

fruitful collaboration between myself and John Ciemniecki ((Wilbert and Newman, 2022) Chapter 4, Figure S2). The observation was that using this relatively simple method of sandwich single cells under agar pads and allowing them to grow into clonal aggregates could be used to differentiate very subtle growth that otherwise would be missed. Two mutant strains of PA were grown in the absence of oxygen and which could not reduce NO_3^-. The strain that contained the genes required for the ATP generating steps of pyruvate fermentation (*ackApta*) underwent more cell divisions then the other lacking these genes. As a reminder, pyruvate fermentation has been observed to contribute to survival, but was thought to not supply enough energy to contribute significantly to cell growth. We can also compare these results to the highest optical density these strains can achieve in a standard growth curve and the difference is not observable, likely due to the difference being within the noise floor of the machine. We thought, if this technique were indeed allowing is to visualize and quantify such a small but significant growth difference, we could continue developing the method and to use it to address the long outstanding question, does phenazines merely support survival, or is there actually growth? Given the importance of tracking and differentiating slow growth from survival, we developed Clonal Aggregate Slow Proliferation Assay (CASPA) and used it to address the role of phenazines in slow growth.

Results

Clonal Aggregate Slow Proliferation Assay (CASPA) method

The general idea of this method is to grow bacterial cells in such a way that after some amount of incubation time one can observe and count the number of cells within a clonal population in order to calculate the number of cell divisions that took place over that time. To begin, we wanted to build upon the method for growing single cells into clonal aggregates as designed and outlined previously (Wilbert and Newman, 2022). Figure 1 graphically represents the CASPA method. Large agar pads are made using orange silicone isolators (Grace BioLabs). Each pad is made from roughly 1 mL of media supplemented with 2% w/v Noble Agar. Next, pads are placed in an anaerobic chamber for at least 24 hours prior to setting up the experiment to allow oxygen to degas from the pads. PA cells are diluted to a final OD of 0.002 in PBS and 20 uL of this dilution is placed on the coverslip of a MatTek dish. Using a metal pallet knife, the pad can then be placed on top of the droplet distributing single cells all throughout the agar surface. Dishes are placed in a Systema 6.7 oz plastic container. Importantly, increasing humidity by placing a wet paper towel here results in too much liquid remaining between agar pad and coverslip promoting swarming and resulting in non-clonal aggregates. Similarly, humidity will differ depending on size of container used and number of samples in container. Therefore, it is recommended that 6.7 oz containers with six MatTek dishes be the standard sample/container set up at all time. Otherwise, timing and dilutions may need to

be optimized for a new set up to ensure clonal aggregates are formed. After incubation for one-seven days in the anaerobic chamber, dishes can be removed and brought to a microscope capable of phase contrast for analysis (Figure 1A). For the following results, at least three 5x5 tile scans at 100x magnification were taken at distinct pad placements using the Nikon Ti2 Eclipse widefield microscope with the 2x Zoom optic in place. Note: aggregates will be dense and remaining single cells will be very small so aim to achieve smallest pixel scaling possible.

Once images are collected, image analysis is performed using a semi-automated FIJI macro (Figure 1B). Briefly, images are background subtracted using a rolling ball radius of 200 pixels. Contrast is enhanced by setting the saturation point 0.025% (this homogenization allows the same threshold to be used on all images). Finally, a 3x3 pixel radius median filter is applied. Processed images are then thresholded based on intensity and holes are filled. Whole aggregate objects are then detected and assigned a number in the ROI manager using the Analyze Particles feature, ignoring noise by selecting only objects above one μm^2. Because our eyes are more reliable than the computer at recognizing the number of cells in each aggregate, the macro will then iterate through each object, zooming in to just the selection and give you an opportunity to specify the number of cells present (in these data sets this typically ranged from 1-40 cells). Figured 1B shows this pipeline and how in the end we have a readout of the number of cells per aggregate which we can use

to find the number of cell divisions by taking log2. This analysis alone is a huge improvement over the methods used in my previous work as cell divisions is likely to be far more accurate of a readout over aggregate size conserving the drastic changes in cell size that bacteria can undergo depending on growth phase and nutrient condition alone.

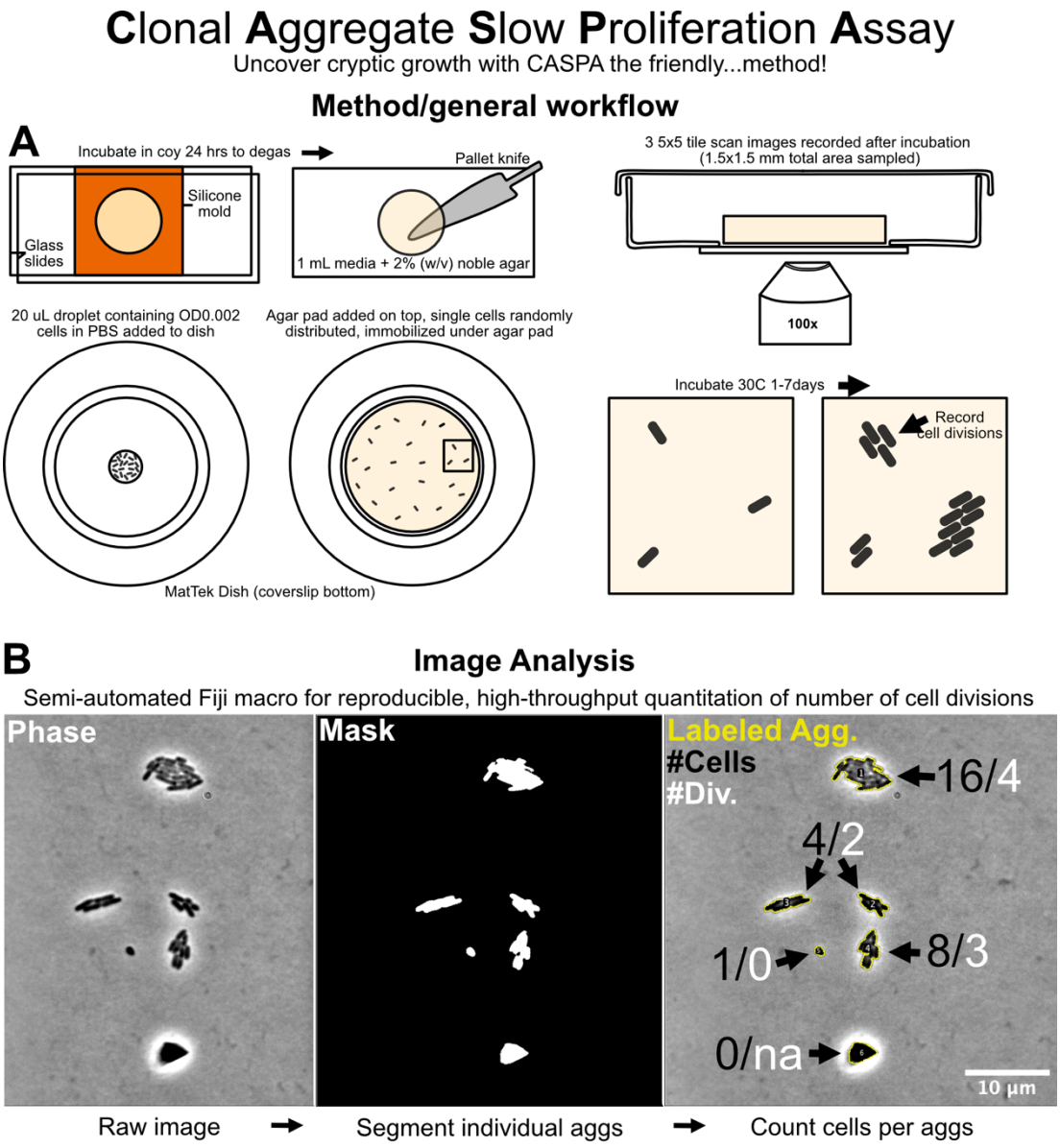

Figure 1. CASPA method. (A) Making pads and setting up imaging dishes. (B) Visual steps of quantitative image analysis pipeline.

PYO promotes anaerobic growth without an exogenous carbon source

After the CASPA method was optimized, we first used it to ask whether or not we could detect more growth of cells in the presence of the phenazine PYO (others were tested but preliminary results suggest PYO is the major contributor to this process). Several pads were prepared in a 2X minimal media containing 40 mM MOPS, 50 mM NH_4Cl, 7.4 mM KH_2PO_4, 2 mM $MgSO_4$, 7.2 μM Fe2O4 and pH adjusted to 7.2 with NaOH. This 2X stock media was then diluted to 1X by combining it 1:1 with a stock of 4% Noble Agar water so that media components were all at a final concentration of half as specified and agar was 2% w/v. For pads containing PYO, it was diluted into agar media to a final concentration at 75 μM from a 5 mM stock in 20 mM HCl at the same time. Pads were then placed in the anaerobic chamber for 24 hours prior to setting up.

The next day, late stationary phase cultures from roughly 20 to 24-hour old 5 mL LB shaking cultures were prepared for inoculation under pads. The optical density was taken (usually in the OD_{500} range of 5-7). OD was used to calculate amount of culture needed to prepare one mL of OD 1 culture. This amount was then centrifuged at 9K RCF for one minute. The supernatant was removed and the pellet was brought into the chamber where it was resuspended in 1X PBS

(left in chamber for days prior to degas) such that we now have one mL OD 1 anoxic culture. 20 uL of culture was placed in the MatTek dish and pads were gently placed on top. Pads were incubated up to size days. One replicate of each pad type (with and without PYO) were taken out at an interval of one day each, imaged and then discarded (Figure 2). Upon visual inspection, there is a clear increase in aggregate size when PYO is present even after one day (Figure 2A compare images). According to the image quantification, there is a slow but steady increase of number of cell divisions over the course of the experiment when PYO is present.

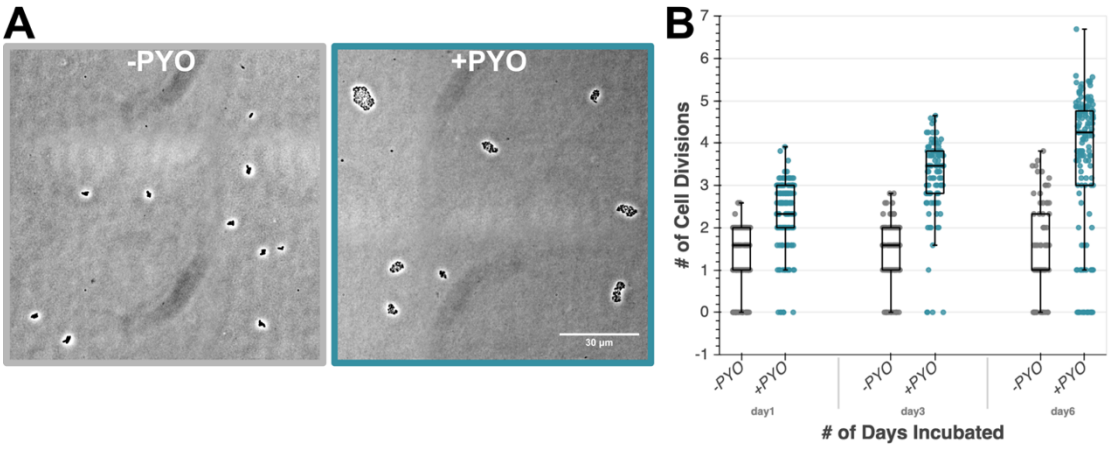

Figure 2. CASPA results for WT PA14 grown in the presence and absence of PYO. (A) Representative images used in analysis. (B) Result of analysis comparing number of cell divisions observed between separate pads taken out of chamber after specific incubation times.

PYO growth can enhances or mimic anaerobic growth on amino acids

We next sought to understand how PYO was promoting the apparent growth we observed. PYO may be acting in a redox balancing role allowing central

metabolism and or fermentation to drive ATP synthesis and thus cell divisions. However, recall that we have not supplied any carbon sources. It is likely that PYO here is instead serving a nutrient harvesting role by acting as a toxin, leading to cell death and release of amino acids non-killed cells could use. If this hypothesis were true, we would expect to see just as much growth when cells are merely supplied with amino acids instead of PYO. When we do this experiment, we end up confirming that growth on amino acids can match that seen with the addition of PYO but, depending on the concentration given, there is another regium where PYO can help increase growth on amino acids above the background. We interpret these results to be overall supportive of the PYO induced lysis hypothesis, but that we cannot rule out PYO acting in a secondary role of redox balancing or even as a terminal electron acceptor. It is likely that both roles are active but will be dependent on concentrations and conditions. One might say, context dependent.

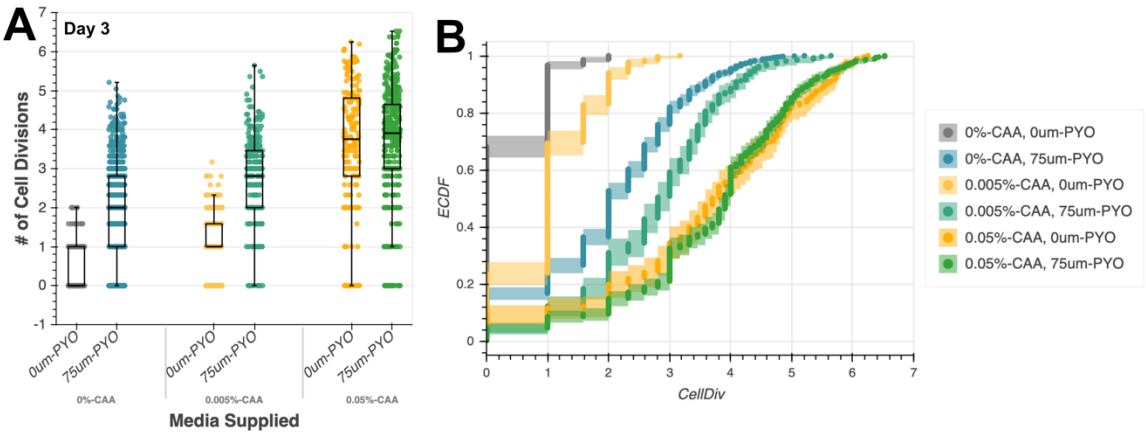

Figure 3. Comparison of synergistic amino acid and PYO growth. (A) Results of aggregates after three days of growth in pads made with specified additions. (B) The same data but as an ECDF plot for better comparison.

PYO interacts with iron leading to lysis under anoxic conditions

If PYO is acting as a toxic to a subpopulation of cells, allowing amino acids to become released and available to others, we should be able to visualize cell lysis with the CASPA method. Most methods of phenazine toxicity involve disrupting cells aerobically respiring with oxygen, resulting in an improper balance of reactive oxygen species, DNA damage and cell death. However, under these conditions there is no oxygen present. Instead, the most likely candidate for this toxicity a previously observed one electron transfer from ferrous iron and PYO resulting in a radical state that similarly to ROS can lead to cell death (Figure 4) (Kang et al., 2022). In order to test whether this was occurring in our system, pads were made as specified with PYO, but iron was either not added, added at normal level or at 10-fold normal level. Visually we can identify more cell lysis of cells within aggregates (Figure 4A). This does not include single cells that may have lysed and are no longer visible. This supports the hypothesis that iron and PYO interactions contribute to cell death and thus release of nutrients. It is also interesting to note that when comparing aggregate sizes between conditions, although they average out the same between all three iron concentrations, the largest aggregates (most cell divisions) observed are when there is the most toxicity from more iron, likely reflecting the nutrients released to the resistant subpopulation that consumes them.

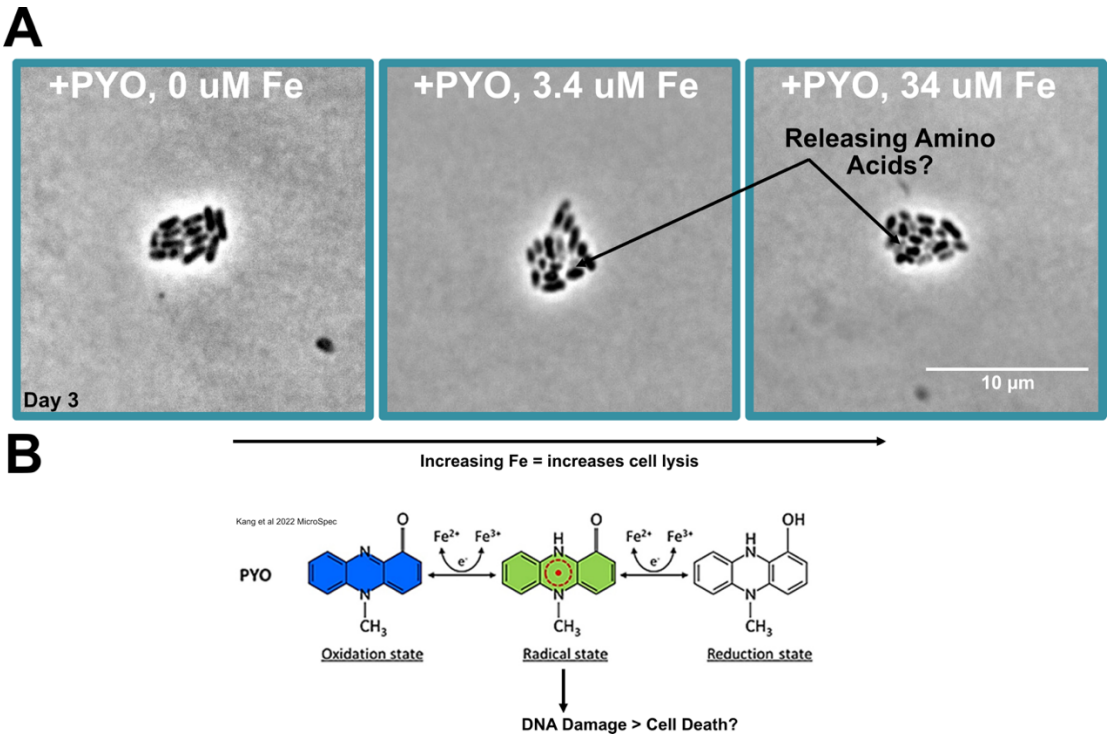

Figure 4. Visual influence of iron concentration on apparent cell lysis. (A) Images showing increasing cell lysis as iron increases. (B) Reproduction of figure showing one electron transfer from ferric iron to form a radical PYO molecule capable of DNA damage and cell death.

Proposed agathokakological role of PYO under anaerobic growth and death

In Figure 5 I attempt to visually summarize the findings here. First, when there are no additions to the agar pads in CASPA experiments there is very little growth. But not absolutely no growth. There appears to be a subpopulation that is able to perform a few divisions based on the spread of the division distribution (look at day 6 of “no PYO” in Figure 1). Some cells divided, most did not. This may represent differences in internal stores (mint green, circle). Recall the starting populations here are from late stationary phase cultures, which are notorious for being heterogenous in their metabolic state. Interestingly, this type

of population was required to maintain CFU survival data (likely because of this cryptic growth).

When supplied with amino acids (AA, yellow, circle) in the pads, we saw significant cell divisions likely due to AA fermentation. Again, the observed distribution in cell divisions per aggregate can be explained by the heterogeneous staring population as shown in the summery figure where the cells with internal stores grow more but all cells do grow.

When we supplied PYO (PYO, blue, circle) but not AA, iron leads to radical forms of PYO that lead to lysis of some cells in the population, presumably releasing AA. However, not all cells seem to undergo lysis. This could be explained again because of the heterogenous starting population. Perhaps cells with more internal stores will have a leg up and are able to better tolerate PYO by upregulating efflux pumps known to prevent PYO toxicity by ensuring internal PYO concentrations remain low (Meirelles and Newman, 2018). Note that this would also suggest that a subpopulation that has no chance at protecting itself from PYO may be a perfect partner for PA under nutrient limiting conditions as a harvesting technique.

Finally, at least under certain concentrations, we saw PYO can improve growth when lower levels of AA are supplied from the beginning. Perhaps under these conditions more of the initial population is able to overcome PYO toxicity with

more available nutrients to upregulate pumps. But clearly there is still another mechanism of PYO stimulation under these conditions otherwise there would not be improved growth. This is where we can start to imagine a scenario where PYO is acting in a redox balancing agent and/or as a TEA. Future experiments will be able to address this by testing mutants incapable of the fermentative arm (pyruvate fermentation via Δ*ackApta*, or AA fermentation such as Δ*arcA*) or removing the potential PMF generating mechanisms of PYO reduction from NADH dehydrogenase mutants.

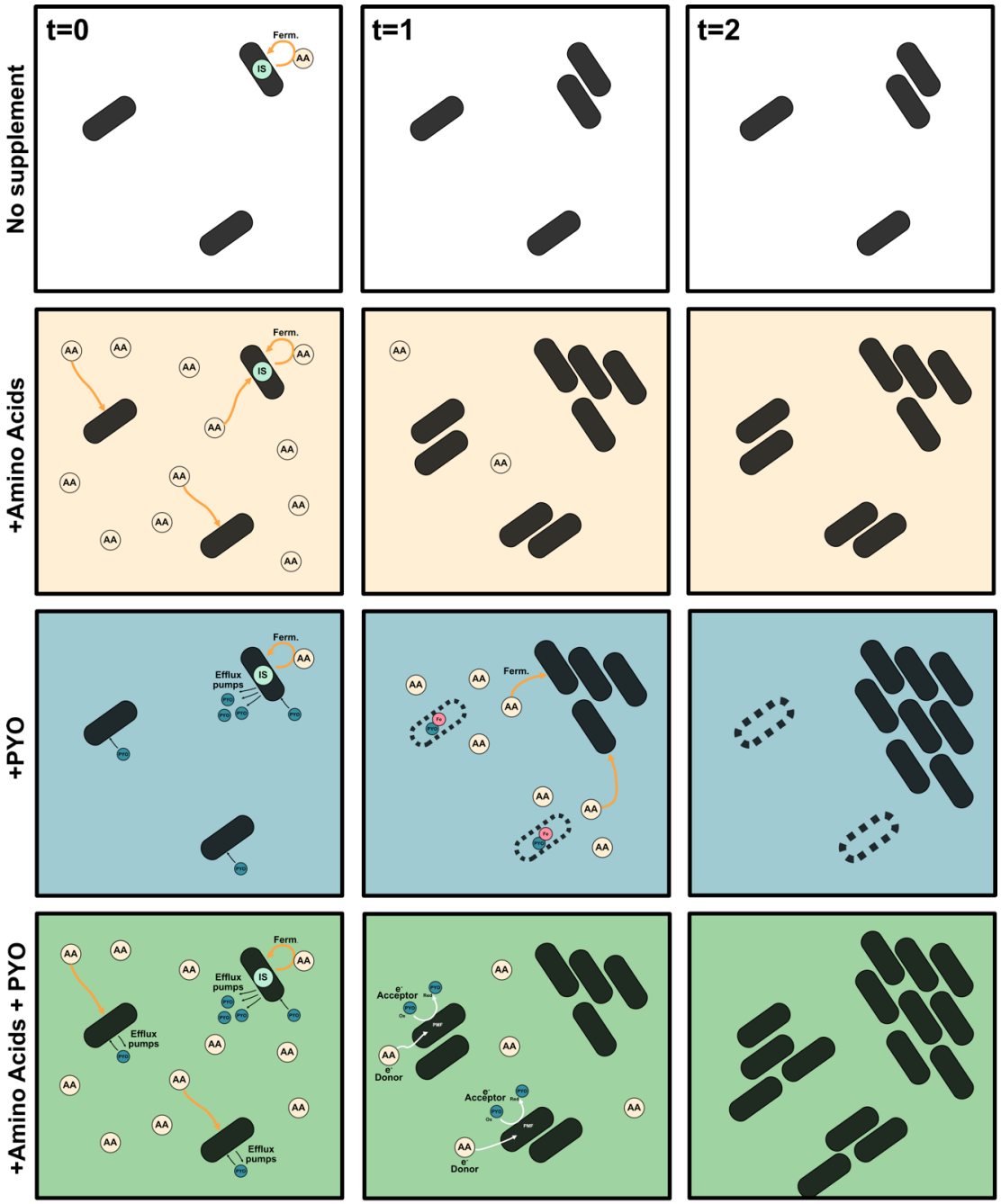

Figure 5. Proposed model of context-dependent effects of PYO.

Discussion and future directions

To the best of our knowledge, these data show for the first time a role for PYO in anaerobic cell growth. While the exact mechanism is still unknown, this methodological framework along with the work of John Ciemniecki to better resolve the site of phenazine reduction in the cell, will hopefully provide some inspiration and tools for future students to continue refining our understanding of agathokakological molecules.

These results suggest a role for PYO in allowing a subpopulation of cells growing even without the addition of new carbon sources. An argument could be made for why such growth would therefore not be very significant to carbon cycles. Yet, no cycle is existing in a vacuum. It is possible that due to this recycling of nutrients, cells could continue modifying other, fresh nutrients in their vicinity such as nitrogen. I can imagine a scenario in which cells deep in soil are starved for oxygen and carbon but due to over fertilization the soil is saturated in nitrogen. Perhaps these cells would then be slowly but surely reducing the nitrogen and releasing it as the potent greenhouse gas nitrous oxide (N_2O). Thanks to this method and framework, such a cryptic contribution to nitrogen cycles could therefore inform models. This idea is supported by other work that shows how capturing cryptic microbial growth of an abundant marine organism uncovered cell division was much faster than previously thought,

disrupting traditional views and how it is thought to play into nutrient cycles (Brüwer et al., 2023).

Previous studies using phenazine to support long term anaerobic survival required an electrode to oxidize the phenazines completing a redox cycle. You may have noticed we have not done so here. We believe this was not required because of the low cell density compared to amount of PYO. Normally dense cultures are used, here the density was very spares. Orders of magnitude lower in fact. Also, the pads appear blue after incubation, indicating it has not all been reduced. We think this change in cell density, while required to ensure confidence of clonal aggregate identification, may play a role as well in our ability to see such subtle differences.

Aside from a slight growth benefit observed with PCA, other phenazines did not appear to result in a significant growth benefit compared what was seen with PYO. One potential reason for this could be the need to complete the redox cycle. One way to overcome this would be to use optically transparent electrodes in contact with the agar pad in order to reoxidize the phenazines for longer term and or higher cell density experiments. Finally, as another alternative, by incubating a phenazine reducer with a phenazine oxidizer using the CASPA method it may be possible to identify how such redox cycle may occur between members of a microbial community (Tsypin and Newman, 2021).

Chapter 6

CONCLUSIONS AND FUTURE DIRECTIONS

I hope that through the development of these methods and strains I have made an impact in the way we think about microbial interactions. Not only in specific intellectual contributions, but also from a standpoint of promoting overcoming hardships, pushing through technological hiccups with troubleshooting, and getting creative not just in what questions you address, but how you address them. Just because there is a classical way to answer a question, does not mean it is the only or the best way.

Creating and characterizing an NO producer and consumer strain led to an appreciation for identifying precise spatiotemporal concentrations of keystone metabolites in order to have a holistic view of its impact. NO has primarily been considered only for its toxic roles. In this thesis, I demonstrate that if the concentration and microenvironment meet certain criteria, it is instead a lifeline. I wonder what other traditionally considered toxic molecules may have such an agathokakological role in shaping microbial communities.

There is a major push from an omics standpoint to map microbial presence in a given site and extrapolate the function based on gene presence or absence. I hope my work highlights the importance of also considering the large impact of how the organisms are arranged in space and time. For example, my NO

producer and consumer strains can range from no interaction, to a commensal interaction to a compulsory dependence on one another for survival depending on local oxygen concentrations as well as whether they are grown planktonically or in a sessile state. The same genes are present in these strains under these different conditions but may or may not be useful predictors of their interactions unless we also know how and where they are expressed in space and time.

Based on this, I think techniques such as SeqFISH that couple the power of imaging spatial patterns of microbes with a readout of their transcriptional landscape will be a vital and fruitful path forward. I can image mapping common transcriptional profiles of neighboring cells and cells within an oxygen gradient, iteratively compared to bulk sequencing profiles as a way to test how such data could drive improvements in our ability to accurate predict metabolic contributions from omics data.

Structure-function relationships are constantly fluctuating as microbes are growing and lysing. Because such dynamic growing and dying are major drivers in these systems, it will also be fruitful to continue expanding upon methods beyond fixed time points. Typically, the more complex an assay, the less specific readouts become. However, it is within that complexity that we can find otherwise hidden or overlooked important and generalizable features contributing to microbial communities.

Appendix I

THE INFLUNCE OF IRON ON AGGREGATE GROWTH IN ABBA

Early on in my PhD I began working with Synthetic Cystic Fibrosis Medium (SCFM), which is a medium designed specifically to mimic the environment found in the sputum layer of lungs of people with cystic fibrosis (Palmer et al., 2007). It is a fairly complex medium, and I began preparing and making it to compare how PA grew in it verse the standard LB medium. Cells were suspending in either LB or SCFM, grown at 37C for 20 hours, stained with the Live/Dead viability kit (Syto9, green, PI, red) and imaged using confocal microscopy (Figure 1). If we compare the first two panels (LB 0 mM KNO_3 vs SCFM 0 mM KNO_3) we see a striking difference. Side note: keep in mind that Syto0 (green) should stain “all cells” as it is cell permeant but can be quenched by phenazines and PI (red) should stain “dead cells” but in reality, at the intensity we see here it is more likely staining non-growing cells with reduced charged membranes allowing the dye to enter.

The ABBA made in LB shows a very typical result. Large aggregates at the top that get smaller as you move deeper into the agar (less oxygen). Aggregates at the top show more green staining, while the deeper aggregates show brighter red (likely starved for a TEA and thus not growing). The ABBA made in SCFM instead shows extremely bright green staining (no real explanation for this aside

from, less nutrients, slower growth, not producing phenazines yet). But most striking is that instead of the largest aggregates being the top agar-oxygen interface, they are several hundred microns deeper than the surface.

Next, I wanted to see what the supplying another TEA would do to the aggregate growth. Now, comparing, the first two top panels to the panels directly below them, we see that in both cases the addition of nitrate, a TEA for when cells lack oxygen, the anoxic aggreges (deepest) are larger and stain brighter). Again, brighter PI staining could mean more dead but also stains stationary phase cells, we can imagine that if the anoxic population is now able to grow, they would be closer to stationary phase at this time point so therefore stain brighter with PI.

Bringing attention back to the apparent inverse gradient in the SCFM medium, I was perplexed and repeated several times always getting this result. It was then that I realized I was accidently forgetting to add an important component: iron. To test if this oversight could be responsible, I first added 1x trace metal from a standard 1000x laboratory stock to the SCFM medium. Low and behold I was able to again achieve growth I was expecting, with largest aggregates at the top agar oxygen interface and getting smaller as you looking deeper. While here I used trace metals, I also tried just mixing LB and SCFM (in case it was something else I was missing) and got the same result. Finally, in the standard

SCFM protocols, they do indicate to prepare a stock of $FeSO_4$ the day of an experiment to add to the medium. This information was just lost in translation from one hand to the next and its addition also returned growth to normal conditions.

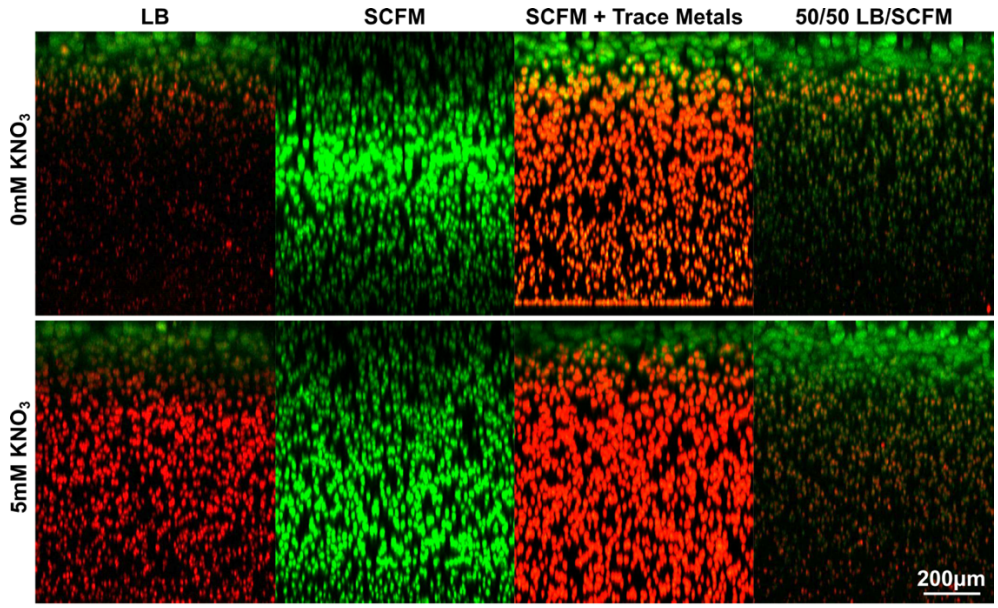

Figure 1. Orthogonal projections of Agar Block Biofilm Assays (ABBA) prepared in different media. Red PI staining intensity. Green Syto9 staining intensity.

This is just an example how mistakes can sometimes turn out to be good things. It also highlights just how useful ABBA can be for visualizing nutrient availability impact on growth and oxygen gradients. Clearly the cells further from oxygen are better off when iron is limiting. It may be a wild speculation, but these results could indicate a requirement for high iron in cytochrome oxidase use or expression.

Appendix II

GENETIC CONTROL OF NO INDUCED CELL LYSIS AT THE CORE VS PERIPHERY OF AN AGGREGATE BIOFILM

In Chapter 4 I went into depth about a strain of PA that produces nitric oxide (NO) and leads to self-lysis under hypoxic conditions. In Figure 1 below I compare patterns of lysis when there are different genes present in the strains. The first step in the production of NO is to reduce the supplied nitrate NO_3^-. PA has two different nitrate reductases: the proton translocating, membrane bound Nar and the redox balancing, periplasmic Nap. Figure 1A shows what is known about the transcriptionally regulation of these two nitrate reductases. Nar is upregulated when oxygen is low and nitrate is high. Nap is upregulated by RpoS, which we can simplify to mean when nutrients are getting low and entering stationary phase. If a NO producer strain contains both reductases, it would make sense then for nitrate to be reduced by either Nap or Nar and therefore throughout the hole depth of a biofilm. Because NO toxicity increases with oxygen, which is likely to be primarily at the periphery, it makes sense that lysis would start at the perimeter and work its way inside. This is exactly what we saw in Chapter 4 Figure 5, and what we see in the time lapse below (Figure 1B).

However, if we remove Nap from the strain and nitrate can only be reduced by Nar and Nar is only going to be expressed in the core due to the regulation by low oxygen, we should instead see no buildup in the core and not the periphery. Though oxygen increases toxicity, it is not required so it makes sense to see lysis in the core.

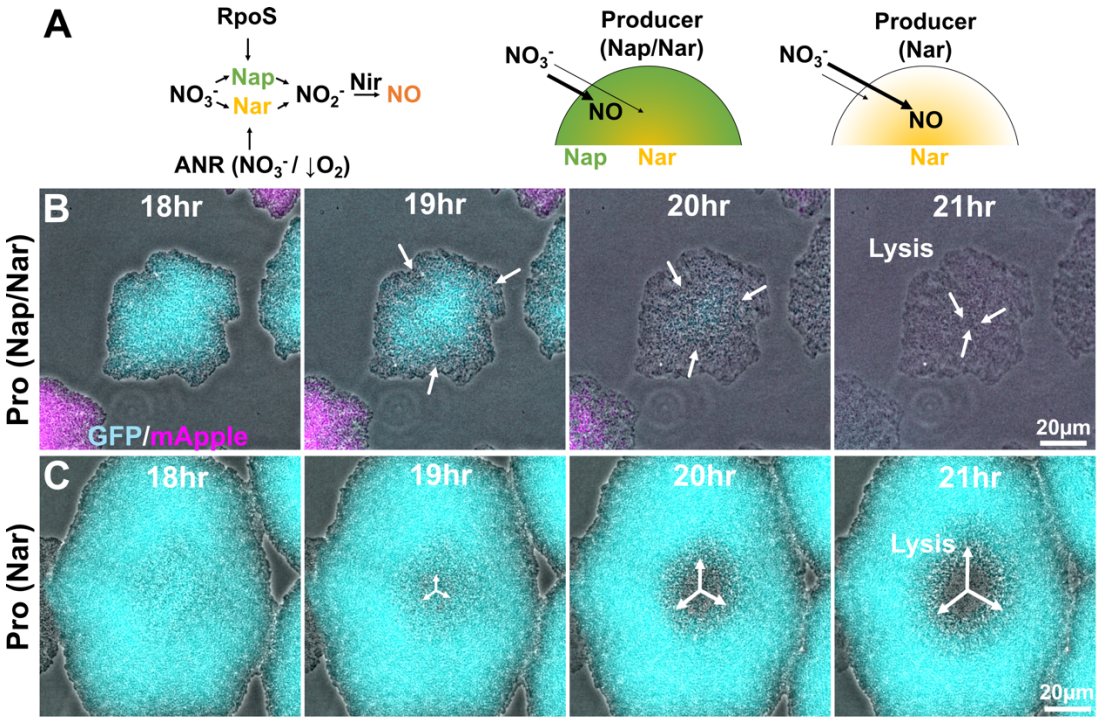

Figure 1. Comparison of nitric oxide producer strains lysis localization. (A) Proposed model of why NO would be produced at different spatial locations with biofilms. (B-C) Still frames from time lapse of producer strains that contain both nitrate reductases (Nap/Nar) or just one (Nar).

Just one change in reductase presence can have huge impacts on whether or not a population would survive under these conditions. I Chapter 4, I showed that if there is a NO consuming strain next to cells producing NO, both can

survive. However, if NO is only being produced in the core of a clonal biofilm as shown here, there may be no hope as other cell types would be too far away to relieve the toxicity.

BIBLIOGRAPHY

Arai, H. (2011). Regulation and Function of Versatile Aerobic and Anaerobic Respiratory Metabolism in *Pseudomonas aeruginosa*. *Front. Microbiol.* **2**, 103.

Basta, D. W., Bergkessel, M. and Newman, D. K. (2017). Identification of fitness determinants during energy-limited growth arrest in *Pseudomonas aeruginosa*. *MBio* **8**, 1–17.

Beckman, J. S. and Koppenol, W. H. (1996). Nitric oxide, superoxide, and peroxynitrite: the good, the bad, and ugly. *Am. J. Physiol.* **271**, C1424-37.

Bois, J. S. (2022). justinbois/iqplot: v0.2.0.

Borer, B., Ciccarese, D., Johnson, D. and Ori, D. (2020). Spatial organization in microbial range expansion emerges from trophic dependencies and successful lineages Benedict. *Commun. Biol.* 1–10.

Brunelli, L., Crow, J. P. and Beckman, J. S. (1995). The comparative toxicity of nitric oxide and peroxynitrite to escherichia coli. *Arch. Biochem. Biophys.* **316**, 327–334.

Brüwer, J. D., Orellana, L. H., Sidhu, C., Klip, H. C. L., Meunier, C. L., Boersma, M., Wiltshire, K. H., Amann, R. and Fuchs, B. M. (2023). In situ cell division and mortality rates of SAR11, SAR86, *Bacteroidetes*, and *Aurantivirga* during phytoplankton blooms reveal differences in population controls. *mSystems* e0128722.

Carlson, C. A. and Ingraham, J. L. (1983). Comparison of denitrification by *Pseudomonas stutzeri*, *Pseudomonas aeruginosa*, and *Paracoccus denitrificans*. *Appl. Environ. Microbiol.* **45**, 1247–1253.

Carr, G. J., Page, M. D. and Ferguson, S. J. (1989). The energy-conserving nitric-oxide-reductase system in *Paracoccus denitrificans*. *Eur. J. Biochem.* **179**, 683–692.

Chen, J. and Strous, M. (2013). Denitrification and aerobic respiration, hybrid electron transport chains and co-evolution. *Biochimica et Biophysica Acta - Bioenergetics* **1827**, 136–144.

Choi, K. H. and Schweizer, H. P. (2006). mini-Tn7 insertion in bacteria with single *att*Tn7 sites: Example *Pseudomonas aeruginosa*. *Nat. Protoc.* **1**, 153–161.

Ciccarese, D., Zuidema, A., Merlo, V. and Johnson, D. R. (2020). Interaction-dependent effects of surface structure on microbial spatial self-

organization. *Philos. Trans. R. Soc. Lond. B Biol. Sci.* **375**, 20190246–20190246.

Ciccarese, D., Tantawi, O., Zhang, I., Plata, D. and Babbin, A. R. (2022). Sinking diatom aggregates provide carbon to drive microscale denitrification in a bulk oxygenated ocean. *bioRxiv* 2022.09.26.509232.

Ciemniecki, J. A. and Newman, D. K. (2023). NADH dehydrogenases are the predominant phenazine reductases in the electron transport chain of *Pseudomonas aeruginosa*. *Mol. Microbiol.* **119**, 560–573.

Cordero, O. X. and Datta, M. S. (2016). Microbial interactions and community assembly at microscales. *Curr. Opin. Microbiol.* **31**, 227–234.

Costa, K. C., Glasser, N. R., Conway, S. J. and Newman, D. K. (2017). Pyocyanin degradation by a tautomerizing demethylase inhibits *Pseudomonas aeruginosa* biofilms. *Science* **355**, 170–173.

Dahlstrom, K. M., McRose, D. L. and Newman, D. K. (2020). Keystone metabolites of crop rhizosphere microbiomes. *Curr. Biol.* **30**, R1131–R1137.

Dal Co, A., van Vliet, S., Kiviet, D. J., Schlegel, S. and Ackermann, M. (2020). Short-range interactions govern the dynamics and functions of microbial communities. *Nat. Ecol. Evol.* **4**, 366–375.

Dar, D., Dar, N., Cai, L. and Newman, D. K. (2021). *In situ* single-cell activities of microbial populations revealed by spatial transcriptomics. *bioRxiv.* 2021.02.24.432792.

DePas, W. H., Starwalt-Lee, R., Van Sambeek, L., Kumar, S. R., Gradinaru, V. and Newman, D. K. (2016). Exposing the three-dimensional biogeography and metabolic states of pathogens in cystic fibrosis sputum via hydrogel embedding, clearing, and rRNA labeling. *MBio* **7**, 1–11.

Eschbach, M., Schreiber, K., Trunk, K., Buer, J., Jahn, D. and Schobert, M. (2004). Long-term anaerobic survival of the opportunistic pathogen *Pseudomonas aeruginosa* via pyruvate fermentation. *J. Bacteriol.* **186**, 4596–4604.

Fang, Y., Koba, K., Makabe, A., Takahashi, C., Zhu, W., Hayashi, T., Hokari, A. A., Urakawa, R., Bai, E., Houlton, B. Z., et al. (2015). Microbial denitrification dominates nitrate losses from forest ecosystems. *Proc. Natl. Acad. Sci. U. S. A.* **112**, 1470–1474.

Findlay, A. J., Bennett, A. J., Hanson, T. E. and Luther, G. W. (2015). Light-dependent sulfide oxidation in the anoxic zone of the chesapeake bay can be explained by small populations of phototrophic bacteria. *Appl. Environ. Microbiol.* **81**, 7560–7569.

Flamholz, A. I., Saccomano, S., Cash, K. and Newman, D. K. (2022). Optical O_2 Sensors Also Respond to Redox Active Molecules Commonly Secreted by Bacteria. *MBio* **13**, e0207622.

Fuhrman, J. A. (2009). Microbial community structure and its functional implications. *Nature* **459**, 193–199.

Glasser, N. R., Kern, S. E. and Newman, D. K. (2014). Phenazine redox cycling enhances anaerobic survival in *Pseudomonas aeruginosa* by facilitating generation of ATP and a proton-motive force. *Mol. Microbiol.* **92**, 399–412.

Goldford, J. E., Lu, N., Bajić, D., Estrela, S., Tikhonov, M., Sanchez-Gorostiaga, A., Segrè, D., Mehta, P. and Sanchez, A. (2018). Emergent simplicity in microbial community assembly. *Science* **361**, 469–474.

Goldschmidt, F., Regoes, R. R. and Johnson, D. R. (2018). Metabolite toxicity slows local diversity loss during expansion of a microbial cross-feeding community. *ISME J.* **12**, 136–144.

Goldschmidt, F., Caduff, L. and Johnson, D. R. (2021). Causes and consequences of pattern diversification in a spatially self-organizing microbial community. *ISME J.* **15**, 2415–2426.

Gowda, K., Ping, D., Mani, M. and Kuehn, S. (2022). Genomic structure predicts metabolite dynamics in microbial communities. *Cell* **185**, 530-546.e25.

Gralka, M., Szabo, R., Stocker, R. and Cordero, O. X. (2020). Trophic Interactions and the Drivers of Microbial Community Assembly. *Curr. Biol.* **30**, R1176–R1188.

Hallatschek, O., Hersen, P., Ramanathan, S. and Nelson, D. R. (2007). Genetic drift at expanding frontiers promotes gene segregation. *Proc. Natl. Acad. Sci. U. S. A.* **104**, 19926–19930.

Hassett, D. J., Cuppoletti, J., Trapnell, B., Lymar, S. V., Rowe, J. J., Yoon, S. S., Hilliard, G. M., Parvatiyar, K., Kamani, M. C., Wozniak, D. J., et al. (2002). Anaerobic metabolism and quorum sensing by *Pseudomonas aeruginosa* biofilms in chronically infected cystic fibrosis airways: rethinking antibiotic treatment strategies and drug targets. *Adv. Drug Deliv. Rev.* **54**, 1425–1443.

Hester, E. R., Jetten, M. S. M., Welte, C. U. and Lücker, S. (2019). Metabolic overlap in environmentally diverse microbial communities. *Front. Genet.* **10**, 1–10.

Jungblut, A. D., Hawes, I., Mackey, T. J., Krusor, M., Doran, P. T., Sumner, D. Y., Eisen, J. A., Hillman, C. and Goroncy, A. K. (2016). Microbial mat communities along an oxygen gradient in a perennially ice-covered Antarctic lake. *Appl. Environ. Microbiol.* **82**, 620–630.

Kang, J., Cho, Y.-H. and Lee, Y. (2022). Pyocyanin and 1-Hydroxyphenazine Promote Anaerobic Killing of *Pseudomonas aeruginosa* via Single-Electron Transfer with Ferrous Iron. *Microbiol. Spectr.* **10**, e0231222.

Kolpen, M., Kühl, M., Bjarnsholt, T., Moser, C., Hansen, C. R., Liengaard, L., Kharazmi, A., Pressler, T., Høiby, N. and Jensen, P. Ø. (2014). Nitrous oxide production in sputum from cystic fibrosis patients with chronic *Pseudomonas aeruginosa* lung infection. *PLoS One* **9**,.

Koskenkorva, T., Aro-Kärkkäinen, N., Bachmann, D., Arai, H., Frey, A. D. and Kallio, P. T. (2008). Transcriptional activity of *Pseudomonas aeruginosa* fhp promoter is dependent on two regulators in addition to *FhpR*. *Arch. Microbiol.* **189**, 385–396.

Krichels, A. H. and Yang, W. H. (2019). Dynamic Controls on Field-Scale Soil Nitrous Oxide Hot Spots and Hot Moments Across a Microtopographic Gradient. *J. Geophys. Res. Biogeosci*. **124**, 3618–3634.

Krichels, A., DeLucia, E. H., Sanford, R., Chee-Sanford, J. and Yang, W. H. (2019). Historical soil drainage mediates the response of soil greenhouse gas emissions to intense precipitation events. *Biogeochemistry* **142**, 425–442.

Krichels, A. H., Homyak, P. M., Aronson, E. L., Sickman, J. O., Botthoff, J., Shulman, H., Piper, S., Andrews, H. M. and Jenerette, G. D. (2022). Rapid nitrate reduction produces pulsed NO and N_2O emissions following wetting of dryland soils. *Biogeochemistry* **158**, 233–250.

Kuhns, D. B., Priel, D. A. L., Chu, J. and Zarember, K. A. (2015). Isolation and Functional Analysis of Human Neutrophils. *Curr. Protoc. Immunol.* **111**, 139–148.

Kuypers, M. M. M., Marchant, H. K. and Kartal, B. (2018). The microbial nitrogen-cycling network. *Nat. Rev. Microbiol.* **16**, 263–276.

Lancaster, J. R. (1994). Simulation of the diffusion and reaction of endogenously produced nitric oxide. *Proc. Natl. Acad. Sci. U. S. A.* **91**, 8137–8141.

Lilja, E. E. and Johnson, D. R. (2016). Segregating metabolic processes into different microbial cells accelerates the consumption of inhibitory substrates. *ISME J.* **10**, 1568–1578.

Livingston, J., Spero, M. A., Lonergan, Z. R. and Newman, D. K. (2022). Visualization of mRNA Expression in *Pseudomonas aeruginosa* Aggregates Reveals Spatial Patterns of Fermentative and Denitrifying Metabolism. *Appl. Environ. Microbiol.* **88**, e0043922.

Lowery, N. V. and Ursell, T. (2019). Structured environments fundamentally alter dynamics and stability of ecological communities. *Proc. Natl. Acad. Sci. U. S. A.* **116**, 379–388.

Lycus, P., Bøthun, K. L., Bergaust, L., Shapleigh, J. P., Bakken, L. R. and Frostegård, Å. (2017). Phenotypic and genotypic richness of denitrifiers revealed by a novel isolation strategy. *ISME J.* **11**, 2219–2232.

Ma, L. and Cordero, O. X. (2018). Solving the structure-function puzzle. *Nat. Microbiol.* **3**, 750–751.

McBee, M. E., Chionh, Y. H., Sharaf, M. L., Ho, P., Cai, M. W. L. and Dedon, P. C. (2017). Production of superoxide in bacteria is stress- and cell state-dependent: A gating-optimized flow cytometry method that minimizes ROS measurement artifacts with fluorescent dyes. *Front. Microbiol.* **8**, 1–17.

Meirelles, L. A. and Newman, D. K. (2018). Both toxic and beneficial effects of pyocyanin contribute to the lifecycle of *Pseudomonas aeruginosa*. *Mol. Microbiol.* **110**, 995–1010.

Momeni, B., Brileya, K. A., Fields, M. W. and Shou, W. (2013). Strong inter-population cooperation leads to partner intermixing in microbial communities. *Elife.* **2013**, 1–23.

Niehaus, L., Boland, I., Liu, M., Chen, K., Fu, D., Henckel, C., Chaung, K., Miranda, S. E., Dyckman, S., Crum, M., et al. (2019). Microbial coexistence through chemical-mediated interactions. *Nat. Commun.* **10**,2052.

Palmer, K. L., Aye, L. M. and Whiteley, M. (2007). Nutritional cues control *Pseudomonas aeruginosa* multicellular behavior in cystic fibrosis sputum. *J. Bacteriol.* **189**, 8079–8087.

Panmanee, W., Su, S., Schurr, M. J., Lau, G. W., Zhu, X., Ren, Z., McDaniel, C. T., Lu, L. J., Ohman, D. E., Muruve, D. A., et al. (2019). The anti-sigma factor MucA of *Pseudomonas aeruginosa*: Dramatic differences of a *mucA22* vs. a *ΔmucA* mutant in anaerobic acidified nitrite sensitivity of planktonic and biofilm bacteria in vitro and during chronic murine lung infection. *PLoS One* **14**, e0216401.

Perry, E. K. and Newman, D. K. (2022). Prevalence and Correlates of Phenazine Resistance in Culturable Bacteria from a Dryland Wheat Field. *Appl. Environ. Microbiol.* **88**, e0232021.

Pessi, I. S., Viitamäki, S., Virkkala, A.-M., Eronen-Rasimus, E., Delmont, T. O., Marushchak, M. E., Luoto, M. and Hultman, J. (2022). In-depth characterization of denitrifier communities across different soil ecosystems in the tundra. *Environ. Microbiome.* **17**, 30.

Price-Whelan, A., Dietrich, L. E. P. and Newman, D. K. (2007). Pyocyanin alters redox homeostasis and carbon flux through central metabolic pathways in *Pseudomonas aeruginosa* PA14. *J. Bacteriol.* **189**, 6372–6381.

Prieto-Barajas, C. M., Valencia-Cantero, E. and Santoyo, G. (2018). Microbial mat ecosystems: Structure types, functional diversity, and biotechnological application. *Electron. J. Biotechnol.* **31**, 48–56.

Proctor, D. M. and Relman, D. A. (2017). The Landscape Ecology and Microbiota of the Human Nose, Mouth, and Throat. *Cell Host Microbe.* **21**, 421–432.

Ratzke, C., Barrere, J. and Gore, J. (2020). Strength of species interactions determines biodiversity and stability in microbial communities. *Nat. Ecol. Evol.* **4**, 376–383.

Rich, J. J., Heichen, R. S., Bottomley, P. J., Cromack, K. and Myrold, D. D. (2003). Community Composition and Functioning of Denitrifying Bacteria from Adjacent Meadow and Forest Soils. *Appl. Environ. Microbiol.* **69**, 5974–5982.

Sasaki, Y., Oguchi, H., Kobayashi, T., Kusama, S., Sugiura, R., Moriya, K., Hirata, T., Yukioka, Y., Takaya, N., Yajima, S., et al. (2016). Nitrogen oxide cycle regulates nitric oxide levels and bacterial cell signaling. *Sci. Rep.* **6**, 1–11.

Schindelin, J., Arganda-Carreras, I., Frise, E., Kaynig, V., Longair, M., Pietzsch, T., Preibisch, S., Rueden, C., Saalfeld, S., Schmid, B., et al. (2012). Fiji: An open-source platform for biological-image analysis. *Nat. Methods* **9**, 676–682.

Shanks, R. M. Q., Caiazza, N. C., Hinsa, S. M., Toutain, C. M. and O'Toole, G. A. (2006). *Saccharomyces cerevisiae*-based molecular tool kit for manipulation of genes from gram-negative bacteria. *Appl. Environ. Microbiol.* **72**, 5027–5036.

Spero, M. A. and Newman, D. K. (2018). Chlorate Specifically Targets Oxidant-Starved, Antibiotic- Tolerant Populations of *Pseudomonas aeruginosa* Biofilms. *MBio* **9**, e01400-18.

Stewart, P. S., Zhang, T., Xu, R., Pitts, B., Walters, M. C., Roe, F., Kikhney, J. and Moter, A. (2016). Reaction-diffusion theory explains hypoxia and heterogeneous growth within microbial biofilms associated with chronic infections. *npj Biofilms Microbiomes.* **2**, 1–8.

Teal, T. K., Lies, D. P., Wold, B. J. and Newman, D. K. (2006). Spatiometabolic stratification of *Shewanella oneidensis* biofilms. *Appl. Environ. Microbiol.* **72**, 7324–7330.

Thalhammer, K. O. and Newman, D. K. (2023). A phenazine-inspired framework for identifying biological functions of microbial redox-active metabolites. *Curr. Opin. Chem. Biol.* **75**, 102320.

Tian, H., Yang, J., Xu, R., Lu, C., Canadell, J. G., Davidson, E. A., Jackson, R. B., Arneth, A., Chang, J., Ciais, P., et al. (2019). Global soil nitrous oxide emissions since the preindustrial era estimated by an ensemble of terrestrial biosphere models: Magnitude, attribution, and uncertainty. *Glob. Chang. Biol.* **25**, 640–659.

Toyofuku, M. and Yoon, S.-S. (2018). Nitric Oxide, an Old Molecule With Noble Functions in *Pseudomonas aeruginosa* Biology. *Adv. Microbial. Phys.* Academic Press. pp. 117–145.

Tsypin, L. M. and Newman, D. K. (2021). Nitrate Reduction Stimulates and Is Stimulated by Phenazine-1-Carboxylic Acid Oxidation by *Citrobacter portucalensis MBL*. *MBio* **12**, e0226521.

Van Rossum, G., Drake, F. L., Harris, C. R., Millman, K. J., van der Walt, S. J., Gommers, R., Virtanen, P., Cournapeau, D., Wieser, E., Taylor, J., et al. (2009). *Python 3 Reference Manual*.

VanDrisse, C. M., Lipsh-Sokolik, R., Khersonsky, O., Fleishman, S. J. and Newman, D. K. (2021). Computationally designed pyocyanin demethylase acts synergistically with tobramycin to kill recalcitrant *Pseudomonas aeruginosa* biofilms. *Proc. Natl. Acad. Sci. U. S. A.* **118**, 118 (12) e2022012118.

VoBwinkel, R., Neidt, I. and Bothe, H. (1991). The production and utilization of nitric oxide by a new, denitrifying strain of *Pseudomonas aeruginosa*. *Arch. Microbiol.* **156**, 62–69.

Wany, A., Pathak, P. K. and Gupta, K. J. (2020). Methods for Measuring Nitrate Reductase, Nitrite Levels, and Nitric Oxide from Plant Tissues. *Methods Mol. Biol.* **2057**, 15–26.

Waskom, M. (2021). Seaborn: Statistical data visualization. *J. Open Source Softw*.

Wessel, A. K., Arshad, T. A., Fitzpatrick, M., Connell, J. L., Bonnecaze, R. T., Shear, J. B. and Whiteley, M. (2014). Oxygen limitation within a bacterial aggregate. *MBio* **5**, e00992.

Widder, S., Allen, R. J., Pfeiffer, T., Curtis, T. P., Wiuf, C., Sloan, W. T., Cordero, O. X., Brown, S. P., Momeni, B., Shou, W., et al. (2016). Challenges in microbial ecology: Building predictive understanding of community function and dynamics. *ISME J.* **10**, 2557–2568.

Wilbert, S. A. and Newman, D. K. (2022). The contrasting roles of nitric oxide drive microbial community organization as a function of oxygen presence. *Curr. Biol.* **32**, 5221-5234.e4.

Wilbert, S. A., Mark Welch, J. L. and Borisy, G. G. (2020). Spatial Ecology of the Human Tongue Dorsum Microbiome. *Cell Rep.* **30**, 4003-4015.e3.

Wingen, M., Potzkei, J., Endres, S., Casini, G., Rupprecht, C., Fahlke, C., Krauss, U., Jaeger, K.-E., Drepper, T. and Gensch, T. (2014). The photophysics of LOV-based fluorescent proteins--new tools for cell biology. *Photochem. Photobiol. Sci.* **13**, 875–883.

Yoon, S. S., Karabulut, A. C., Lipscomb, J. D., Hennigan, R. F., Lymar, S. V., Groce, S. L., Herr, A. B., Howell, M. L., Kiley, P. J., Schurr, M. J., et al. (2007). Two-pronged survival strategy for the major cystic fibrosis pathogen, *Pseudomonas aeruginosa*, lacking the capacity to degrade nitric oxide during anaerobic respiration. *EMBO J.* **26**, 3662–3672.

Yu, K., Mitchell, C., Xing, Y., Magliozzo, R. S., Bloom, B. R. and Chan, J. (1999). Toxicity of nitrogen oxides and related oxidants on mycobacteria: *M. tuberculosis* is resistant to peroxynitrite anion. *Tuber. Lung Dis.* **79**, 191–198.

Zhang, I. H., Mullen, S., Ciccarese, D., Dumit, D., Martocello, D. E., Toyofuku, M., Nomura, N., Smriga, S. and Babbin, A. R. (2021). Ratio of Electron Donor to Acceptor Influences Metabolic Specialization and Denitrification Dynamics in *Pseudomonas aeruginosa* in a Mixed Carbon Medium. *Front. Microbiol.* **12**, 1–13.

Zumft, W. G. (1997). Cell biology and molecular basis of denitrification. *Microbiol. Mol. Biol. Rev.* **61**, 533–616.

Zuñiga, C., Zaramela, L. and Zengler, K. (2017). Elucidation of complexity and prediction of interactions in microbial communities. *Microb. Biotechnol.* **10**, 1500–1522.